INVESTIGATION OF SUSPENDED WALKWAY DISTRESS BY LABORATORY STUDIES OF FOUR CONCRETE CORES AND A POST-POCKET GROUT SAMPLE

EXECUTIVE SUMMARY

Four concrete cores identified as P-1 through P-4 and an anchoring grout sample (PP-1) used to embed steel guardrail posts were received from the PROJECT. Severe corrosion of reinforcing steel and associated extensive delamination of concrete cover over corroded steel has occurred from various locations in five exterior elevated reinforced concrete walkways and adjoining reinforced concrete stairways (e.g., at the locations of Cores P-1 and P-2). Additionally, many anchoring grout pockets (e.g., at the location of the grout sample PP-1) have reportedly shown swelling at the surface. The purposes of laboratory investigations are to determine the compositions, conditions and evidence of any potential chemical and/or physical deterioration of concretes and anchoring grout to understand the field distress. Protective coatings are found at the exposed top and bottom ends of all four cores from which one core was requested for examination of coating applied at the bottom end to investigate the chemical make-up and if the coating is breathable.

The concrete cores were examined by: (a) optical microscopy to determine the compositions, types and potential deteriorations, if any in coarse and fine aggregates, hardened cement pastes in concretes, and air-void systems within (through-depth) and between the cores; and (b) scanning electron microscopy and energy-dispersive X-ray microanalysis (SEM-EDS) of paste composition and microstructure of concrete. Protective coatings applied at both ends of the concrete slabs were examined by: (a) optical microscopy, (b) SEM-EDS, and, (c) Fourier-Transform Infrared (FT-IR) spectroscopy of peeled portions of coatings from the exposed and adhered ends. Anchoring grout sample was examined by: (a) optical microscopy and (b) SEM-EDS to examine composition and microstructure of paste fractions of grout, (c) X-ray diffraction (XRD) to determine bulk mineralogy and possible presence of gypsum, if any, (d) X-ray fluorescence (XRF) to determine bulk chemical composition and sulfate content of grout to investigate possible use of a gypsum-based grout; and (e) thermal analysis of grout to determine the presence of gypsum in grout. Petrographic examinations (optical and electron microscopy and microanalysis *a la* ASTM C 856 and C 1723, respectively), XRD, chemical analysis (XRF), thermal analysis, and FT-IR are the techniques used for examinations of concretes, coatings, and grout.

Concretes present in all four cores are compositionally similar to each other and made using essentially similar concrete ingredients, e.g., (a) crushed granite and crushed chlorite schist coarse aggregate (alkali granite content is higher than chlorite schist) having nominal maximum sizes of $^{3}/_{4}$ in. in. (19 mm) (b) natural siliceous (quartz-quartzite) sand fine aggregate having nominal maximums sizes of $^{3}/_{8}$ in. (9.5 mm); (c) Portland cement pastes having water-cement ratios similar within and between cores and estimated to be 0.45 to 0.50 and cement contents similar between cores and estimated to be from $5^{1}/_{2}$ to 6 bags per cubic yard; and (d) air contents variable within and between the cores indicating variable air-void systems from non-air-entrained concrete at the ends to air-entrained concrete in the interior where absence of air especially at the top and/or bottom ends of cores have created essentially a non-air-entrained appearance of concrete as opposed to detection of higher amount of 'entrained' air in the body to indicate potential air entrainment in the body (e.g., in Cores P-2, and P-4), or, to even absence of any air entrainment all throughout the depth of a core (e.g., in Core P-3), or adequate air entrainment throughout the depth (in Core P-1). Therefore, air content and air entrainment showed lack of quality assurance of concrete being delivered at the locations of examined cores.

Carbonation of concrete has occurred from both top and bottom ends and measured to be from as low as 2 mm in Core P-4 to as high as 30 mm in Core P-3 (15 to 20 mm in Cores P-1 and P-2) from their top ends and from 25 mm (in Cores P-2 and P-4) to 35 mm in Core P-1 and as deep as 45 mm in Core P-3 from their bottom ends. Besides carbonations to as deep as 15 to 30 mm from the exposed end of the cores (which are higher than that normally anticipated for a well-consolidated concrete impermeable to atmospheric carbon dioxide) there is no evidence of any chemical or physical deterioration of concrete detected in the concrete in all cores.

Despite lack of air entrainment at the exposed surface ends of some cores to depths of $^{1}/_{2}$ to 1 in. (e.g., in Cores P-2, P-3, and P-4) and reported exposure to possible freezing, there is, however, no evidence of any cracking of other distress in the concrete at the exposed surface ends that could be contributed to cyclic freezing and thawing of a non-air-entrained concrete at critically saturated conditions. Carbonation is the only mechanism detected in the cores from prolonged exposures to atmospheric carbon dioxide that has penetrated deep enough to promote potential carbonation-induced corrosion of reinforcing steel, if steel is present within the carbonated zone, especially when the concrete cover over steel is shallow. Pastes in the concrete have water-cement ratios and consolidation that have promoted deep penetration of atmospheric carbon dioxide. Carbonation-induced corrosion of steel especially over shallow concrete cover can cause

cracking and delamination of concrete cover over the exposed corroded steel. Both coarse and fine aggregates are present in sound condition and did not contribute to any distress.

All four cores showed two protective coatings at their exposed ends (Coat #1 and 2), and, two protective coats at the bottom ends (Coat #3 and 4) that are compositionally similar for each coat across the cores. Coat #1 is an elastomeric non-breathable urethane waterproofing membrane, gray to beige in color, less than 0.1 to 1.2 mm non-uniform thickness (maximum thickness is at the locations of quartz filler and minimum where filler is absent), showing characteristic titanium-enrichment from Ti-oxide pigment, and magnesium and silica in SEM-EDS and characteristic FT-IR absorption bands from Talc filler. Coat #2 beneath #1 at the top end is directly adhered to concrete, which is a non-breathable epoxy-based binder, gray to ash in color, 0.8 mm nominal thickness, more uniform in thickness than Coat# 1 due to the absence of any coarse quartz fillers, but contain potential silicate (slag, fine silt-sized quartz) fillers as detected in SEM-EDS and silicate absorption bands in FT-IR studies. Coat #3 at the bottom end is directly adhered to concrete, which is a non-breathable poly-vinyl acetate (PVA)-based paint, off-white in color, 0.5 to 0.8 mm non-uniform thickness, showing characteristic titanium-enrichment from Ti-oxide pigment in SEM-EDS studies and also characteristic absorption bands for china clay pigment, silicate (slag, fine silt-sized quartz) and calcite fillers from FT-IR studies. Coat #4 applied over #3 at the bottom end directly exposed to the environment is another PVA-based paint, milky white in color, 0.5 to 0.6 mm and non-uniform thickness, showed multi-layered applications that appeared opaque in transmitted plane-polarized light observations in a petrographic microscope. FT-IR studies showed characteristic absorption bands for urethane in Coat #1, epoxy in Coat #2, and PVA in Coat #3 and 4. Protective coatings are mostly well-bonded to each other and to concrete for those directly applied on concrete surfaces over the area of examinations in the cores.

Core Nos. P-1 and P-2 were reportedly collected respectively from areas exhibiting: (a) extensive delaminations; near excavation revealed severe rebar corrosion at the location of P-1, and (b) nearby walkway soffit delamination at the location of P-2; low cover soffit reinforcement is corroded – higher cover rebar minimally corroded in nearest excavation. No visible distress was noted at the locations of Cores P-3 and P-4.

As mentioned, except carbonation of concrete to depths as deep as 30 mm from top exposed end and 45 mm from bottom end, and potential carbonation-induced corrosion of steel in concrete if steel is present within the carbonated zone (especially at the locations of shallow concrete covers over top layer of steel) there is no other evidence of any chemical or physical deterioration of concrete detected in the cores. Reported field evidence of extensive delaminations over severely corroded rebar at the location of P-1, and walkway soffit delamination at the location of P-2 over low cover, and minimal rebar corrosion over higher concrete cover over rebar are consistent with petrographic observations.

The examined fragmented but dense, hard, intact pieces of distressed anchoring grout (PP-1) showed a blended Portland cement and calcium aluminate/sulfoaluminate-based formulation, and its application in a moist outdoor environment, where the grout was exposed to moisture during service to facilitate post-hardening sulfate-aluminate reactions in the presence of moisture during service. As a result, the grout has undergone expansion not only during hardening to provide the anchoring but also after hardening, from exposure to water with further disintegration during service from continued sulfate-aluminate reactions in the hydration products of cementitious binders. Mineralogy and microstructure of the grout shows quartz sand in a Portland cement and calcium aluminate/sulfoaluminate-based binder formulation. No free gypsum was detected in optical, SEM-EDS, XRD, or thermal studies but compositions of paste in SEM-EDS studies indicated blended Portland and calcium sulfoaluminate-based formulation as opposed to gypsum-based formulation of grout. Bulk sulfate (as SO_3) content in the distressed grout is 4.3 percent, which is less than that of a gypsum-based grout but higher than that of a Portland cement-based grout, indicating presence of a sulfate component in the binder, which is not gypsum but a calcium sulfoaluminate cement. Reported swelling is judged to be due to a combination of continued sulfate-aluminate reactions in the presence of moisture during service along with possible freezing-related expansion at saturated conditions, both of which are related to easy accessibility of moisture to the grout during service. Unfortunately, the best method to mitigate the existing swelling problem is to remove the distressed grout and reinstall the anchoring grout with a more durable and acceptable material with a proven service-record in the moist outdoor environment, and installed by strictly following the manufacturer's application guidelines. Access of moisture to the grout during service must also be restricted.

INTRODUCTION

Reported herein are the results of detailed laboratory studies of four (4) hardened concrete cores and a fragmented "post-pocket" grout sample received from CLIENT. The samples were, reportedly, taken from suspended walkways at the PROJECT.

BACKGROUND INFORMATION & TESTING STRATEGY

The following background information was received with the samples:

Project: PROJECT

Building Location: LOCATION

Extraction Date: 5/24/2018

Site Samples for ASTM C 856 – Petrographic Examination of Hardened Concrete

The general characteristics of samples are provided in the following table.

Note: White coating on bottom of one petrographic sample should be analyzed via FTIR. The intent of this testing is to determine the type of coating and if it is generally a breathable material.

Sample ID	Sample Type	Proximate Distress
P-1	4″ Core	Extensive delaminations; near excavation revealed severe rebar corrosion
P-2	4″ Core	Walkway soffit delaminated nearby; low cover soffit reinforcement is corroded – higher cover rebar minimally corroded in nearest excavation
P-3	4″ Core	No Distress
P-4	4″ Core	No Distress

Site Sample for Scanning Electron Microscopy (SEM). Sample is from grout used to embed steel guardrail posts. Intent of testing is to determine if grout material is reactive. Reactive grout material is suspected because many pockets are visibly swelling at the surface.

Sample ID	Sample Type	Proximate Distress
PP-1	4″ Core	No visible distress or anomalies around the grout pocket

Background Information:

- Subject Building: Barbee Hall – Student Dormitory at North Carolina A&T University
- Subject Structures: Five exterior elevated reinforced concrete walkways and adjoining reinforced concrete stairways.
- Coatings: Urethane deck coating applied on top of walkways. Age of coating unknown. Bottom of walkways coated with unknown white paint. Goal of FTIR coating is to classify this white paint material and determine if it is generally breathable.

- Distress: Walkways are generally in good condition with the exception of isolated delaminations. Stairways are dilapidated.
- Reinforcement cover generally sufficient in evaluated areas (at least 1-1/2″ on average).
- Steel guardrails are embedded in grouted post pockets. Swelling, staining, and significant post corrosion at these pockets is common. An SEM sample has been included (PP-1) to determine if the grout material is reactive.

FIELD PHOTOGRAPHS

The following figures show the field photographs of the elevated walkways and visible distress.

Figure 1: Field photograph showing an overview of the elevated concrete walkway slabs.

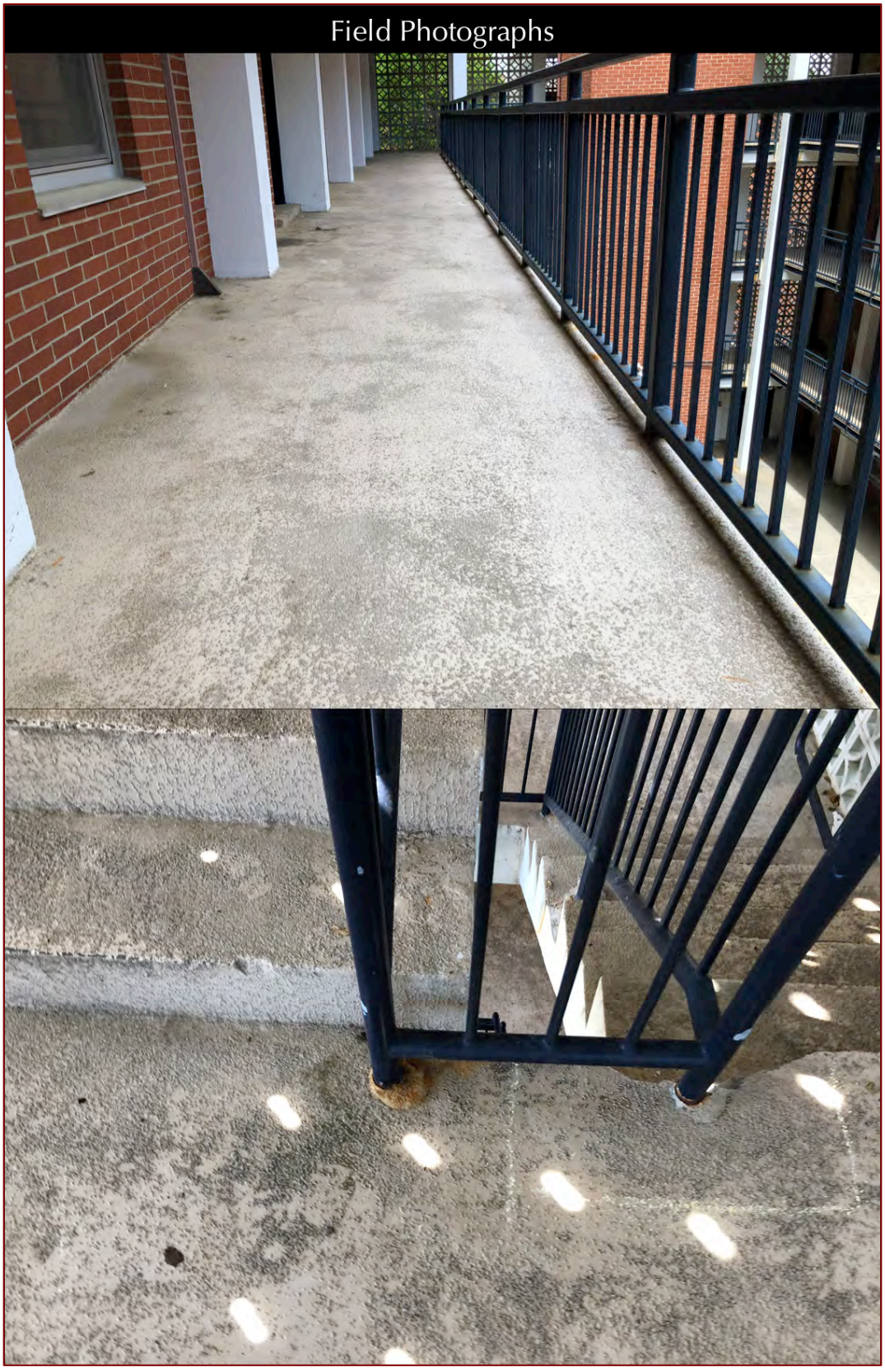

Figure 2: Field photographs showing the condition of the walkway surface (top), and the conditions of the concrete stairs and rail-post grout (bottom).

PURPOSE OF PRESENT INVESTIGATION

Of the samples received, four concrete cores (P-1, P-2, P-3, and P-4) were requested for petrographic examinations, one core (P-4) was requested for FT-IR analysis of the white coating on the bottom surface, and the 'post-pocket' sample (PP-1) was requested for scanning electron microscopy. Based on the background information provided, the purposes of the present investigation are to determine:

a. The compositions, qualities, and overall conditions of concretes in the cores;
b. Evidence of any physical or chemical deterioration of concretes in the cores;
c. Thickness, condition, bonding characteristics, and type of protective coatings on concrete;
d. The composition, quality, and condition of the rail-post grout; and,
e. Finally, based on detailed laboratory investigation, investigation of overall qualities and conditions of existing concrete, protective coatings, and anchoring grout samples.

SAMPLES

PHOTOGRAPHS, IDENTIFICATIONS, INTEGRITY, AND DIMENSIONS

Received for detailed laboratory studies were four (4) concrete cores identified as Nos. P-1, P-2, P-3, and P-4. The cores have nominal diameters of 3⅝ in. (90 mm) to 3¾ in. (95 mm), and nominal lengths of 4¾ in. (120 mm) to 5⅛ in. (130 mm). All four cores were received in intact condition with no evidence of joints or large voids within the concretes. Figures 4 to 7 show the cores as received.

ID	Diameter	Length	Top Surface	Bottom Surface	Cracking	Embedded Items	Condition
P-1	3⅝ in. (90 mm)	4¾ in. (120mm)	Tan Urethane Coating	White Protective Coating	None	None	Intact (Figure 4)
P-2	3¾ in. (95 mm)	5 in. (125mm)	Tan Urethane Coating	White Protective Coating	None	None	Intact (Figure 5)
P-3	3⅝ in. (90 mm)	5⅛ in. (130)	Tan Urethane Coating	White Protective Coating	Large horse-shoe-shaped crack on side surface extending from 1 in. to 4 in. from top surface	None	Intact (Figure 6)
P-4	3⅝ in. (92 mm)	5⅛ in. (130mm)	Tan Urethane Coating	White Protective Coating	None	None	Intact (Figure 7)

Table 1: Overall dimensions and conditions of the cores, as received.

Sample PP-1 was received as several fragmented pieces (Figure 3). Grout sample is medium grey, dense and hard.

END SURFACES

Top surfaces of all four cores are finished tan urethane coating, and the bottom surfaces of all four cores show a white paint coating. Figures 4 through 7 show the top and bottom surfaces of the cores, as received.

CRACKING & OTHER VISIBLE DISTRESS

Core P-3 contains a major horse-shoe-shaped crack on the cylindrical side surface extending from a depth of 1 in. to 4 in. from the top surface (Figure 6). There is no evidence of any other distress of concrete found in the other three cores received.

EMBEDDED ITEMS

There is no evidence of fibers, wire mesh, reinforcing steel, or other embedded items found in the cores.

RESONANCE

The cores have a ringing resonance, when hammered.

Figure 3: Shown are the rail-post grout sample PP-1 as received in a plastic Ziploc bag (left), and the individual pieces after removal from the bag (right). Notice the overall hard intact nature of individual pieces, despite the fragmented nature of overall grout.

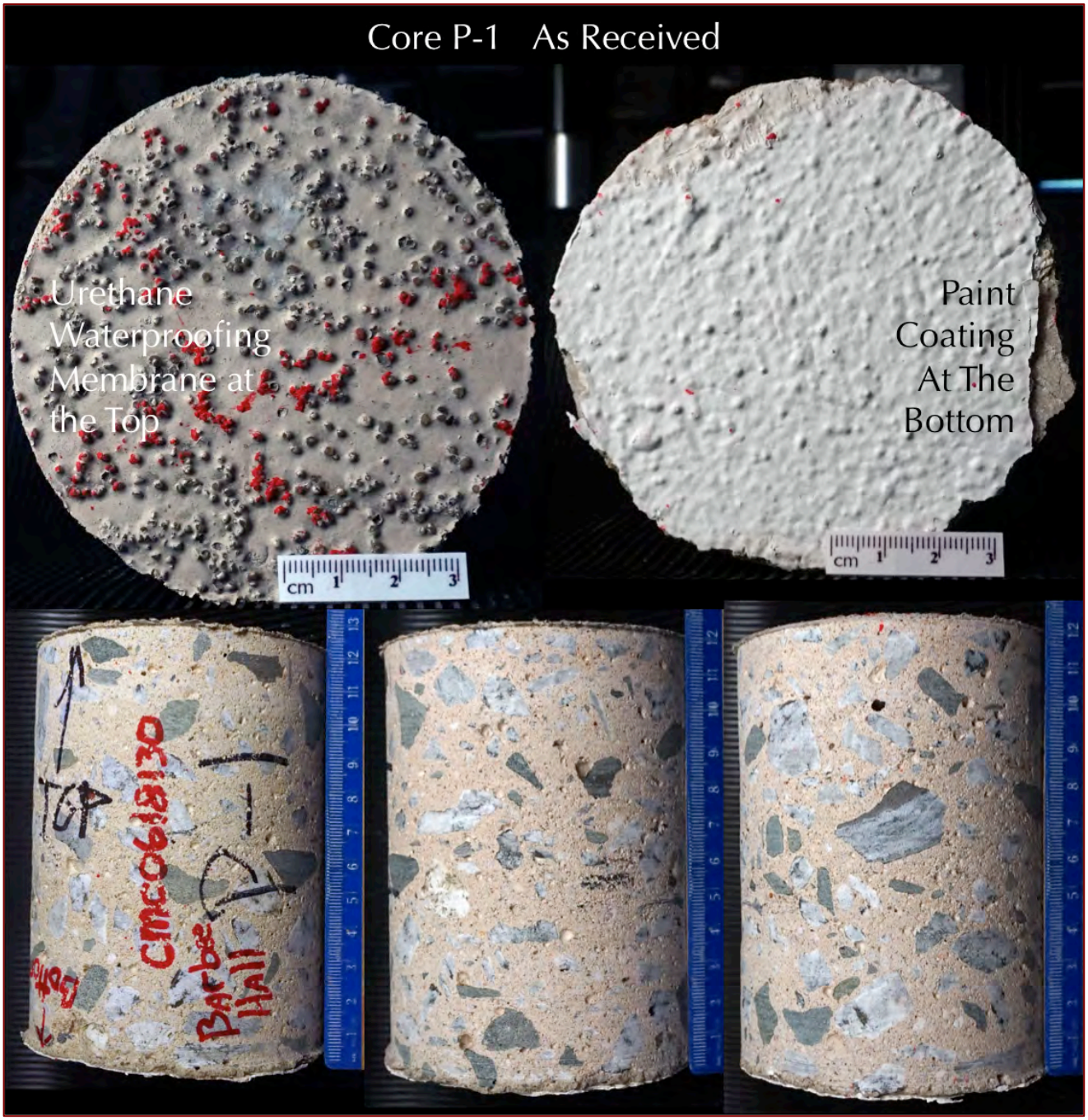

Figure 4: Shown are: (a) the top surface with tan urethane-type waterproofing membrane (top left); (b) the bottom surface with white coating (top right); and (c) cylindrical side views of Core P-1 (bottom photos), as received. Notice the overall beige color of concrete in the cylindrical surfaces.

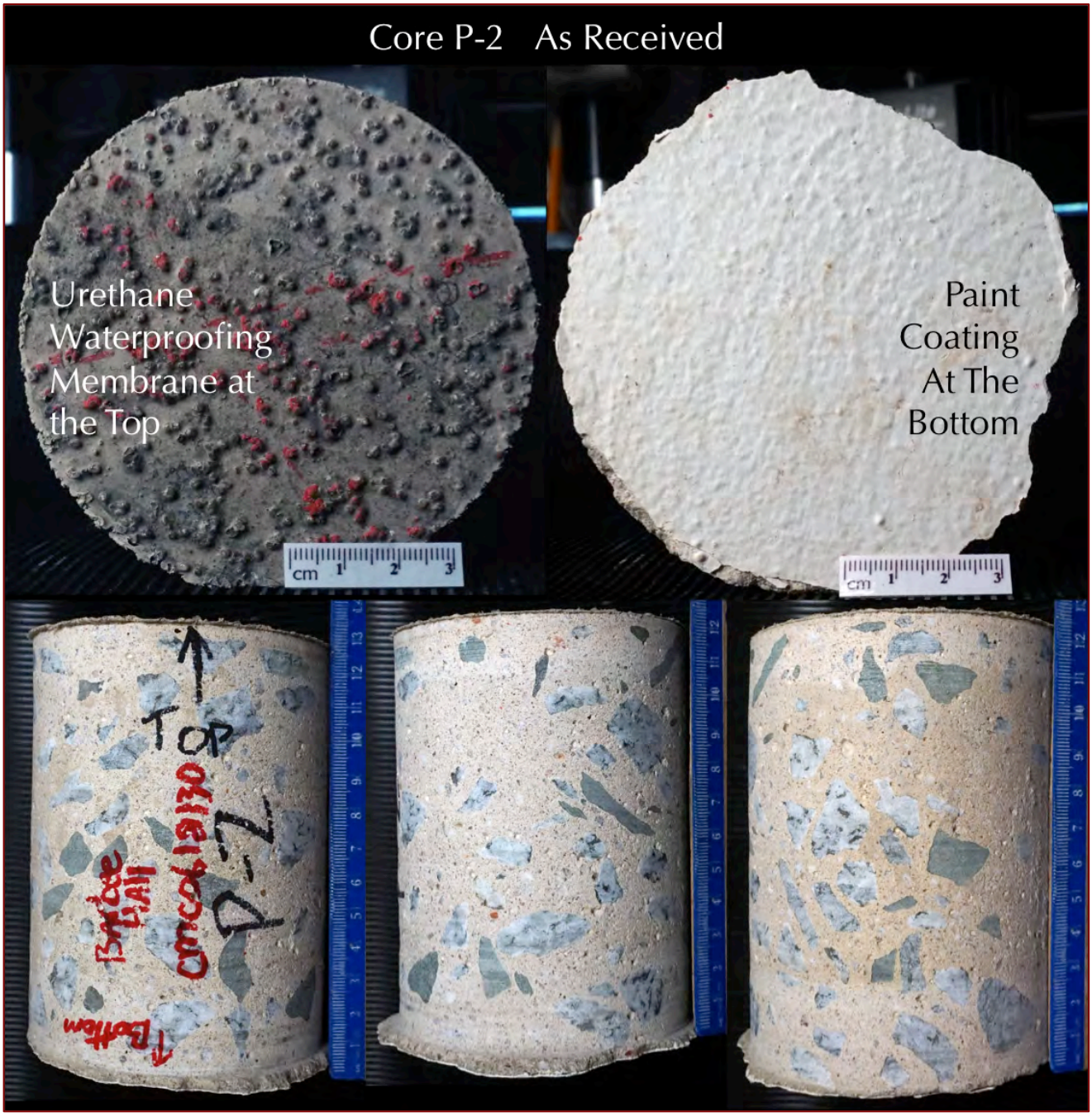

Figure 5: Shown are: (a) the top surface with tan urethane-type waterproofing membrane (top left); (b) the bottom surface with white coating (top right); and (c) cylindrical side views of Core P-2 (bottom photos), as received.

Figure 6: Shown are: (a) the top surface with tan urethane-type waterproofing membrane (top left); (b) the bottom surface with white paint coating (top right); and (c) cylindrical side views of Core P-3 (bottom photos), as received. Red arrows in the bottom middle photo indicate the horse-shoe-shaped crack, which extends from 1 in. to 4 in. from the top surface.

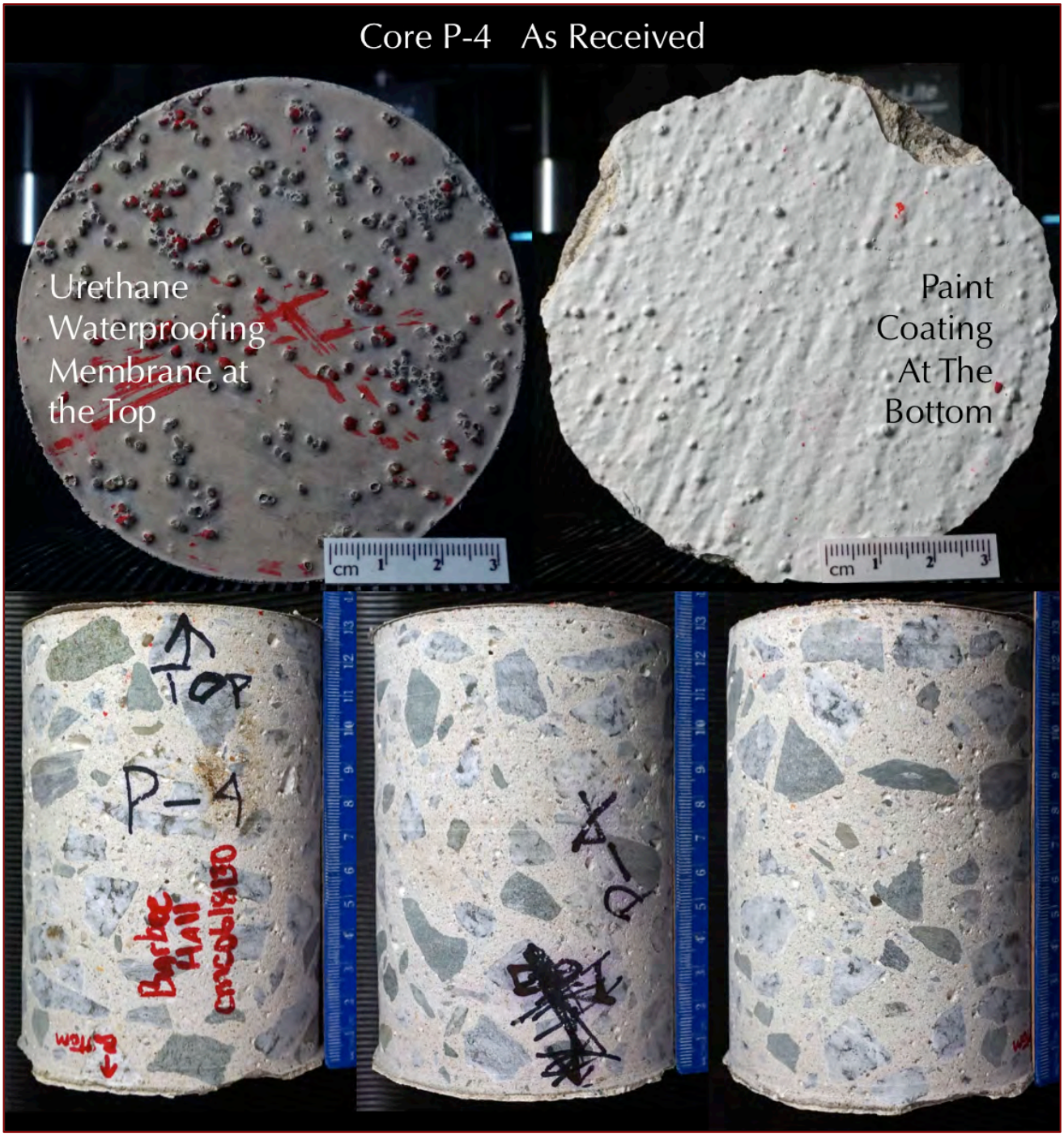

Figure 7: Shown are: (a) the top surface with tan urethane-type waterproofing membrane (top left); (b) the bottom surface with white paint coating (top right); and (c) cylindrical side views of Core P-4 (bottom photos), as received.

METHODOLOGIES

OPTICAL MICROSCOPY

Cores P-1, P-2, P-3, and P-4 were tested and examined by following the methods of ASTM C 856 "Standard Practice for Petrographic Examination of Hardened Concrete." Details of concrete petrography, and sample preparation techniques for petrographic examinations of concrete are provided in Jana (1997a, 1997b, 2005, 2006).

Briefly, the steps followed during petrographic examination of the cores include:

i. Visual examinations of the cores, as received, including adequate documentation of dimensions, measurements, condition, physical properties, integrity, etc.;

ii. Low-power stereomicroscopical examinations of as-received, saw-cut and freshly fractured sections, and lapped cross sections of cores for evaluation of texture, air-void systems, and compositions;

iii. Examinations of oil immersion mounts in a petrographic microscope for mineralogical compositions of specific areas of interests;

iv. Examinations of blue dye-mixed (to highlight open spaces, cracks, etc.) low-viscosity epoxy-impregnated large area (50 mm × 75 mm) thin sections of concretes in a petrographic microscope for detailed compositional and microstructural analyses (Figure 8);

v. Photographing the cores, as received and at various stages of preparation with a digital camera and a flatbed scanner;

vi. Photomicrographs of lapped sections and thin sections of cores taken from stereomicroscope and petrographic microscope, respectively, to provide detailed compositional and mineralogical information of concretes; and,

vii. A Jenoptik Progres GRYPHAX camera attached to a Nikon Eclipse 600 POL petrographic microscope (equipped with reflected, transmitted, polarized and fluorescent-light facilities), a Jenoptik Progres C14 camera attached to an Olympus SZH reflected and transmitted-light stereomicroscope, and an OMAX digital camera attached to a Nikon SMZ-10A low-power stereomicroscope were used together for detailed optical microscopical examinations and associated digital photomicrography.

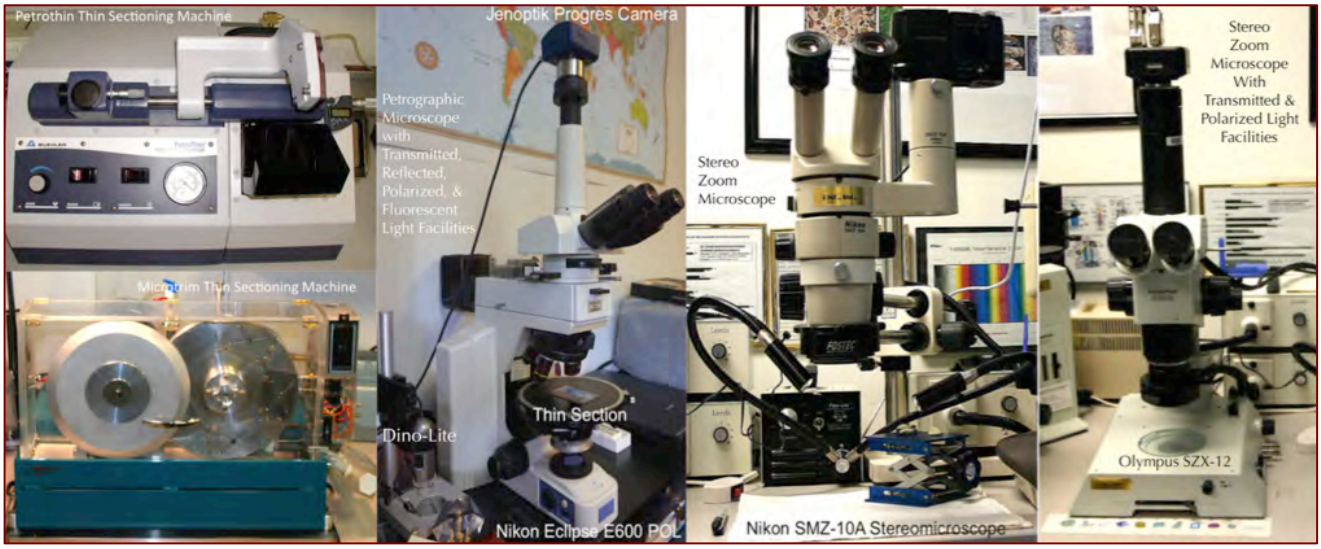

Figure 8: Thin sectioning equipments (left), petrographic micorscope (2nd from left), stereozoom microscope (3rd from left), and transmitted-light stereozoom microscope (rightmost) used in optical micorscopy.

SCANNING ELECTRON MICROSCOPY & ENERGY-DISPERSIVE X-RAY SPECTROSCOPY (SEM-EDS)

SEM-EDS studies were employed for examination of: (a) protective coatings and (b) composition of paste in the concrete in Core P-4, and (c) microstructural and microchemical analyses of the anchoring grout sample. Thin sections of these samples already prepared for optical microscopy were polished and portions of thin sections were coated with a conductive gold-palladium film for SEM-EDS studies and examined in a Cambridge CamScan Series II scanning electron microscope equipped with a backscatter detector, a secondary electron detector, and x-ray fluorescence spectrometer (Figure 9) to determine composition and microstructures of the materials.

Methods followed in scanning electron microscopy and energy-dispersive X-ray fluorescence spectroscopy (SEM-EDS) include: (a) secondary electron imaging (SEI) to determine the surface texture, microstructure and morphology of the examined surface, (b) backscatter electron (BSE) imaging to determine compositions of various phases from various shades of darkness/grayness from average atomic numbers of phases from the darkest pore spaces to brightest iron minerals (via minerals e.g., thaumasite, periclase, ettringite, quartz, dolomite, monosulfate, gypsum, calcite, C-S-H, aluminate, calcium hydroxide, belite, alite, free lime, and ferrite having progressively increasing average atomic numbers and brightness in BSE image), (c) X-ray elemental mapping (dot mapping) of an area of interest to differentiate various phases, (d) point-mode or area (raster)-mode analysis of specific area/phase of interest on a polished thin or solid section, and (e) average compositional analysis of a specific phase or an area on a polished thin or solid section or small subset of a sample.

Figure 9: SEM-EDS: Cambridge CamScan Series II Scanning Electron Microscope and 4Pi Revolution software, backscatter detector, secondary electron detector, and energy-dispersive X-ray fluorescence spectrometer.

Procedures for SEM examinations are described in ASTM C 1723. Sarkar et al. (2000) described various applications of SEM-EDS in concrete and other construction materials. Polished and coated thin section (or polished solid encapsulated block) of mortar is examined in an SEM equipped with backscatter detector, secondary electron detector, and energy-dispersive X-ray fluorescence spectrometer.

X-RAY DIFFRACTION

Bulk mineralogical composition, particularly the potential presence of gypsum in the anchoring grout sample was determined by X-ray diffraction (XRD) in a Siemens D 5000 powder diffractometer ((θ-2θ goniometer, Figure 10) by employing a long line focus Cu X-ray tube, divergent and anti-scatter slits fixed at 1 mm, a receiving slit (0.6 mm), diffracted and incident beam Soller slits (0.04 rad), a curved graphite diffracted beam monochromator, and a sealed proportional counter. Generator settings used are 45 kV and 30mA. A dry, finely ground sample pulverized to pass US 325 sieve (44-µm) is placed in a 1-in. diameter circular sample holder and excited with the copper radiation of 1.54 angstroms. Tests are performed at a 2-theta range from 4° to 64° with a step of 0.02° and a dwell time of one second.

The resulting diffraction patterns are collected by using DataScan 4 software of Materials Data, Inc. (MDI), analyzed by using Jade 9.0 software of MDI with ICDD PDF-4 (Minerals 2017) diffraction data, and, phase identification, and quantitative analyses were carried out with MDI's Search/Match and Easy Quant modules, respectively.

Figure 10: Siemens D 5000 X-ray diffractometer used for mineralogical composition of grout.

ENERGY-DISPERSIVE X-RAY FLUORESCENCE SPECTROSCOPY (ED-XRF)

An energy-dispersive bench-top x-ray fluorescence unit from Rigaku Americas Corporation (NEX-CG, Figure 11) is used for determination of bulk chemical (oxide) composition of grout, particularly the sulfate content. Unlike conventional EDXRF analyzers, the NEX CG was engineered with a unique close-coupled Cartesian Geometry (CG) optical kernel that dramatically increases signal-to-noise. By using monochromatic secondary target excitation, instead of conventional direct excitation, sensitivity is further improved. The resulting dramatic reduction in background noise, and simultaneous increase in element peaks, result in a spectrometer capable of routine trace element analysis even in difficult sample types. The instrument is calibrated by using various certified (CCRL, NIST, GSA, and Brammer) reference standards of cements and rocks. The same pellet used for XRD for mineralogical compositions is used for XRF to determine the chemical composition.

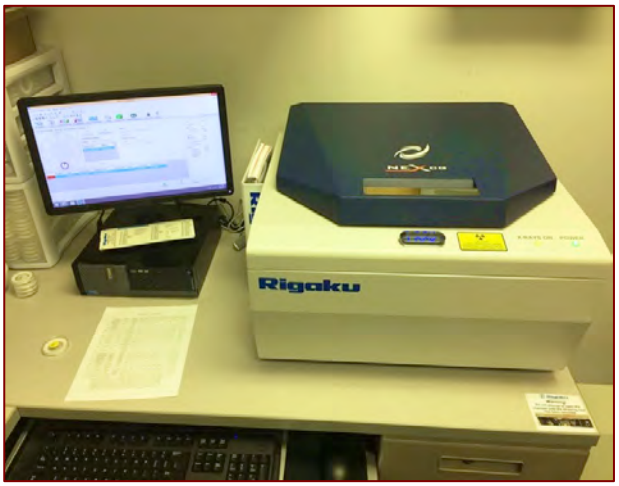

Figure 11: Rigaku NEX-CG bench-top ED-XRF unit used for bulk chemical composition of grout.

A representative portion of grout (about 8 grams) is pulverized down to minus US 325 sieve (finer than 45 microns size) in a Rocklab pulverizer with a grinding aid/binder (7.5% binder by weight of sample), and then pelletized (approximately 7 grams) to a 31-mm diameter pellet in a 25-ton press.

FOURIER-TRANSFORM INFRARED SPECTROSCOPY

For Core P-4 compositions of coatings present on the top and bottom ends were further studied by Fourier Transform Infrared Spectroscopy (FT-IR). FT-IR is particularly useful for detection of admixture, additives, and polymer resins through identification of various organic components (functional groups) (e.g., methyl CH_3, organic acids CO-OH, carbonates CO_3) from their characteristic spectral fingerprints in FTIR spectrum. FTIR can also be used for detection of main mineral phases in a hydraulic binder, CSH, carbonates, gypsum, and clays. Organic compounds such as synthetic (e.g., acrylics, polyesters) and natural resins, carbohydrates, colorants, oils and fats, proteins, waxes as well as inorganic compounds, e.g., corrosion products, minerals, pigments, paints, fillers, stone, glass, and ceramics can be detected by this technique.

Figure 12: Perkin Elmer Spectrum 100 FT-IR with Universal ATR.

For analyses of coatings, FT-IR is done in a Perkin Elmer Spectrum 100 FTIR spectrophotometer (Figure 12) running with Spectrum 10 software. Coating samples were collected from Core P-4 with a razor blade and measured using attenuated total reflection (ATR) on a single bounce diamond/ZnSe ATR crystal. Opposite side of peeled coating sample was measured between a frequency range of 4000 to 650 cm^{-1}. Each run was collected at 4 cm^{-1} resolution with Strong Beer-Norton apodization. Data were collected with a temperature-stabilized deuterated triglycine sulfate (DTGS) detector by placing the sample in contact with the ATR crystal and by applying force from the pressure applicator supplied with the ATR accessory. The application of pressure enabled the coating to be in intimate contact with the ATR crystal, ensuring a high-quality spectrum was achieved.

THERMAL ANALYSES

In addition to XRD, mineralogical compositions of anchoring grout, particularly sulfate in grout is further determined from thermal analysis. Thermal analyses are usually done to determine the presence and quantitative amounts of: (a) hydrates (e.g., detection of CSH by its decomposition at 150-250ºC); (b) sulfates (gypsum from decompositions at 125ºC, and 185-200ºC, ettringite at 120-130ºC, thaumasite at 150ºC); (c) hydrate water, e.g., calcium silicate hydrate from decomposition at 180-190ºC, Portlandite from decomposition at 400-600ºC; (d) quartz from polymorphic transformation (α to β form) at 573ºC; (e) cryptocrystalline calcite in the carbonated lime matrix from decomposition at 620-690ºC, magnesite at 450-520ºC, or (f) coarsely crystalline calcite e.g., in limestone by decomposition at 680-800ºC or (g) dolomite at 740-800ºC and 925ºC, (h) phase transition of belite (C_2S) at 693ºC, etc. Phases are determined from their characteristic decomposition temperatures occurring mostly as endothermic peaks or polymorphic transition temperatures as for quartz. Simultaneous TGA and DSC analyses (Figure 13) were done in a Mettler Toledo TGA/DSC 1 unit on 30-70 mg of finely ground (<0.6 mm) sample in alumina crucible (70 µl, no lid) from 30°C to 1000°C at a heating rate of 10°C/min with high purity nitrogen as purge gas at a flow rate of 75.0 ml/min. By using one of the three removable sensor types the TGA/DSC 1 simultaneously measures heat flow in addition to weight change. The instrument offers high resolution (ultra-microgram resolution over the whole measurement range), efficient automation (with a reliable sample robot for high sample throughput), wide measurement range (measure small and large sample masses and volumes) broad temperature scale (analyze samples from ambient to 1100°C), superior ultra-micro balance, simultaneous DSC heat flow measurement (for simultaneous detection of thermal events, e.g., polymorphic alpha-to-beta transition of quartz and quartz content), and a gastight cell (ensures a properly defined measurement environment).

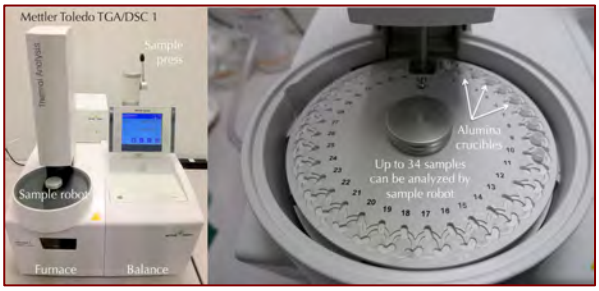

Figure 13: Mettler-Toledo TGA/DSC1 unit for simultaneous thermogravimetric analysis (TGA), and differential scanning calorimetry (DSC).

PETROGRAPHIC EXAMINATIONS – CONCRETE AND COATINGS

LAPPED AND PHENOLPHTHALEIN-TREATED SAW-CUT CROSS SECTIONS

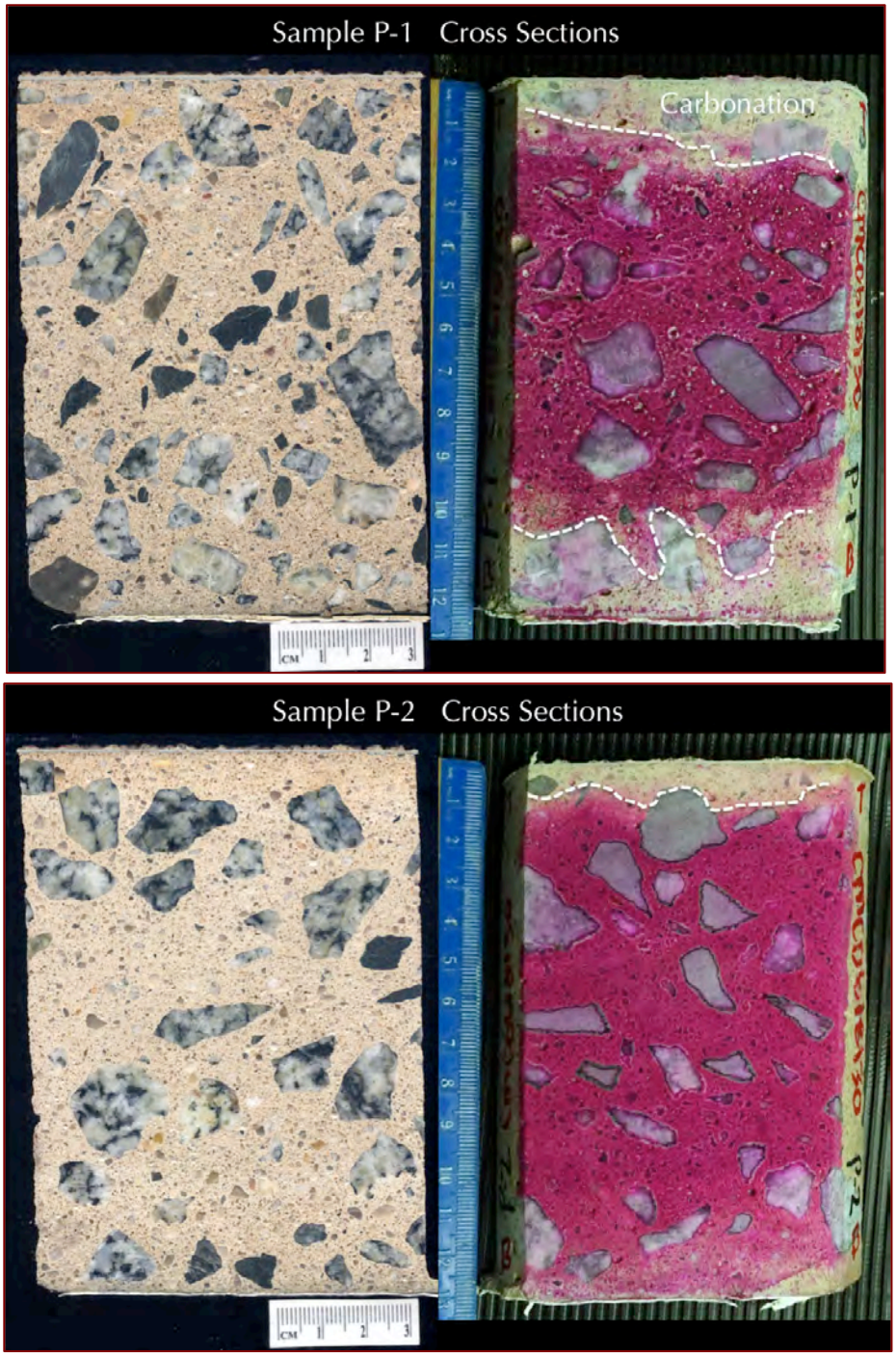

Figure 14: Lapped cross section (left) and saw-cut cross section treated with phenolphthalein alcoholic solution (right) of Core P-1 (top) and P-2 (bottom) showing: (a) size, shape, angularity, gradation, and distribution of crushed stone coarse aggregate, (b) overall dense and well-consolidated nature of concrete; (c) carbonation of concrete from both ends as indicated by the cream-colored carbonated surface regions as opposed to pink discolored interior non-carbonated concrete.

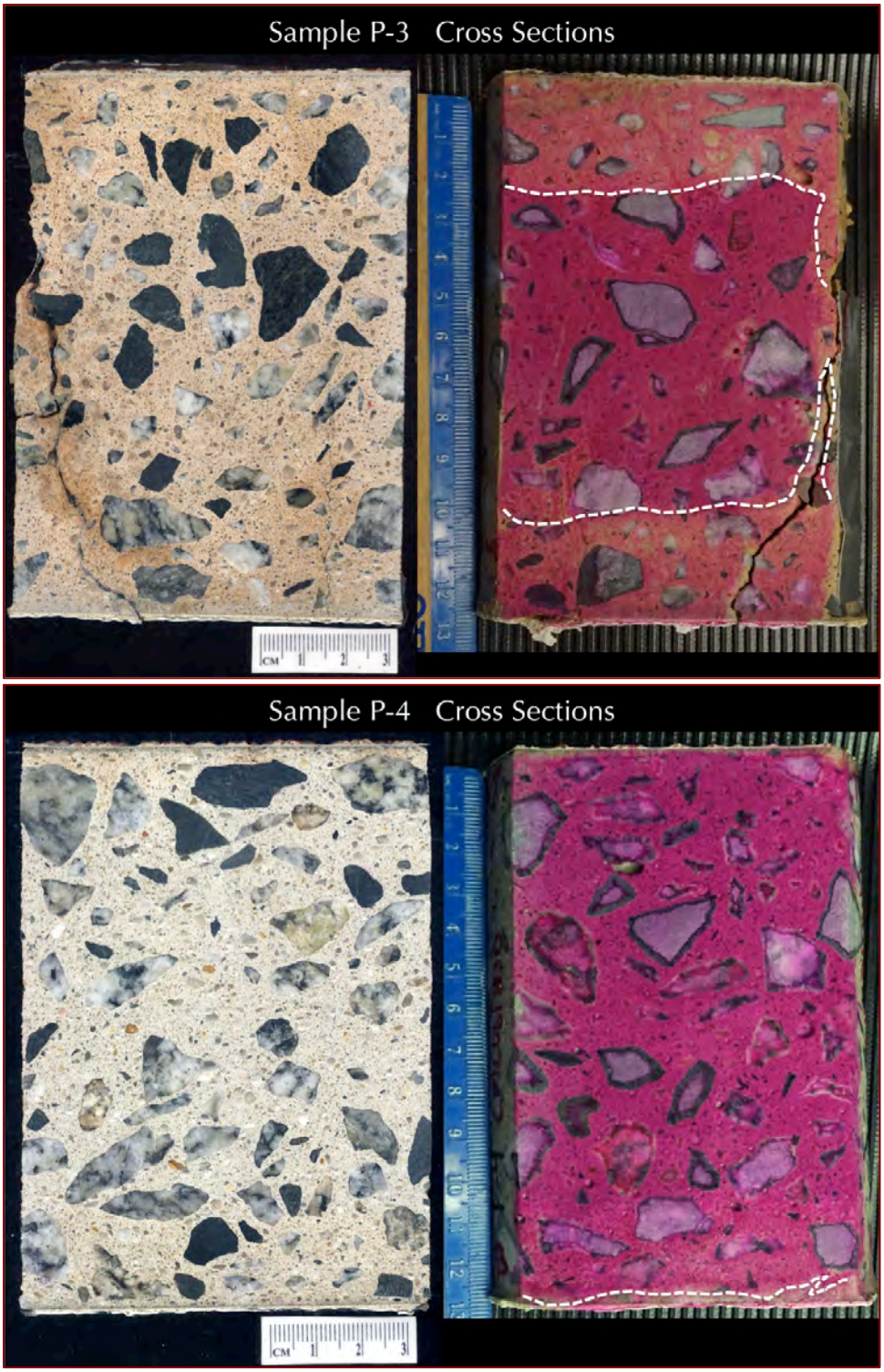

Figure 15: Lapped cross section (left) and saw-cut cross section treated with phenolphthalein alcoholic solution (right) of Core P-3 (top) and P-4 (bottom) showing: (a) size, shape, angularity, gradation, and distribution of crushed stone coarse aggregate, (b) overall dense and well-consolidated nature of concrete; (c) carbonation of concrete from both ends as indicated by the cream-colored carbonated surface regions as opposed to pink discolored interior non-carbonated concrete.

PHOTOMICROGRAPHS OF LAPPED CROSS SECTIONS OF CORES

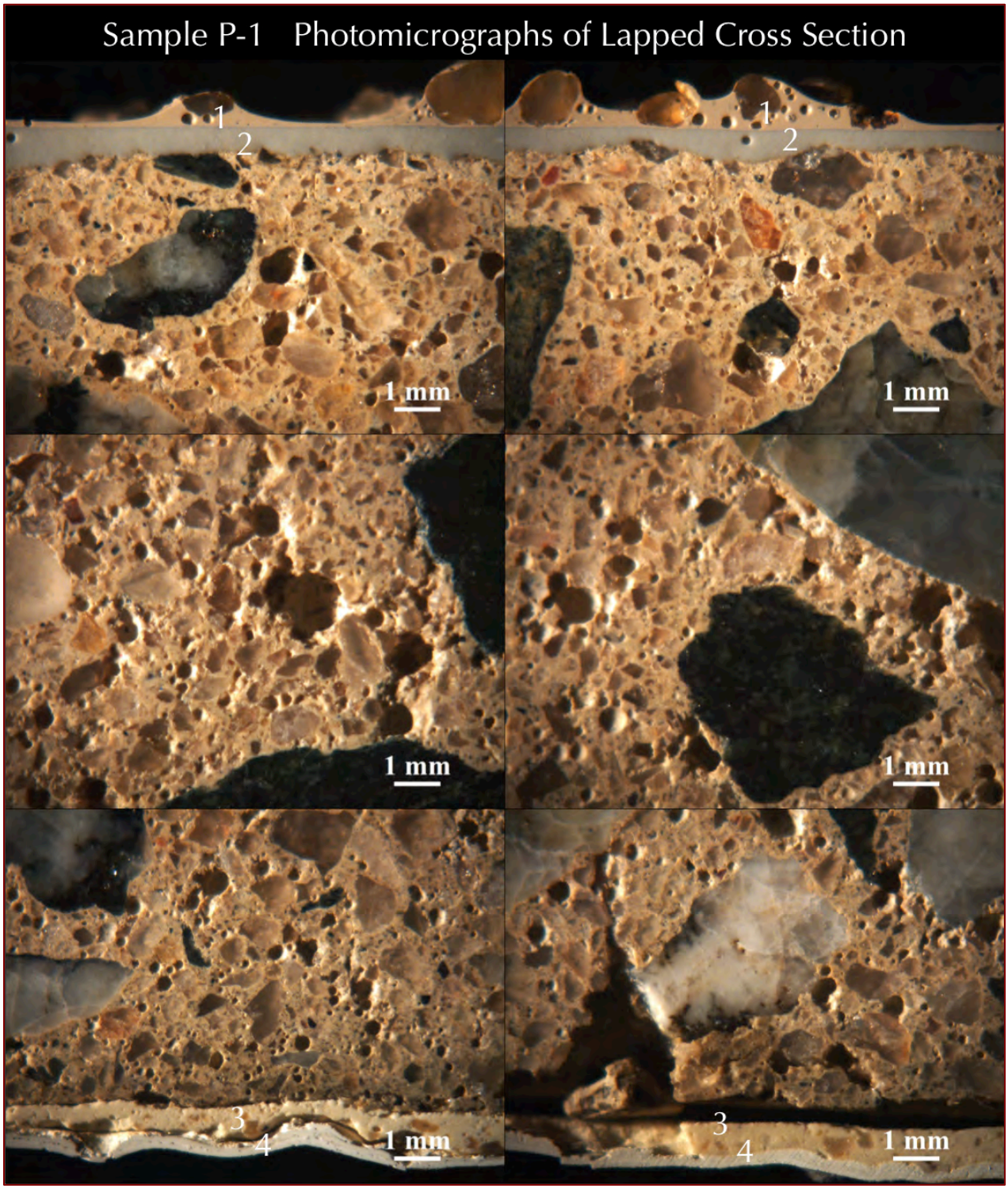

Figure 16: Photomicrographs of lapped cross section of Core P-1 showing: (a) two protective coatings #1 and 2 at the top, and another two coatings #3 and 4 at the bottom end; and (b) air-entrained (AE) nature of the concrete with many spherical voids less than one mm in size but non-uniform distribution of air (all photos). Air is higher in the interior than at both ends. Air varied from 5-6% (AE) at top $^{3}/_{4}$ in., to 9-10% (AE) from $^{3}/_{4}$ to to $3^{3}/_{4}$ in. depth, then 7-8% (AE) from $3^{3}/_{4}$ to $4^{3}/_{4}$ in. depth from top.

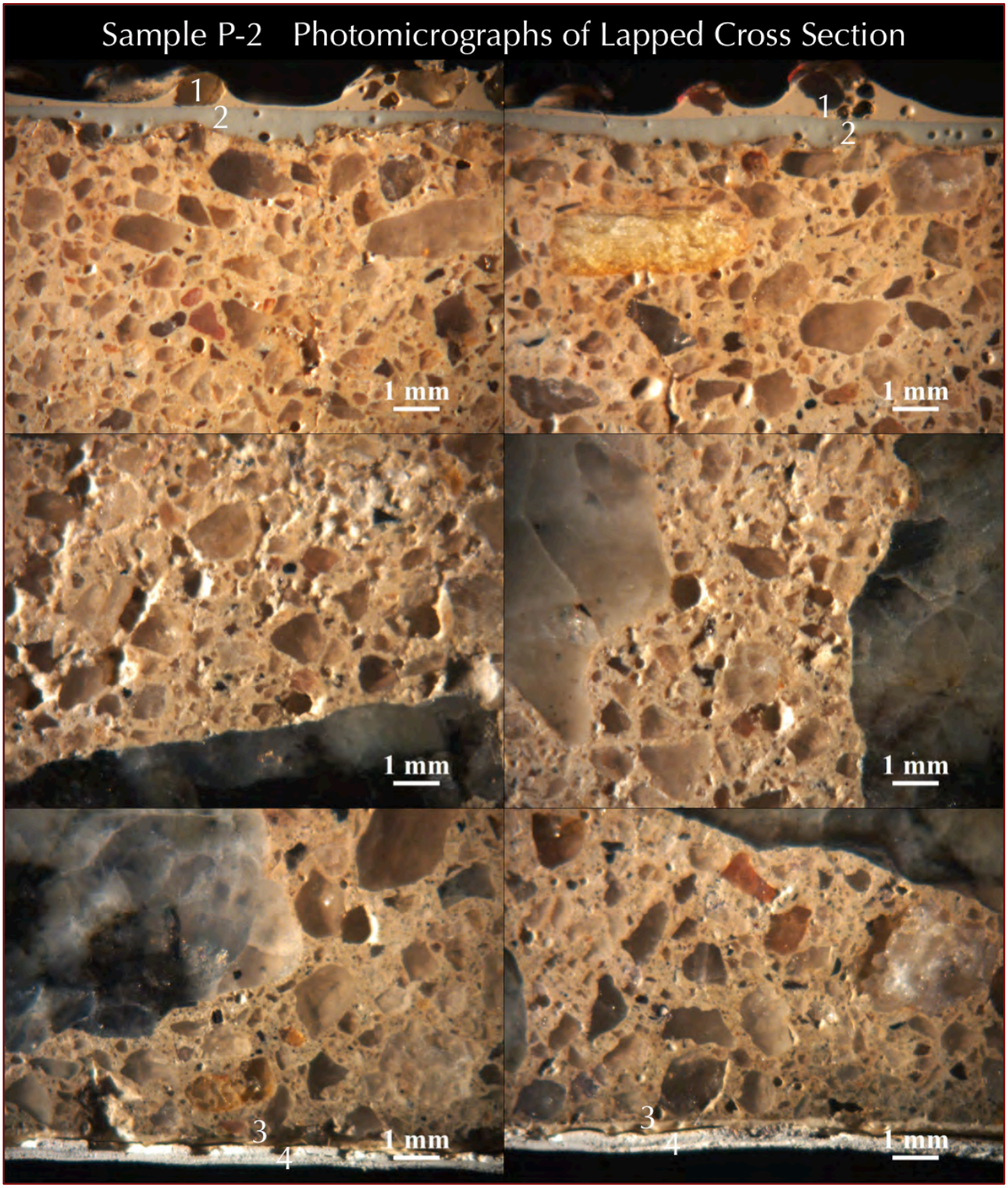

Figure 17: Photomicrographs of lapped cross section of Core P-2 showing: (a) two protective coatings #1 and 2 at the top and another two coatings #3 and 4 at the bottom end; and (b) no air at the ends to air-entrained (AE) nature of the interior concrete with a few spherical voids less than one mm in size but non-uniform distribution of air (all photos). Air is higher in the interior than at both ends. Air varied from 1-2% (non-AE) at top 1 in. depth to 5-6% (AE) from 1 to 4 in. depth, then droped to $1^1/_2$ to $2^1/_2$% (non-AE) at 4 to 5 in. depth.

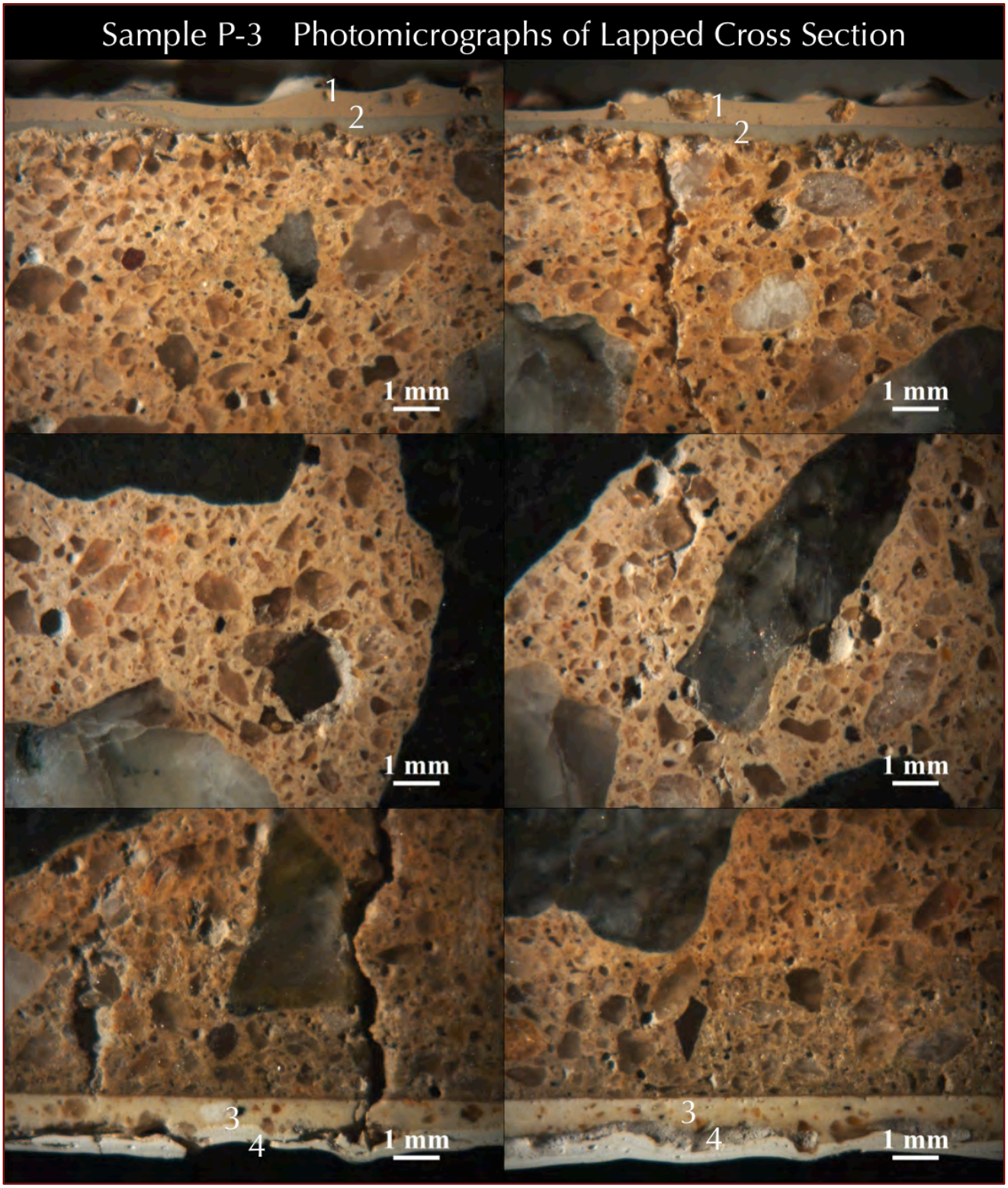

Figure 18: Photomicrographs of lapped cross section of Core P-3 showing: (a) two protective coatings #1 and 2 at the top, and another two coatings #3 and 4 at the bottom end; (b) non-air-entrained nature of the concrete (all photos); and (c) visible cracking in concrete at both ends that are truncated against the protective coatings at the top but transected the coating at the bottom end. Air varied from 0-1% (non-AE) at the top $^{1}/_{2}$ in. depth, to $1^{1}/_{2}$ to $2^{1}/_{2}$% (non-AE) at $^{1}/_{2}$ to $4^{1}/_{2}$ in. interior, then dropped to 0-1% (non-AE) at $4^{1}/_{2}$ to $5^{1}/_{4}$ in. depth from top.

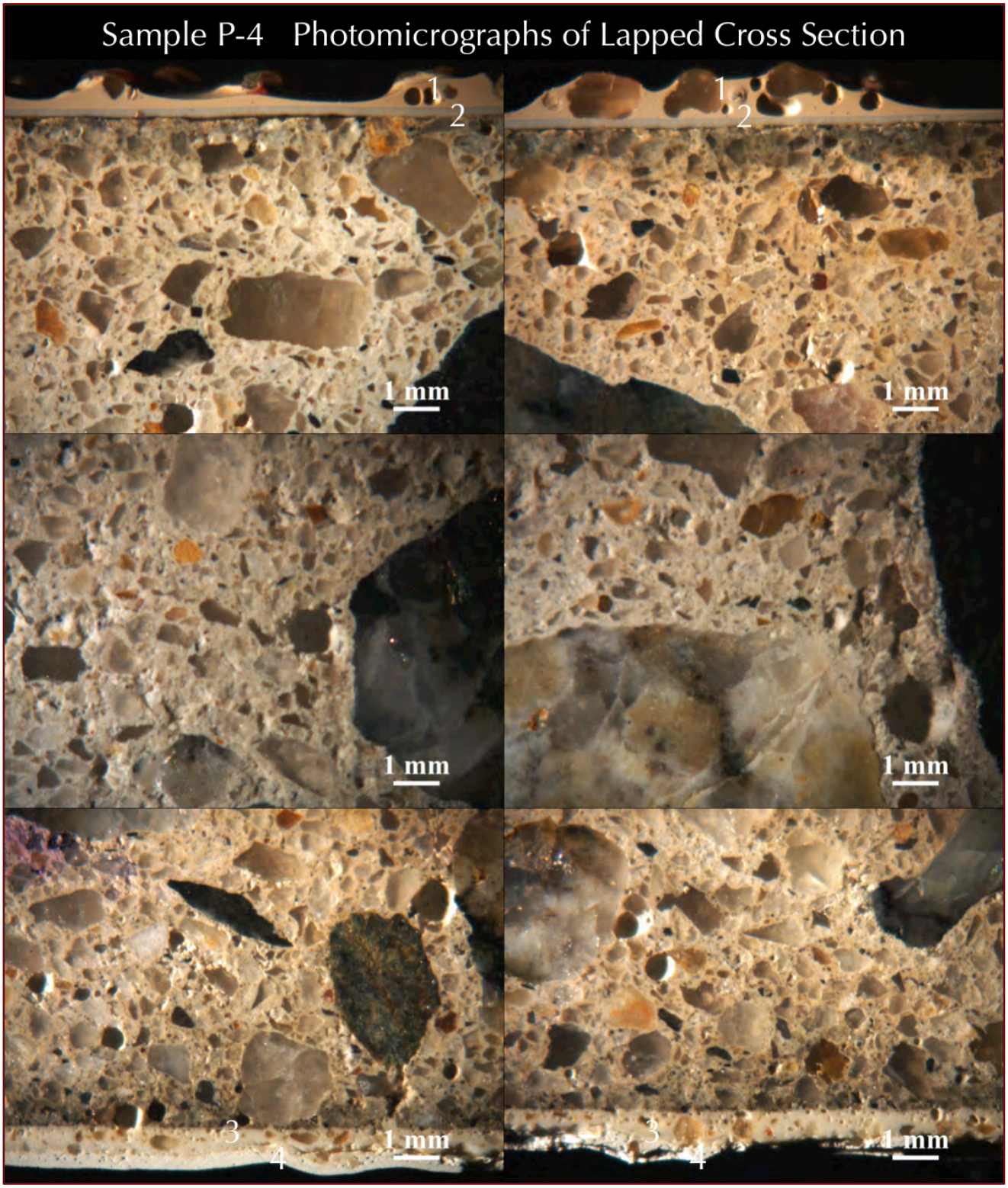

Figure 19: Photomicrographs of lapped cross section of Core P-4 showing: (a) two protective coatings #1 and 2 at the top, and another two coatings #3 and 4 at the bottom end; and (b) non-air-entrained nature of the concrete (all photos). Air varied from 0-1% at the top 1 in. depth (non-AE), to 5-6% from 1 to 4 1/4 in. interior (AE), then dropped to 1-2% (non-AE) from 4 1/4 to 5 1/4 in. depth from top.

PHOTOMICROGRAPHS OF LAPPED CROSS SECTIONS SHOWING PROTECTIVE COATINGS

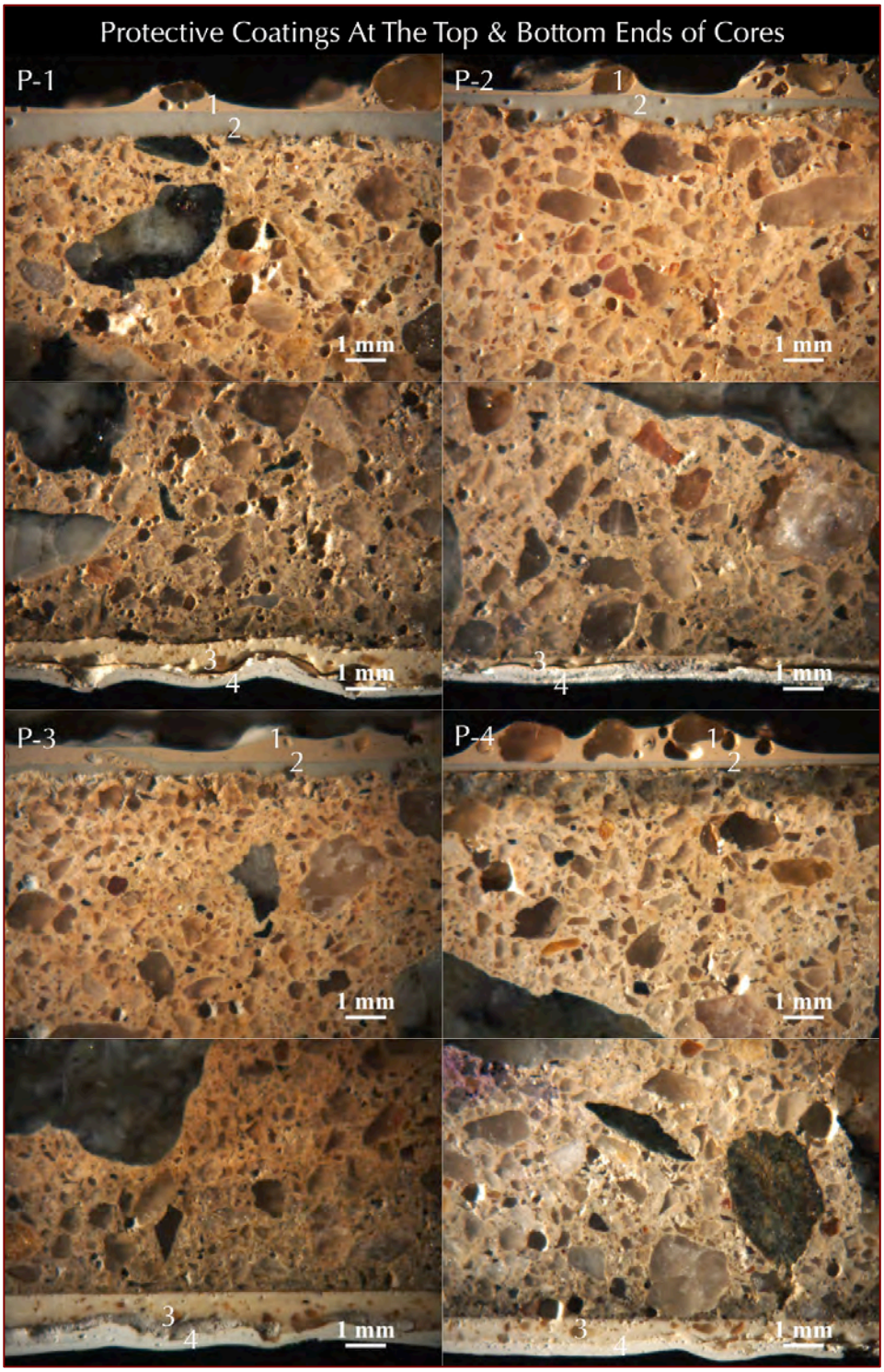

Figure 20: Photomicrographs of lapped cross sections of cores showing the presence of two layers of protective coatings at both ends in all four cores that appeared to be visually similar for each coat in all four cores (i.e. #1 is similar in all cores, and so on and so forth). Notice the coats directly adhered to concrete at both ends (i.e. #2 and 3) are well-bonded to the concrete but some de-bonding has occurred especially at the bottom coats between #3 and 4.

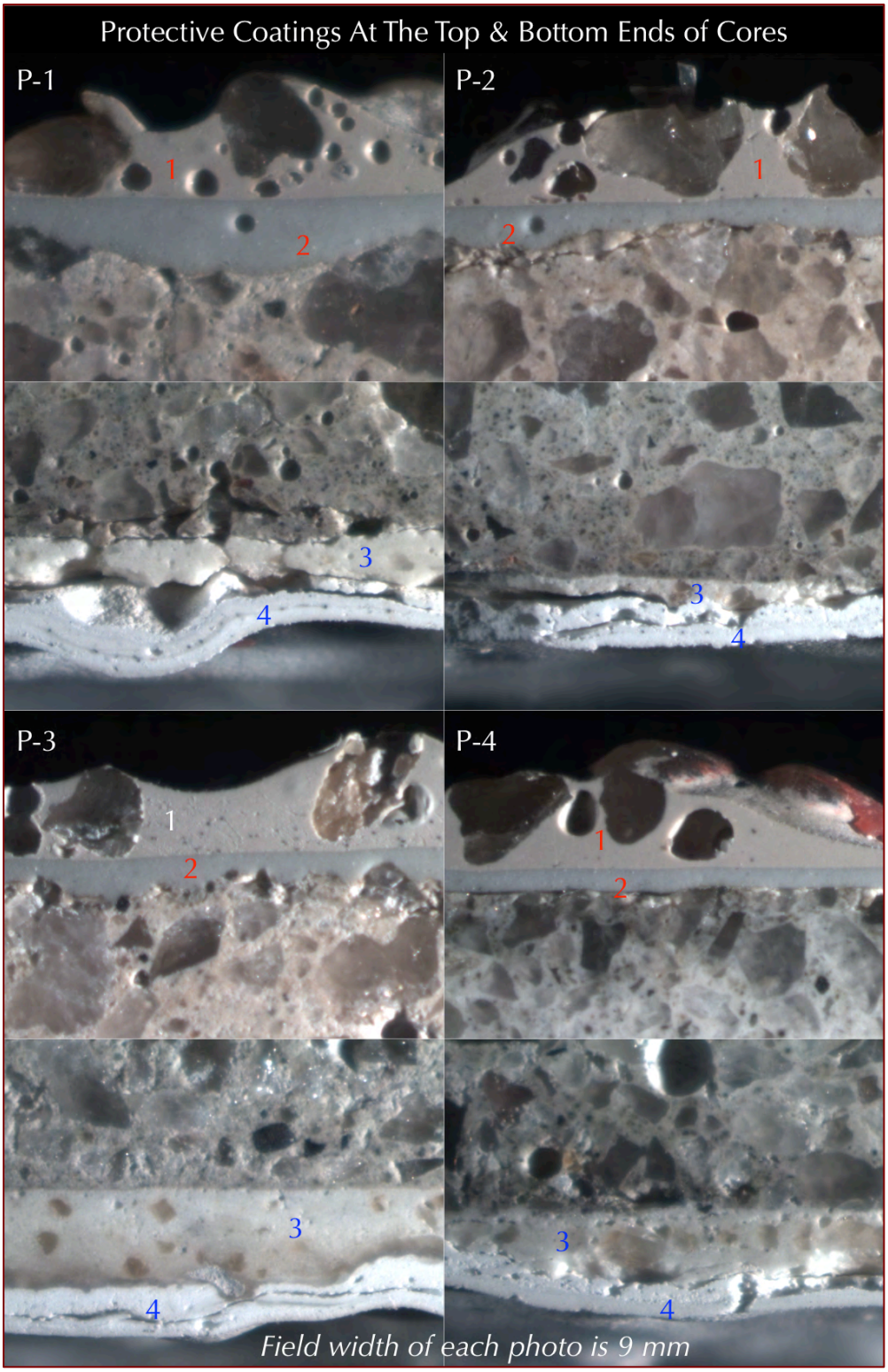

Figure 21: Photomicrographs of lapped cross sections of cores showing the presence of two layers of protective coatings at both ends in all four cores that appeared to be visually similar for each coat in all four cores (i.e. #1 is similar in all cores, and so on and so forth). Notice the coats directly adhered to concrete at both ends (i.e. #1 and 3) are well-bonded to the concrete but some de-bonding has occurred especially at the bottom coats between #3 and 4. Notice the presence of quartz filler in Coat #1 and finer more angular filler in Coat #3 but absence of such visible fillers in Coat #2 and 4. Notice multiple layers of de-bonding in Coat #4.

THIN SECTIONS

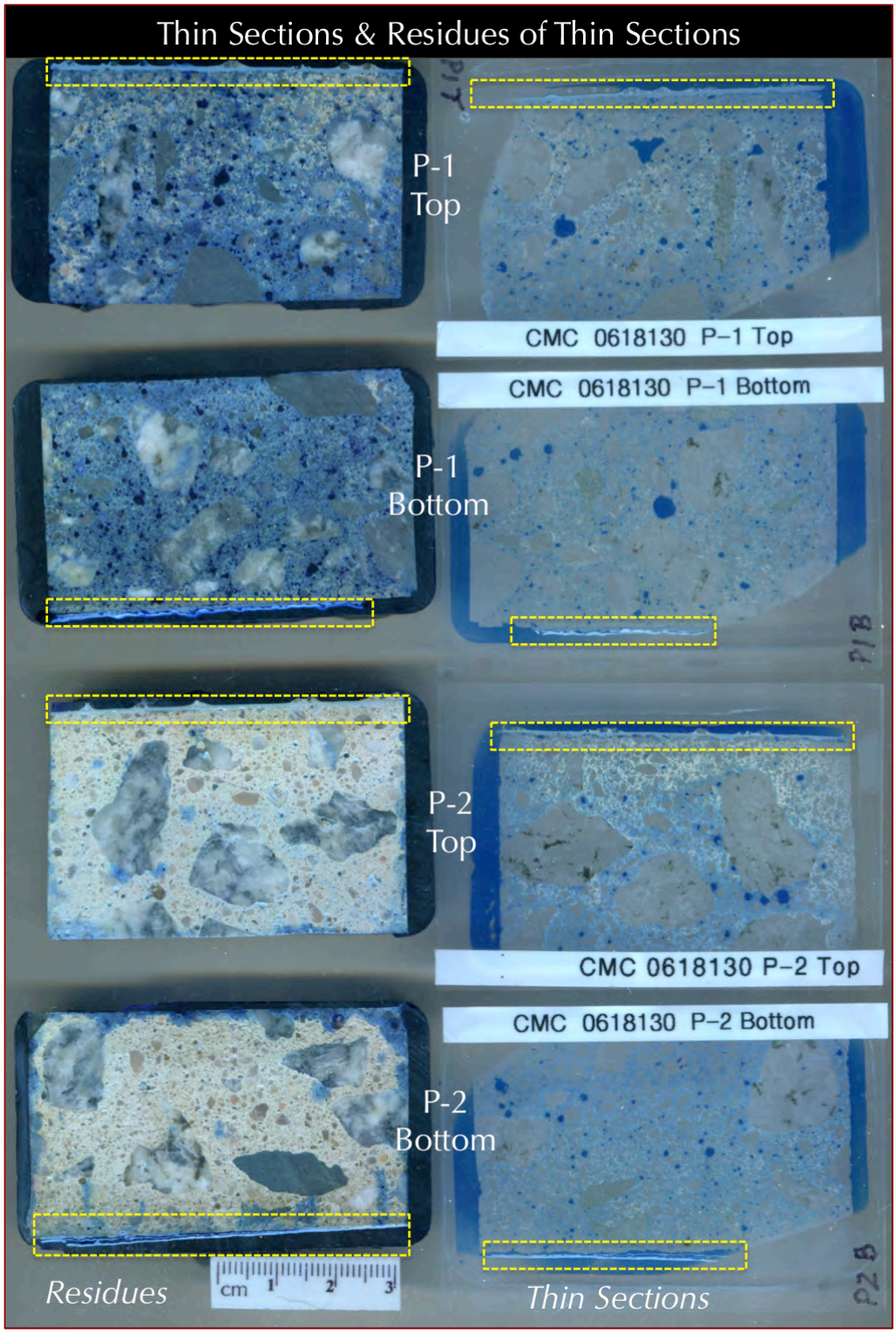

Figure 22: Blue dye-mixed epoxy-impregnated thin sections of the top and bottom portions of Core Nos. P-1 and P-2 in right column and corresponding residues left from thin section preparation in left column showing the surface coatings at both ends that are marked in boxes. Blue dyed epoxy highlights voids, pore spaces in paste and cracks in concrete.

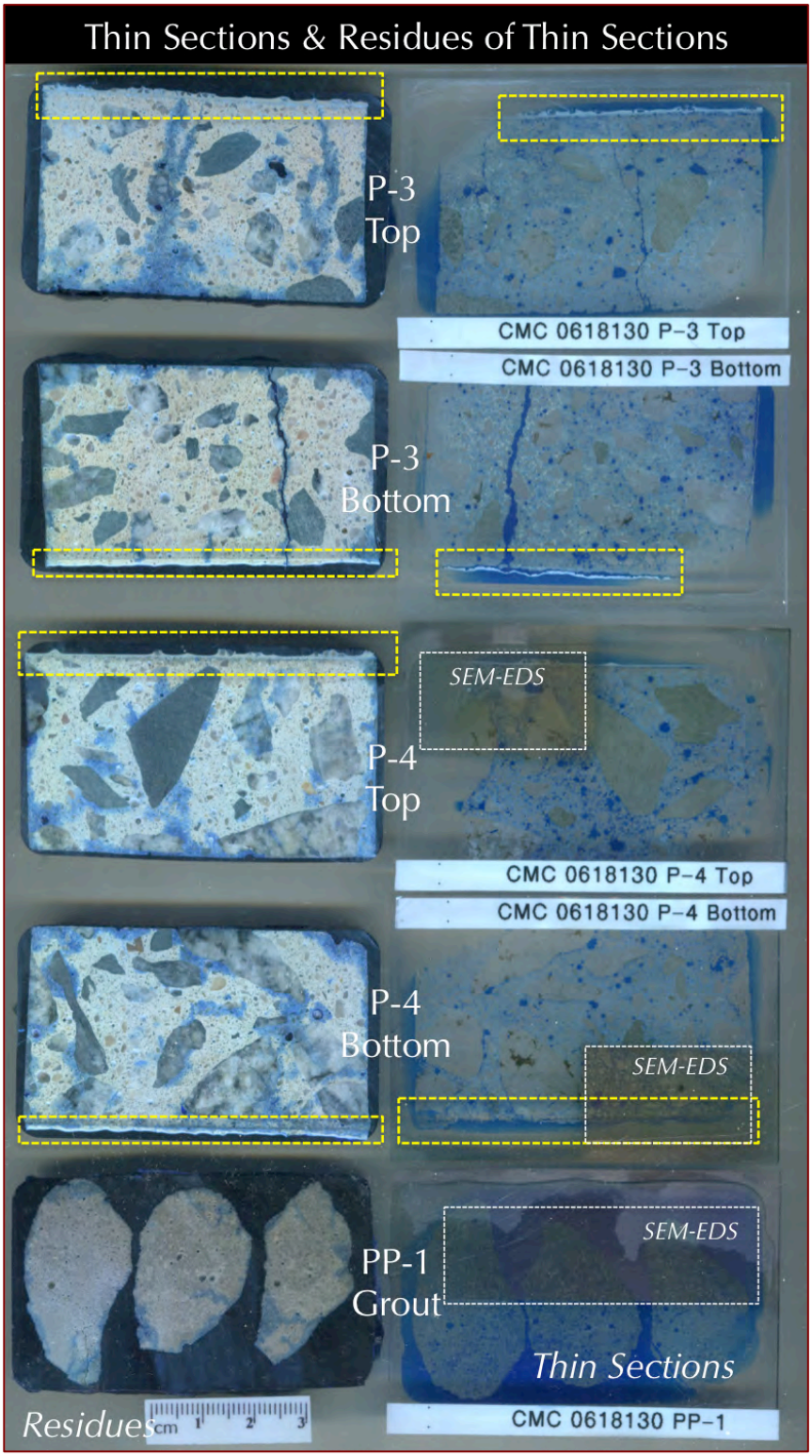

Figure 23: Blue dye-mixed epoxy-impregnated thin sections of the top and bottom portions of Core Nos. P-3, P-4 and the anchoring grout sample in right column and corresponding residues left from thin section preparation in left column showing the surface coatings at both ends that are marked in boxes. Blue dyed epoxy highlights voids, pore spaces in paste and cracks in samples. Portions further studied in SEM-EDS are boxed in dashed white lines.

PHOTOMICROGRAPHS OF THIN SECTIONS OF CONCRETES AND PROTECTIVE COATINGS

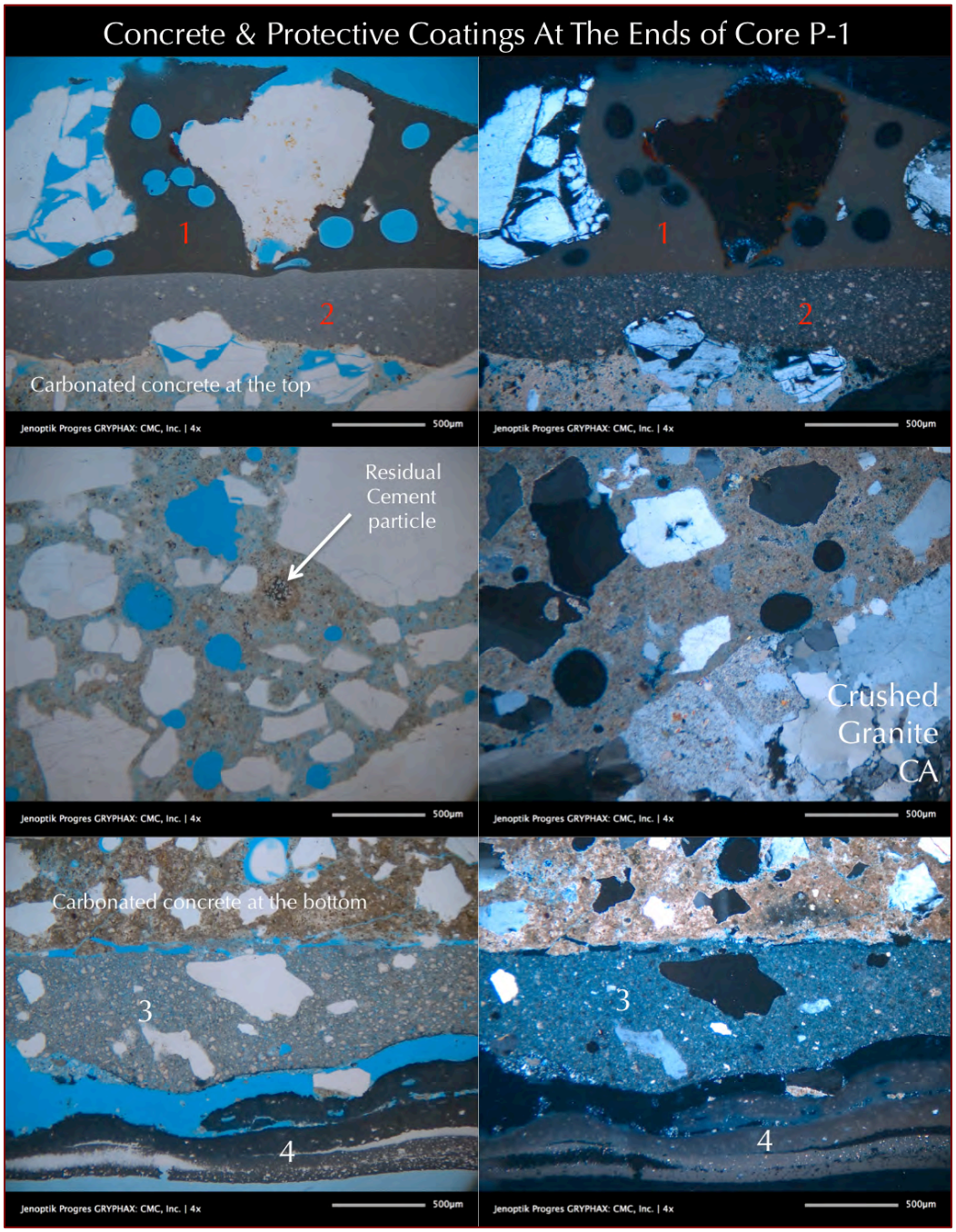

Figure 24: Photomicrographs of blue dye-mixed epoxy-impregnated thin section from the top and bottom ends of Core P-1 showing: (a) two layers of protective coatings at both ends (#1 and 2 at the top, and #3 and 4 at the bottom end); (b) air bubbles and rounded to subangular quartz fillers in Coat #1 in a polymer medium, whereas (c) lack of such fillers in Coat #2, (d) many fine silt-sized fillers in a polymer medium in Coat #2, (e) presence of fine angular quartz and much finer particulate materials in a polymer medium in Coat #3, (f) multi-layered more opaque-like Coat #4, (g) presence of crushed granite and schist (not shown) coarse aggregate and silica (quartz) sand fine aggregate in concrete, (h) Portland cement paste having a few residual cement particles; (i) a few air voids highlighted by blue epoxy, and (j) carbonated concrete especially at ends adjacent to the protective coatings.

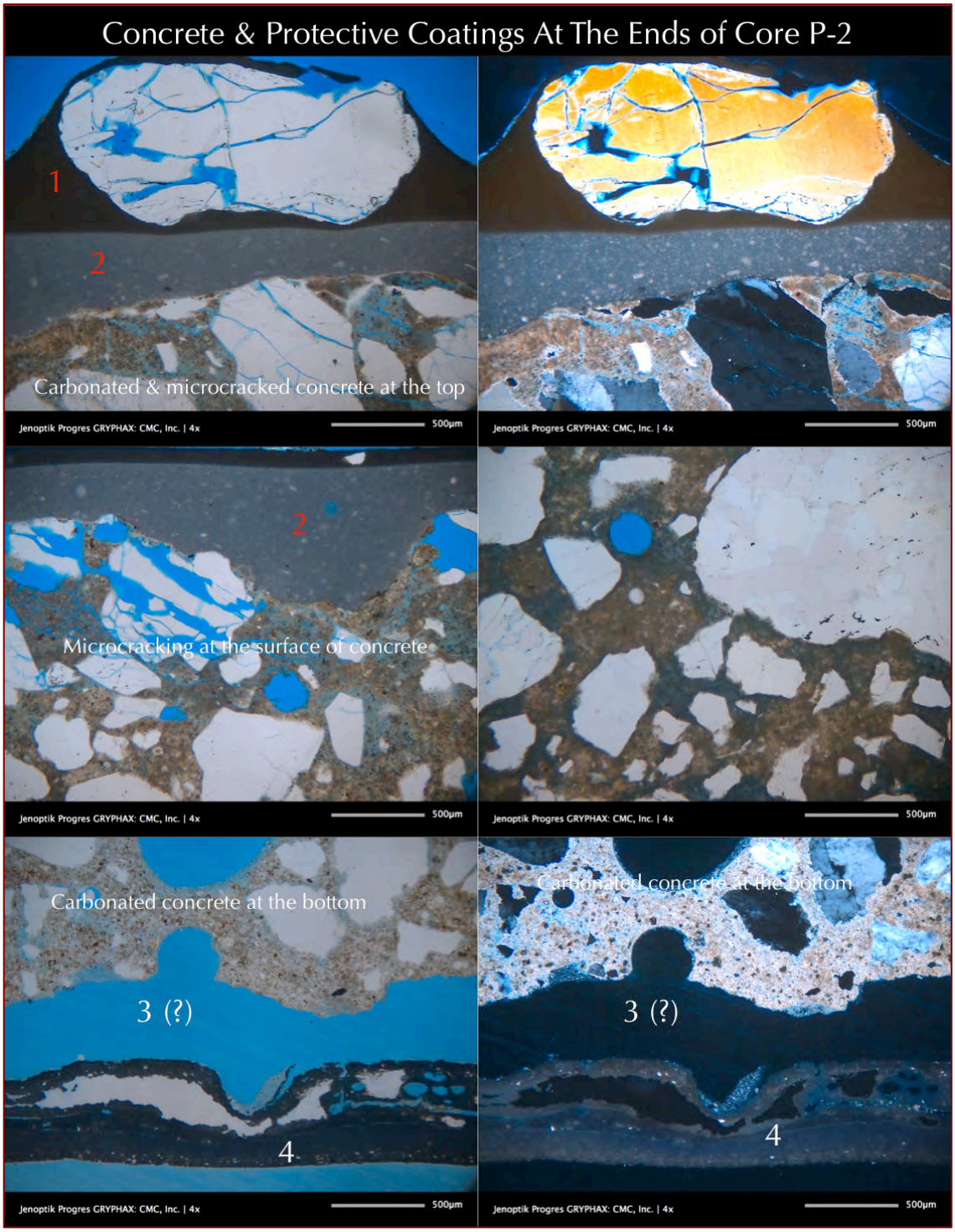

Figure 25: Photomicrographs of blue dye-mixed epoxy-impregnated thin section from the top and bottom ends of Core P-2 showing: (a) two layers of protective coatings at both ends (#1 and 2 at the top, and #3 and 4 at the bottom end); (b) rounded to subangular quartz fillers in Coat #1 in a polymer medium, whereas (c) lack of such fillers in Coat #2, (d) many fine silt-sized fillers in a polymer medium in Coat #2, (e) absence of Coat #3 in this portion of thin section, (f) multi-layered more opaque-like Coat #4, (g) presence of crushed granite and schist (not shown) coarse aggregate and silica (quartz) sand fine aggregate in concrete, (h) Portland cement paste having a few residual cement particles; (i) a few air voids in concrete highlighted by blue epoxy, and (j) carbonated concrete especially at both ends adjacent to the protective coatings.

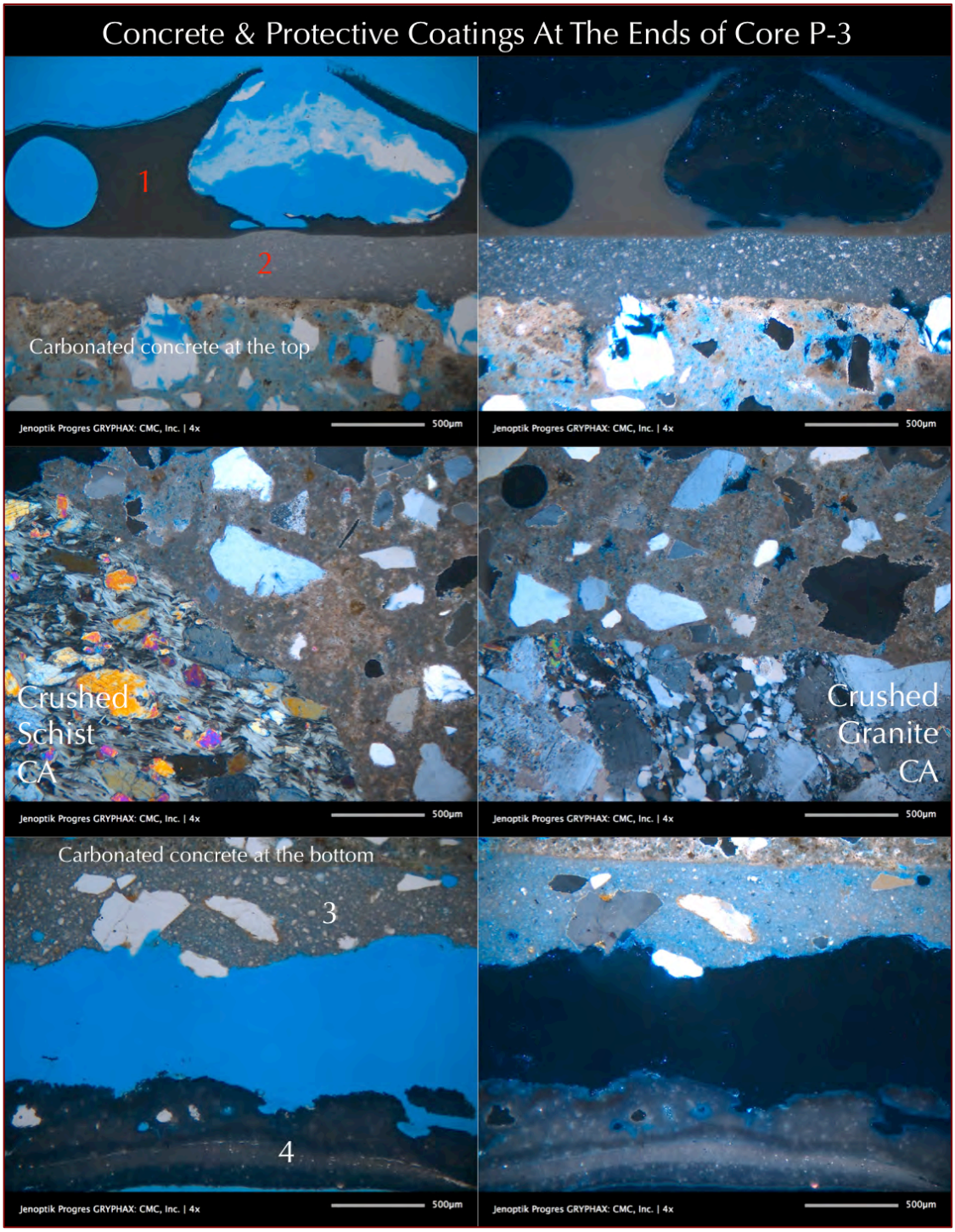

Figure 26: Photomicrographs of blue dye-mixed epoxy-impregnated thin section from the top and bottom ends of Core P-3 showing: (a) two layers of protective coatings at both ends (#1 and 2 at the top, and #3 and 4 at the bottom end); (b) air bubbles and rounded to subangular quartz fillers in Coat #1 in a polymer medium, whereas (c) lack of such fillers in Coat #2, (d) many fine silt-sized fillers in a polymer medium in Coat #2, (e) presence of fine angular quartz and much finer particulate materials in a polymer medium in Coat #3, which is de-bonded from (f) multi-layered more opaque-like Coat #4, (g) presence of crushed granite and schist coarse aggregate and silica (quartz) sand fine aggregate in concrete, (h) Portland cement paste having a few residual cement particles; (i) a few air voids in concrete highlighted by blue epoxy, and (j) carbonated concrete especially at both ends adjacent to the protective coatings.

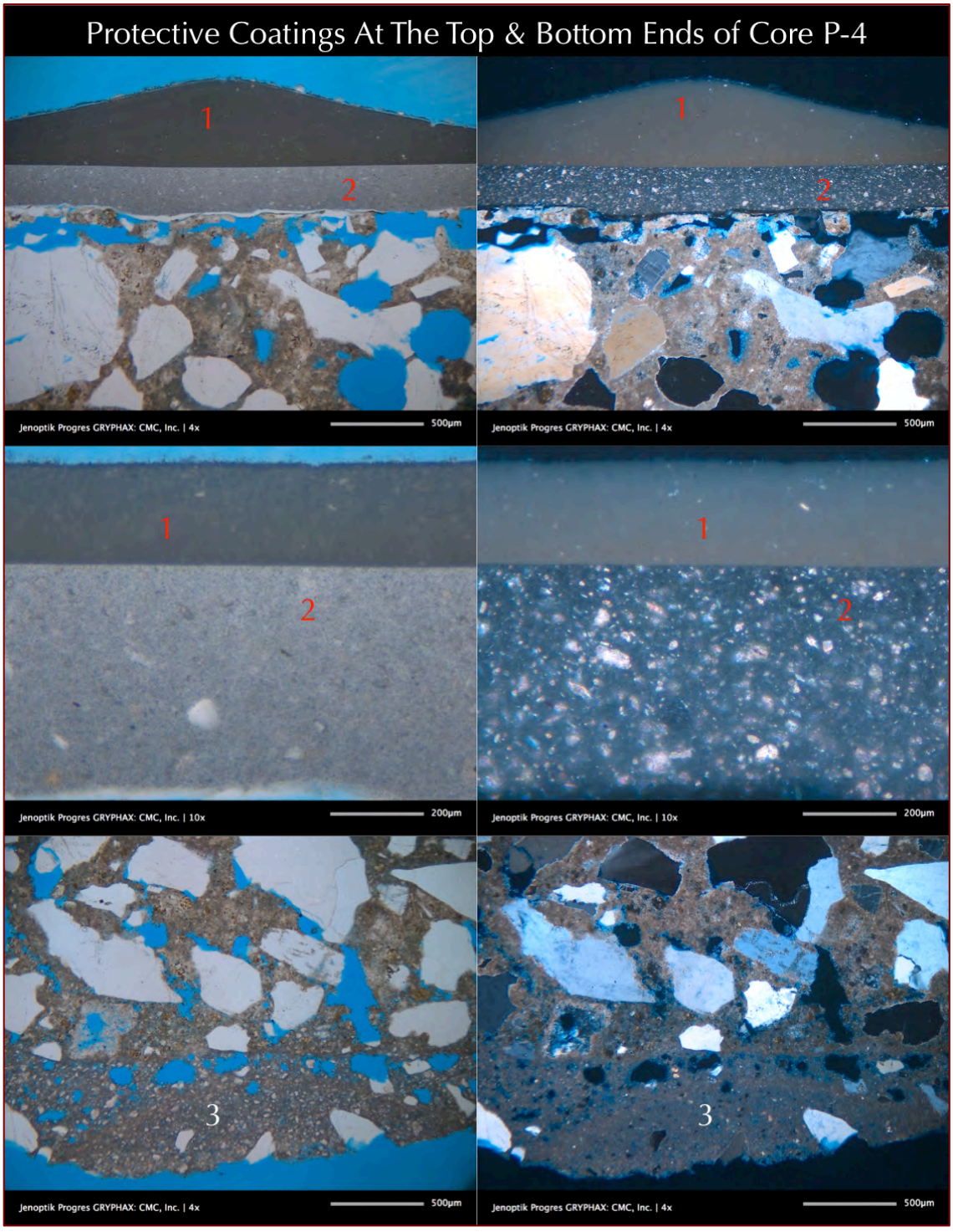

Figure 27: Photomicrographs of blue dye-mixed epoxy-impregnated thin section from the top and bottom ends of Core P-4 showing: (a) two layers of protective coatings at both ends (#1 and 2 at the top, and #3 and 4 (not shown here) at the bottom end); (b) air bubbles and rounded to subangular quartz fillers in Coat #1 in a polymer medium, whereas (c) lack of such fillers in Coat #2, (d) many fine silt-sized fillers in a polymer medium in Coat #2, (e) presence of fine angular quartz and much finer particulate materials in a polymer medium in Coat #3, (f) missing of multi-layered more opaque-like Coat #4 in this section, (g) presence of silica (quartz) sand fine aggregate in concrete, (h) Portland cement paste having a few residual cement particles; (i) a few air voids highlighted by blue epoxy, and (j) carbonated concrete especially at both ends adjacent to the protective coatings.

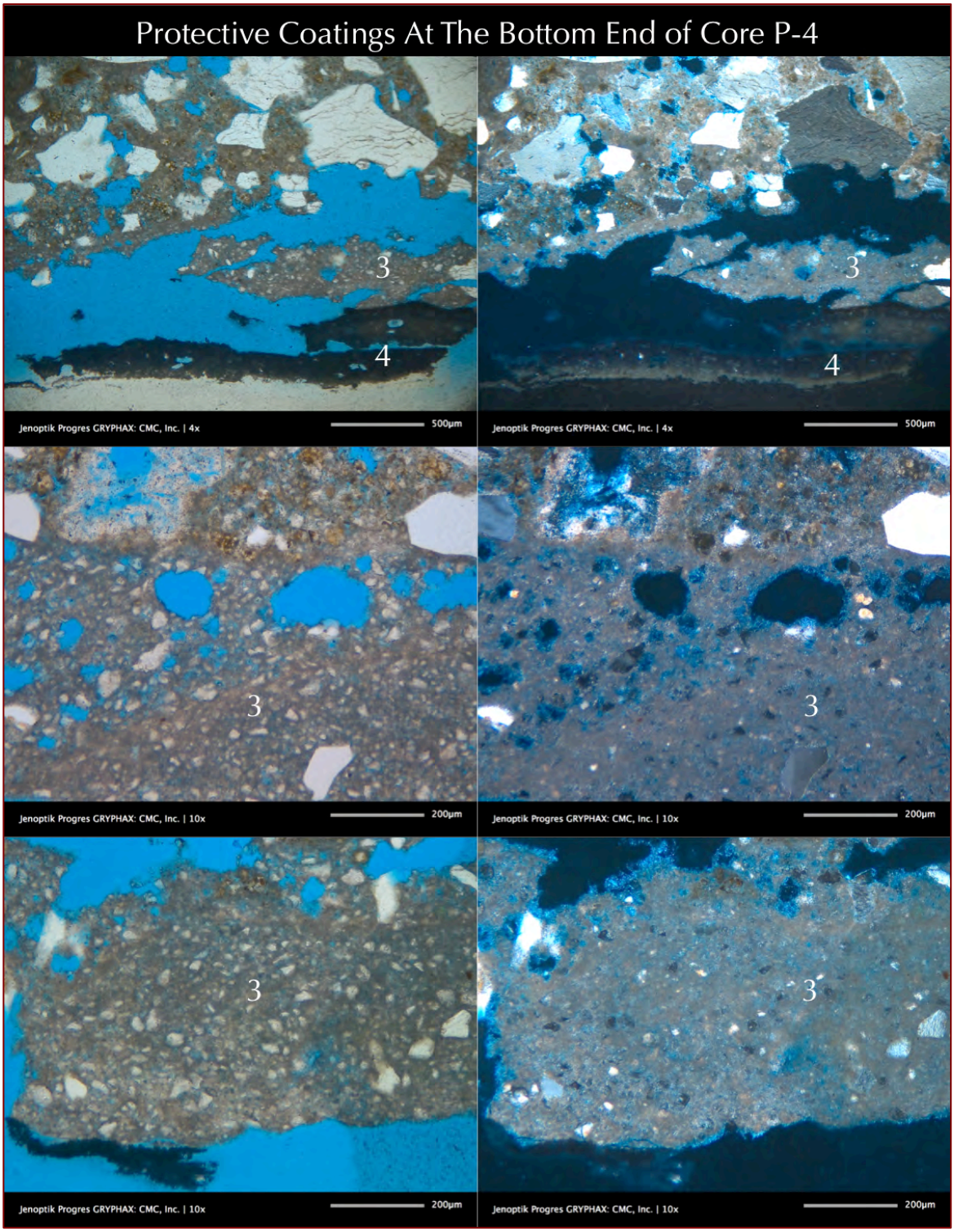

Figure 28: Photomicrographs of blue dye-mixed epoxy-impregnated thin section from the bottom end of Core P-4 showing: (a) two layers of protective coatings #3 and 4 at the bottom end; (b) presence of fine angular quartz and much finer particulate materials in a polymer medium in Coat #3, which is de-bonded from (c) opaque-like Coat #4, (d) presence of silica (quartz) sand fine aggregate in concrete, (e) Portland cement paste having a few residual cement particles; and (f) carbonated concrete especially at both ends adjacent to the protective coatings.

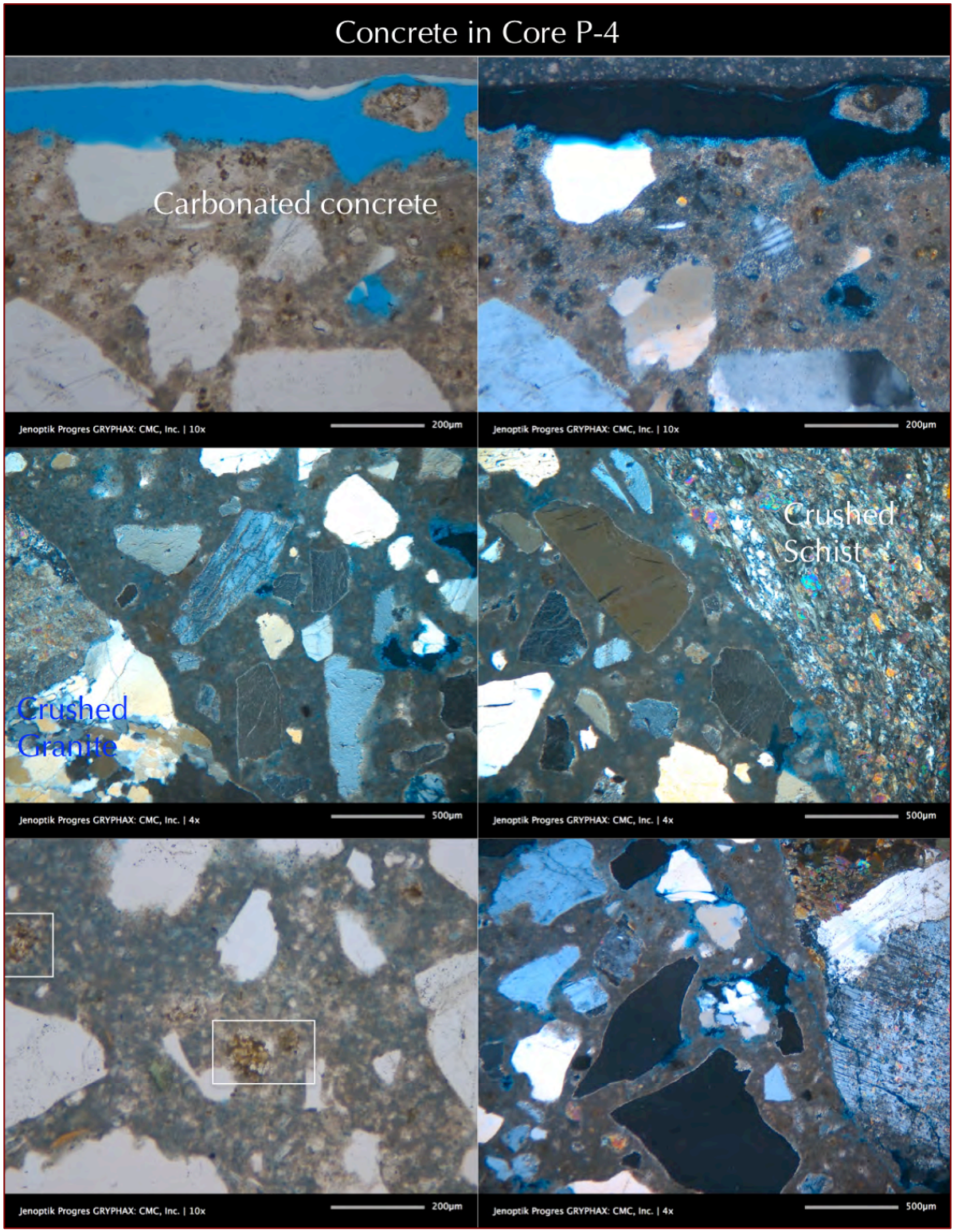

Figure 29: Photomicrographs of blue dye-mixed epoxy-impregnated thin section from the bottom end of Core P-4 showing: (a) carbonated concrete at the top beneath the Coat #2, which is de-bonded from concrete in this portion, (b) crushed granite and schist coarse aggregate and silica (quartz) sand fine aggregate, and (c) Portland cement paste having a few residual cement particles.

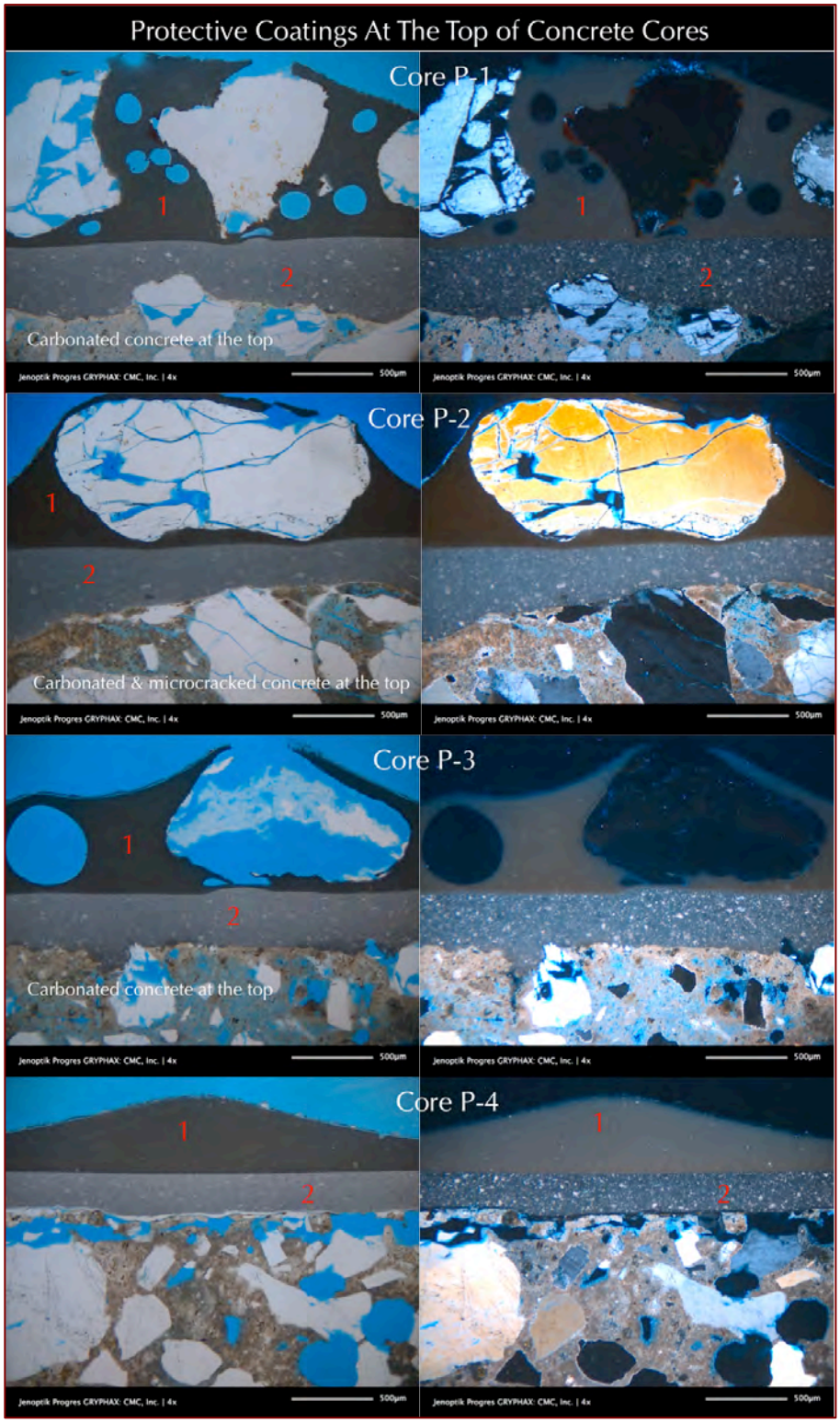

Figure 30: Photomicrographs of thin sections from top ends of all four cores showing the two protective coatings #1 and 2 – their compositional similarity for each coat in all four cores where Coat #1 contains rounded quartz fillers in a polymer medium in all four cores, whereas Coat #2 contains fine silt-sized particles in a polymer medium. Both coats are well-bonded to each other and also to the underlying concrete for the most part. Concrete beneath the coats are carbonated in all four cores indicating prolonged periods of exposures to atmopsheric carbon dioxide prior to the installation of protective coats.

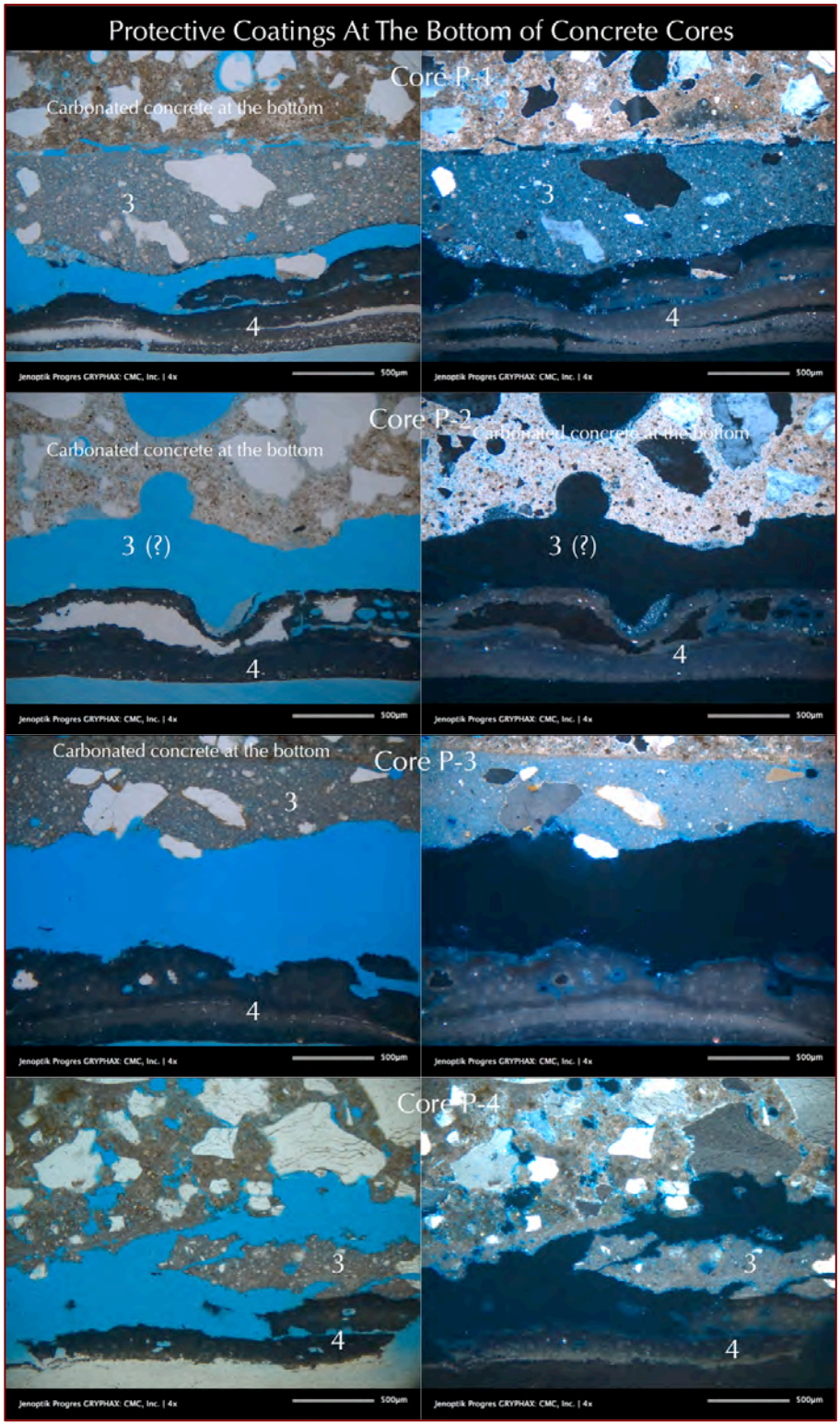

Figure 31: Photomicrographs of thin sections from bottom ends of all four cores showing the two protective coatings #3 and 4 – their compositional similarity for each coat in all four cores where Coat #3 contains fine angular quartz and fine silt-sized silicate fillers in a polymer medium in all four cores, whereas Coat #4 contains no such filler and appears dark opaque in all cores. Both coats are poorly bonded to each other. Concrete adjacent to the coats are carbonated in all four cores indicating prolonged periods of exposures to atmopsheric carbon dioxide prior to the installation of protective coats.

SEM-EDS ANALYSES OF PROTECTIVE COATINGS IN CORE P-4

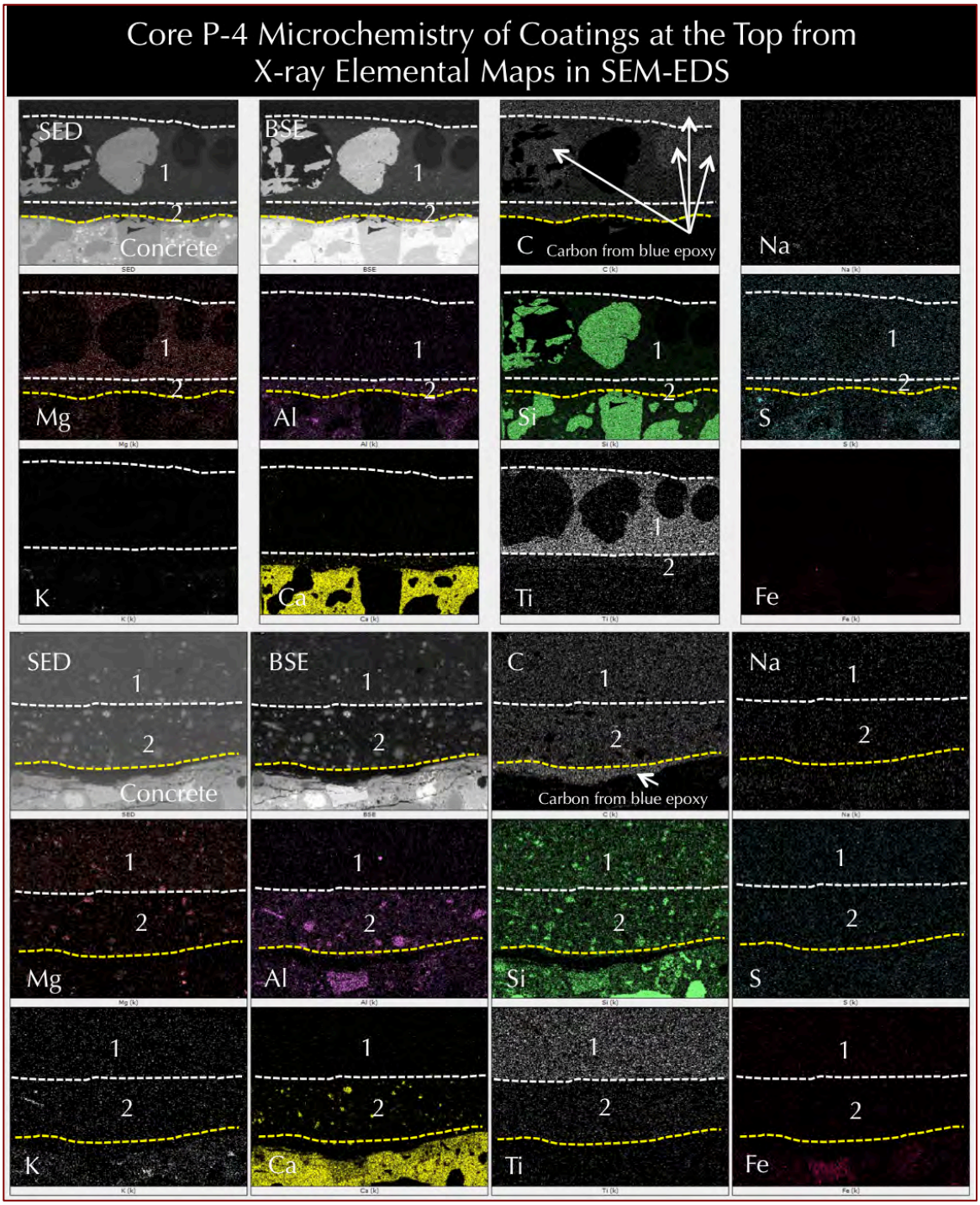

Figure 32: X-ray elemental mapping of top two coatings (#1 and 2) in Core P-4 showing: (a) characteristic titanium enrichment in Coat #1 from incorporation of titanium oxide pigment; (b) presence of silica in both coats from fine silicate fillers and rounded coarse quartz filler in Coat #1; (c) magnesium enrichment in Coat #1 but not in #2; (d) carbon in both coats from carbon-based polymer (separate from carbon footprint from blue epoxy used to impregnate the sample for thin sectioning); (e) calcium enrichment in Portland cement paste in concrete beneath the coatings; (f) some aluminum enrichment in Coat #2 as opposed to Coat #1; and (g) potential slag filler in Coat #2 from Ca, Al, Si highlighted spots in their maps.

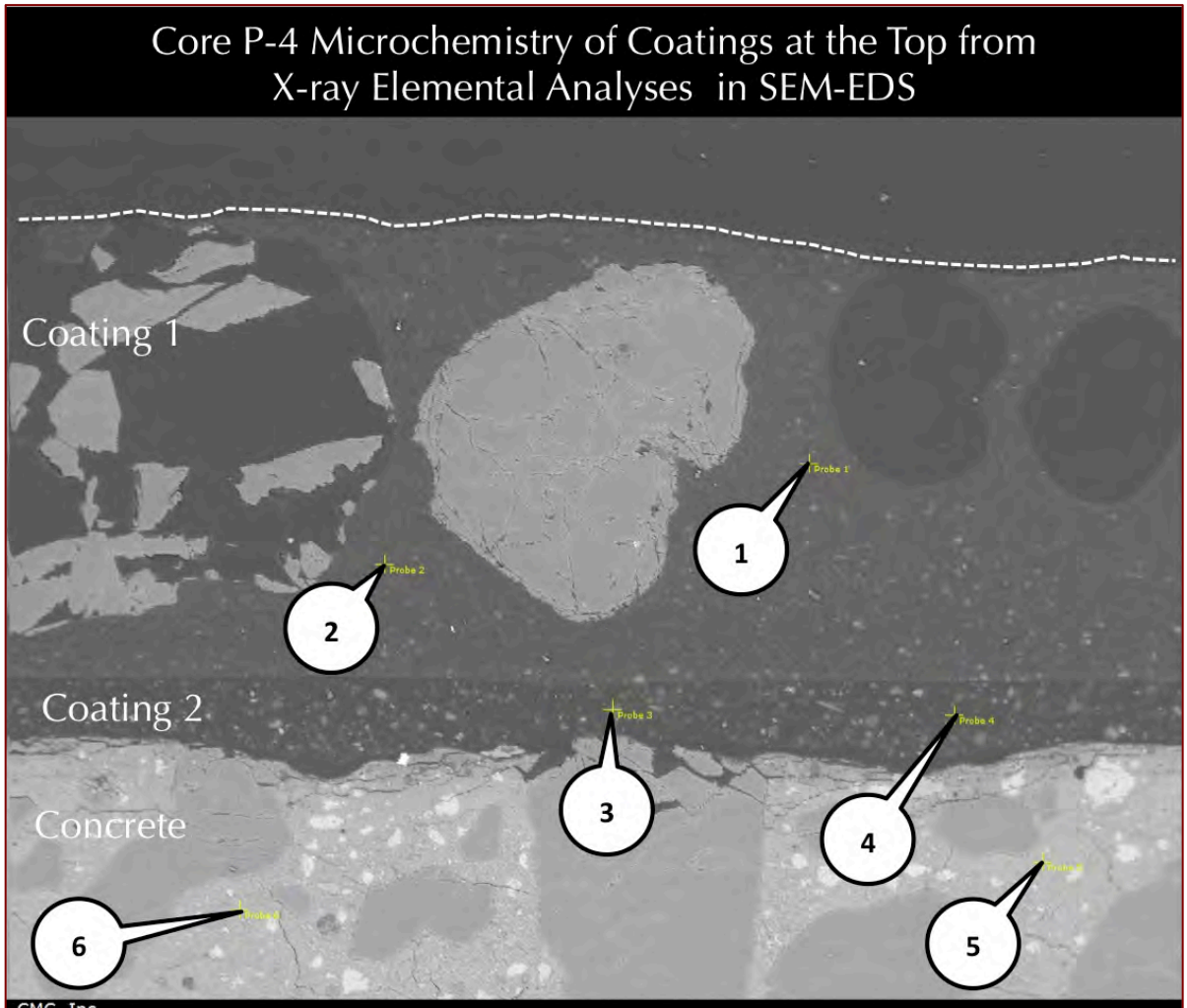

Probe	CaO	SiO2	Al2O3	Na2O	MgO	SO3	K2O	TiO2	FeO	CO2	Total	Phase
1	0.00	6.24	0.40	0.00	1.36	0.00	0.01	8.66	0.70	82.63	100.00	Coat 1
2	0.00	9.61	0.88	0.00	2.27	0.00	0.01	11.21	0.80	75.22	100.00	Coat 1
3	0.00	45.49	26.80	0.00	0.01	0.00	0.00	3.67	0.81	23.22	100.00	Coat 2
4	1.05	10.27	1.71	0.12	0.34	0.00	0.13	2.36	0.19	83.82	99.99	Coat 2
5	0.01	44.18	8.05	0.02	0.53	0.01	47.09	0.02	0.03	0.06	100.00	Grain
6	0.00	31.03	9.17	0.00	49.31	0.07	0.00	1.18	0.51	8.72	99.99	Grain

Figure 33: Secondary electron image (top) and X-ray elemental analyses (bottom Table) of selected locations (at the tips of callouts) in the top two protective coatings (#1 and 2 for Probe #1 to 4) in Core P-4 as well as two near-surface locations in Portland cement paste (Probe #5 and 6) showing compositional variations in coats. Coat #2 has low overall titanium but higher aluminum and silica than Coat #1.

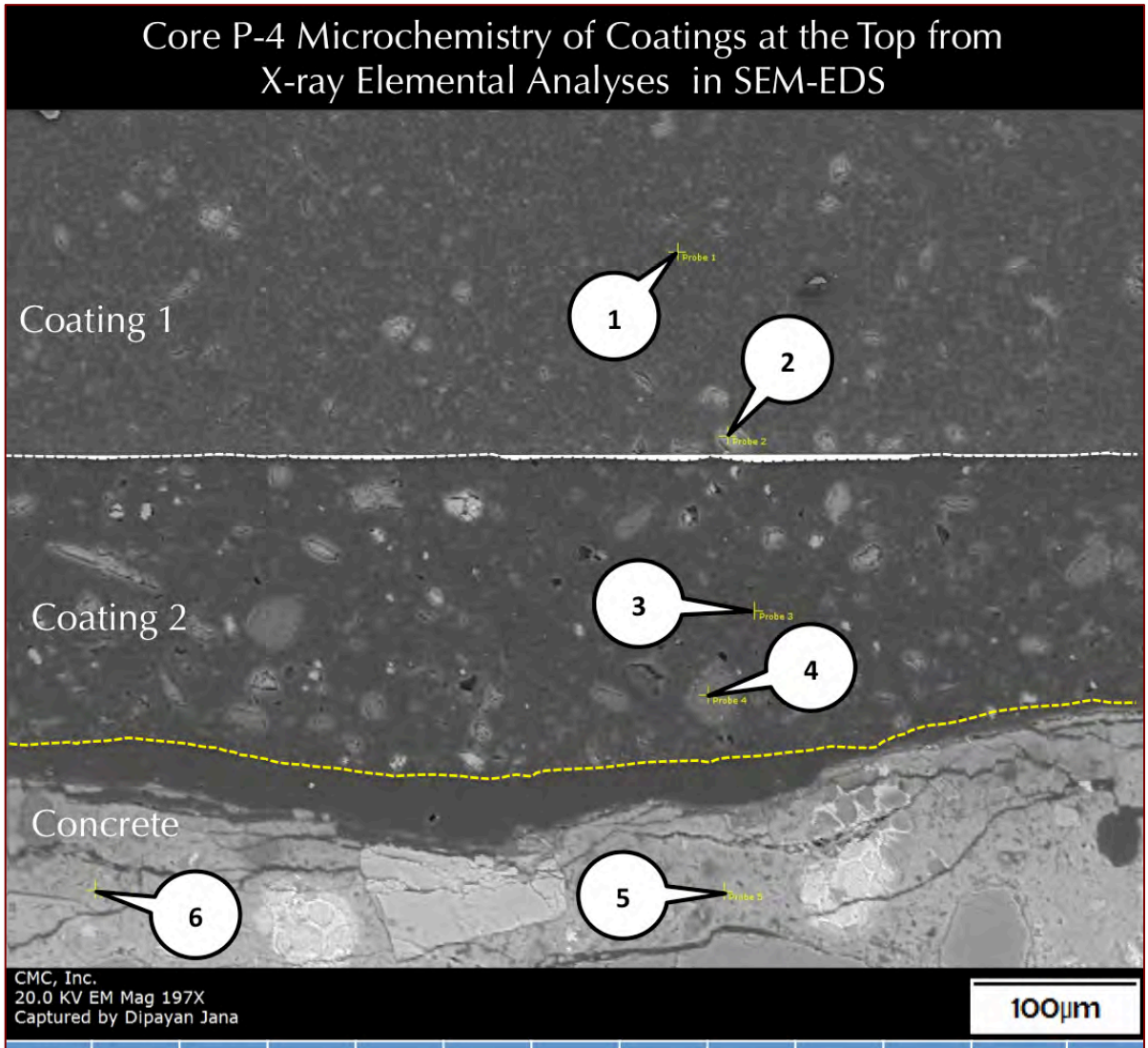

Probe	CaO	SiO2	Al2O3	Na2O	MgO	SO3	K2O	TiO2	FeO	CO2	Total	Phase
1	0.00	8.69	0.31	0.00	0.95	0.00	0.00	15.32	1.33	73.39	99.99	Coat 1
2	0.00	70.62	1.62	0.01	19.54	0.00	0.04	0.23	3.98	3.96	100.00	Coat 1
3	6.18	33.52	12.62	0.00	2.63	0.00	0.26	11.92	1.88	30.99	100.00	Coat 2
4	0.00	13.72	34.98	33.09	17.67	0.00	0.00	0.19	0.34	0.01	100.00	Coat 2
5	2.18	12.67	1.22	0.18	1.52	0.00	0.05	5.46	0.50	76.22	100.00	Grain
6	0.01	28.36	39.33	0.01	0.01	0.02	31.68	0.02	0.37	0.19	100.00	Grain

Figure 34: Secondary electron image (top) and X-ray elemental analyses (bottom Table) of selected locations (at the tips of callouts) in the top two protective coatings (#1 and 2 for Probe #1 to 4) in Core P-4 as well as two near-surface locations in Portland cement paste (Probe #5 and 6) showing compositional variations in coats. Coat #2 has low overall titanium but higher aluminum and silica than Coat #1 (except Probe 2 that is on a silica filler in Coat #1).

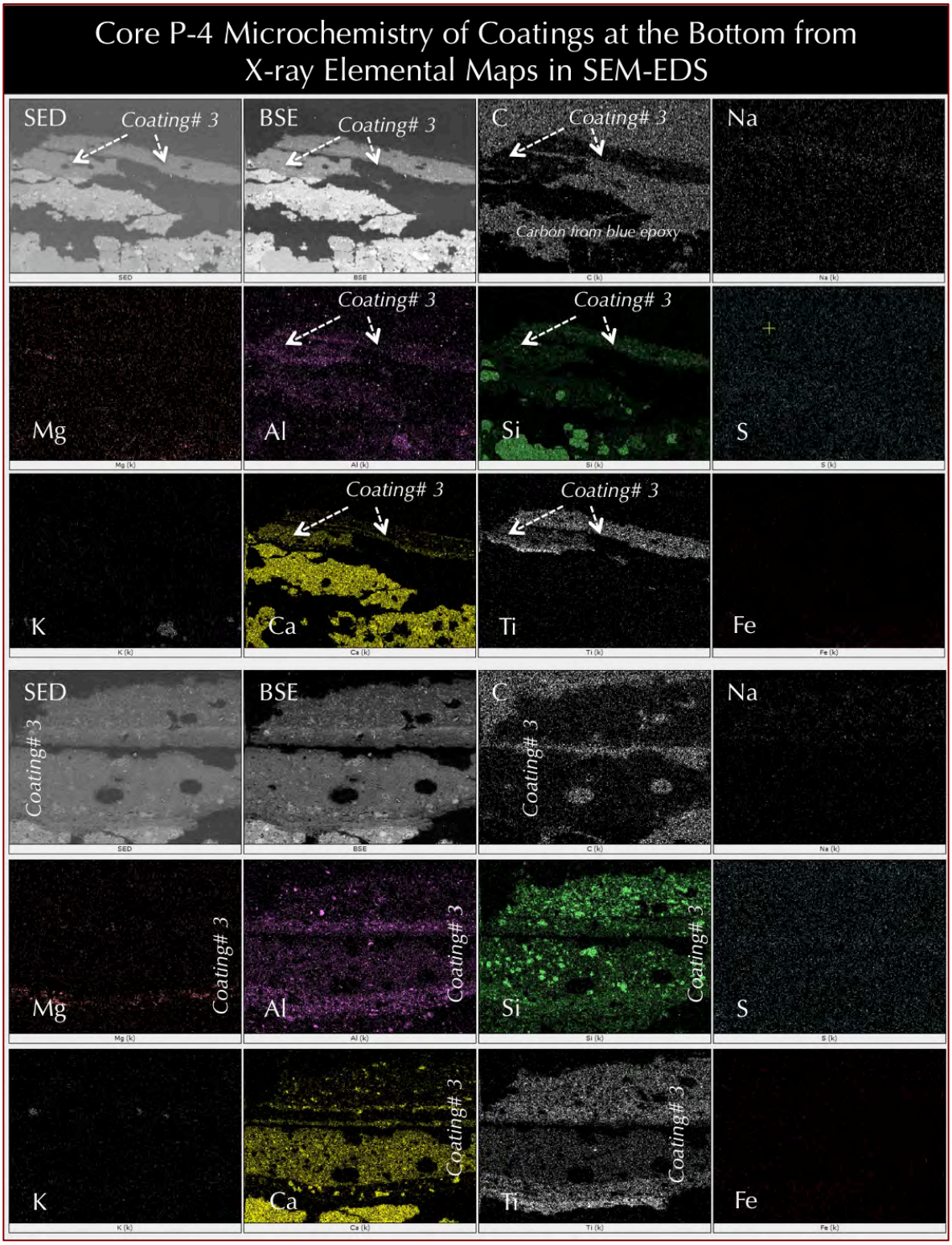

Figure 35: X-ray elemental mapping of bottom coating (#3) in Core P-4 showing: (a) characteristic but variable titanium enrichment in layers or bands in Coat #3 from incorporation of titanium oxide pigment; (b) presence of silica in Coat #3 from fine silicate fillers; (c) magnesium enrichment in some layers within Coat #3; (d) carbon depletion in Coat #3 as opposed to carbon from blue epoxy used to impregnate the sample for thin sectioning; and (e) variable aluminum enrichment in Coat #3.

SEM-EDS ANALYSES OF CONCRETE IN CORE P-4

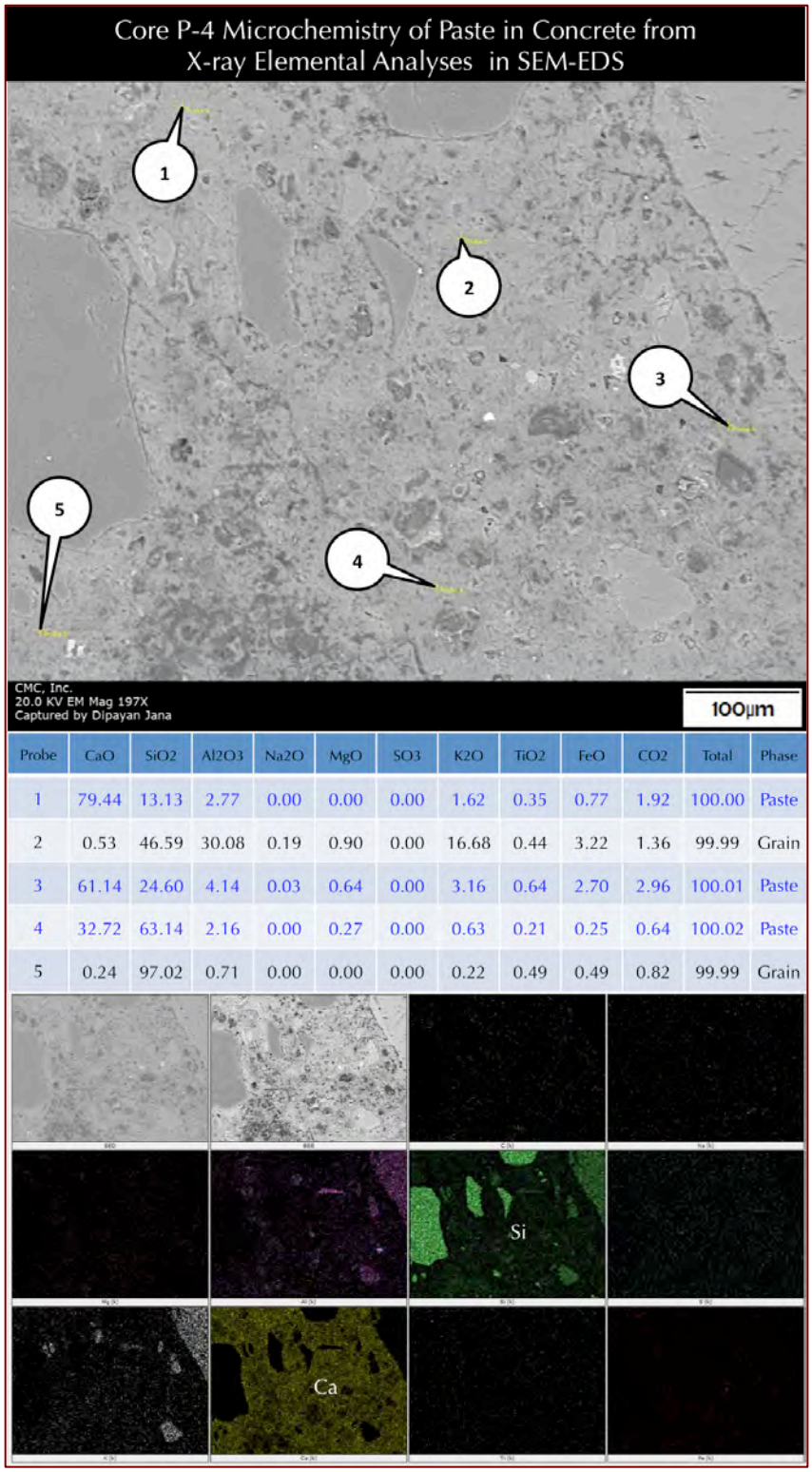

Probe	CaO	SiO2	Al2O3	Na2O	MgO	SO3	K2O	TiO2	FeO	CO2	Total	Phase
1	79.44	13.13	2.77	0.00	0.00	0.00	1.62	0.35	0.77	1.92	100.00	Paste
2	0.53	46.59	30.08	0.19	0.90	0.00	16.68	0.44	3.22	1.36	99.99	Grain
3	61.14	24.60	4.14	0.03	0.64	0.00	3.16	0.64	2.70	2.96	100.01	Paste
4	32.72	63.14	2.16	0.00	0.27	0.00	0.63	0.21	0.25	0.64	100.02	Paste
5	0.24	97.02	0.71	0.00	0.00	0.00	0.22	0.49	0.49	0.82	99.99	Grain

Figure 36: Secondary electron image (top), X-ray elemental analyses (middle Table) of selected locations (at the tips of callouts), and X-ray elemental mapping (bottom) of Portland cement paste in concrete in Core P-4 showing the characteristic calcium silicate hydrate composition of paste as shown in blue rows in the Table.

FT-IR SPECTROSCOPY OF COATINGS IN CORE P-4

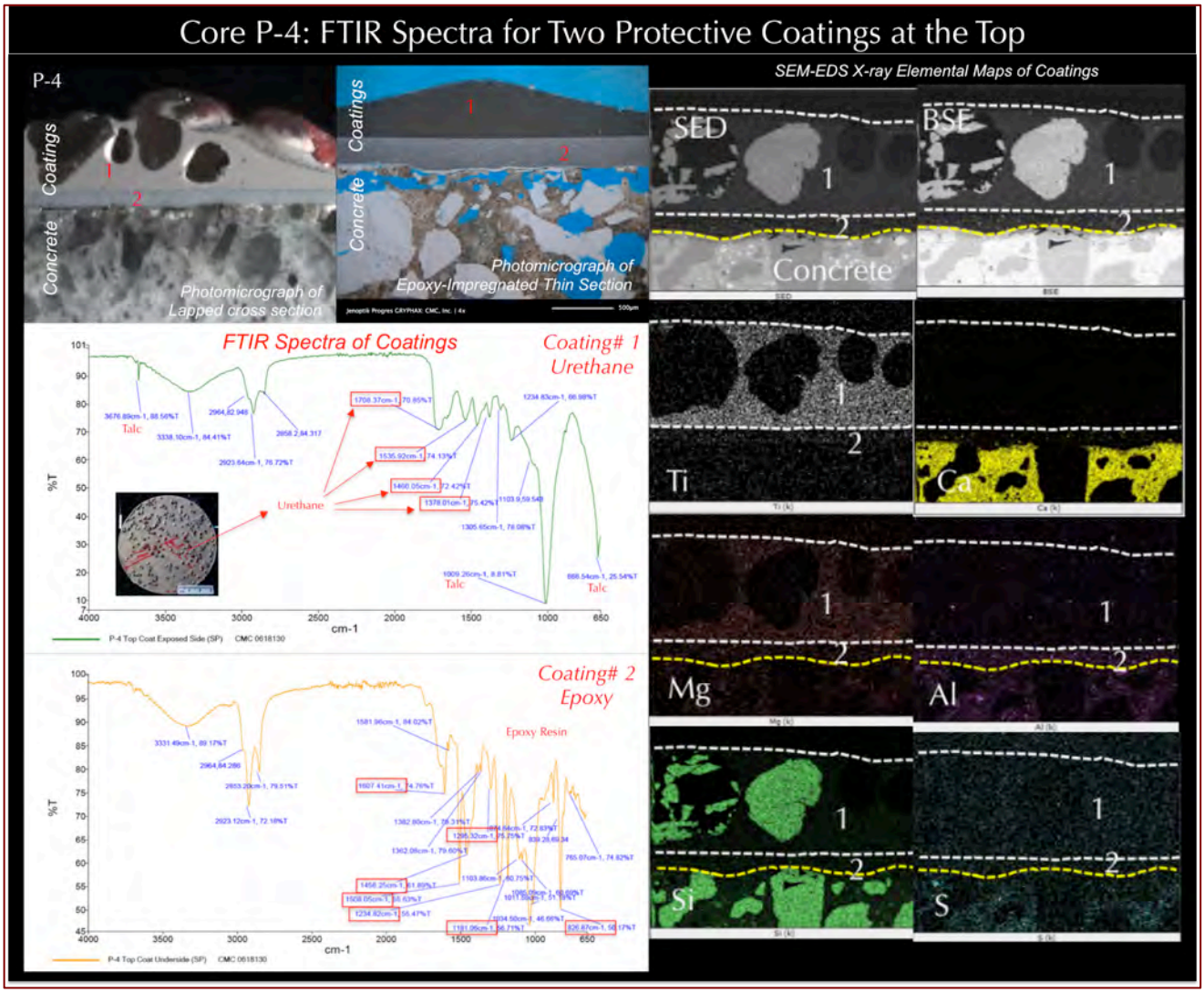

Figure 37: Coating #1 - The resin is consistent with a urethane as evidenced by the bands near 1710, 1680, 1535, 1460, 1380 cm^{-1}. The large band near 1010 cm^{-1} with the sharp band near 3700 cm^{-1} and the band near 670 cm^{-1} indicated the presence of talc. Coating #2 - The resin is consistent with an epoxy by bands near 1610, 1510, 1460, 1295, 1230, 1180, and 830 cm^{-1}.

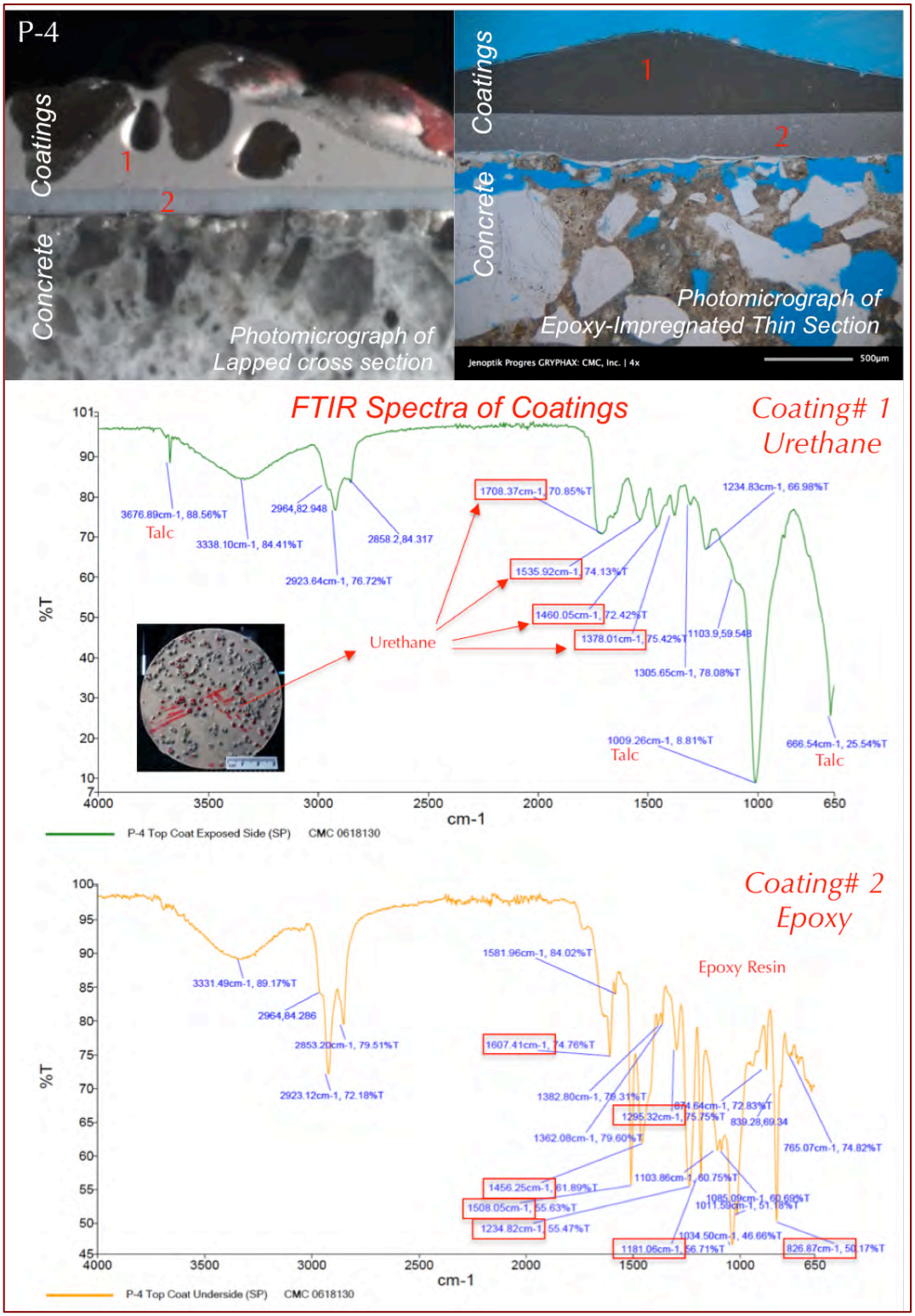

Figure 38: Coating #1 - The resin is consistent with a urethane as evidenced by the bands near 1710, 1680, 1535, 1460, 1380cm^{-1}. The large band near 1010 cm^{-1} with the sharp band near 3700 cm^{-1} and the band near 670 cm^{-1} indicated the presence of talc. Coating #2 - The resin is consistent with an epoxy by bands near 1610, 1510, 1460, 1295, 1230, 1180, and 830 cm^{-1}.

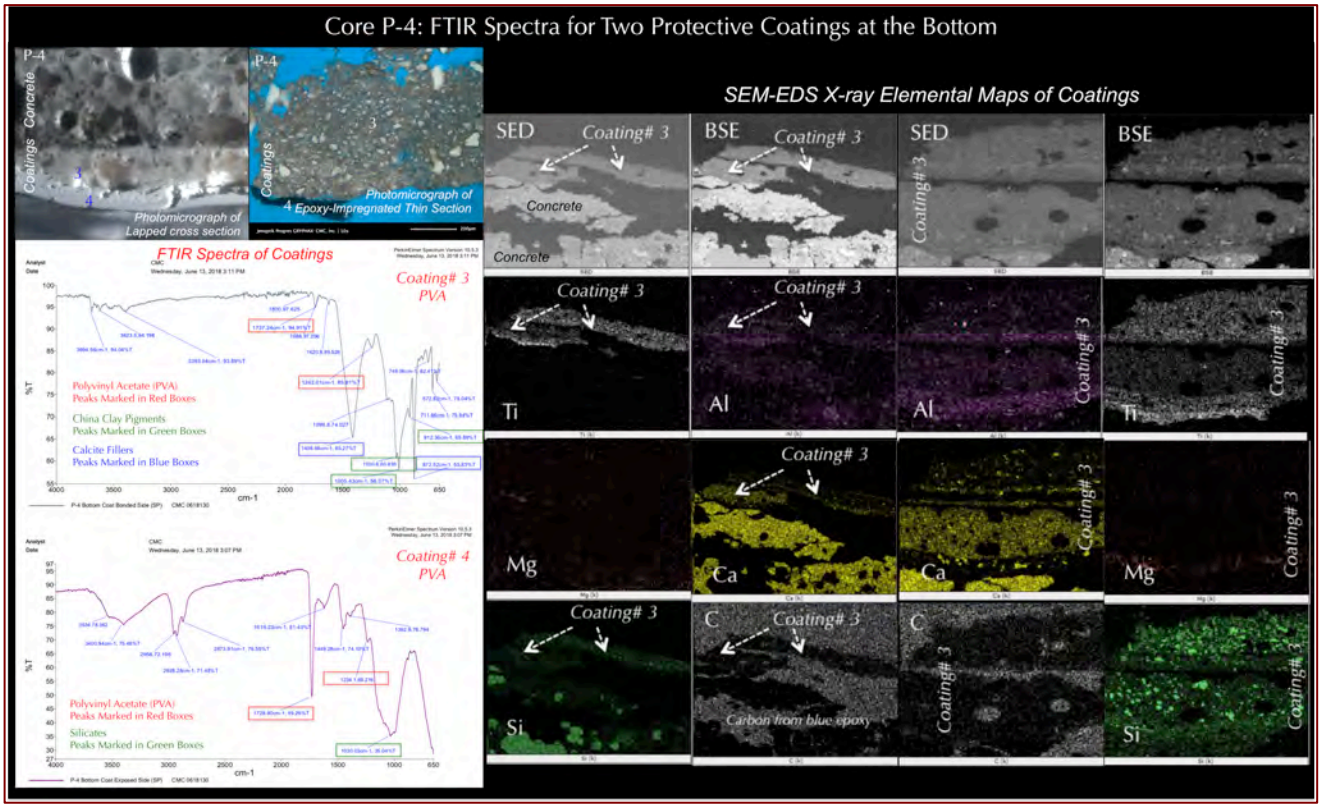

Figure 39: Coating #3 - The resin bands are small. From the bands near 1740 and 1240 cm^{-1}, the resin is most consistent with a vinyl (polyvinyl acetate, PVA). The pigmentation is china clay as indicated by the bands near 1030, 1010, 915 cm^{-1}. The bands near 1410 and 875 cm^{-1} are a carbonate material (a little low for $CaCO_3$). Coating #4 - The resin is another layer of vinyl as confirmed from bands near 1728 and 1234 cm^{-1}. The large band between 1100 and 1000 cm^{-1} is consistent with silicate materials, which, from SEM-EDS studies is judged to be from slag and fine quartz fillers.

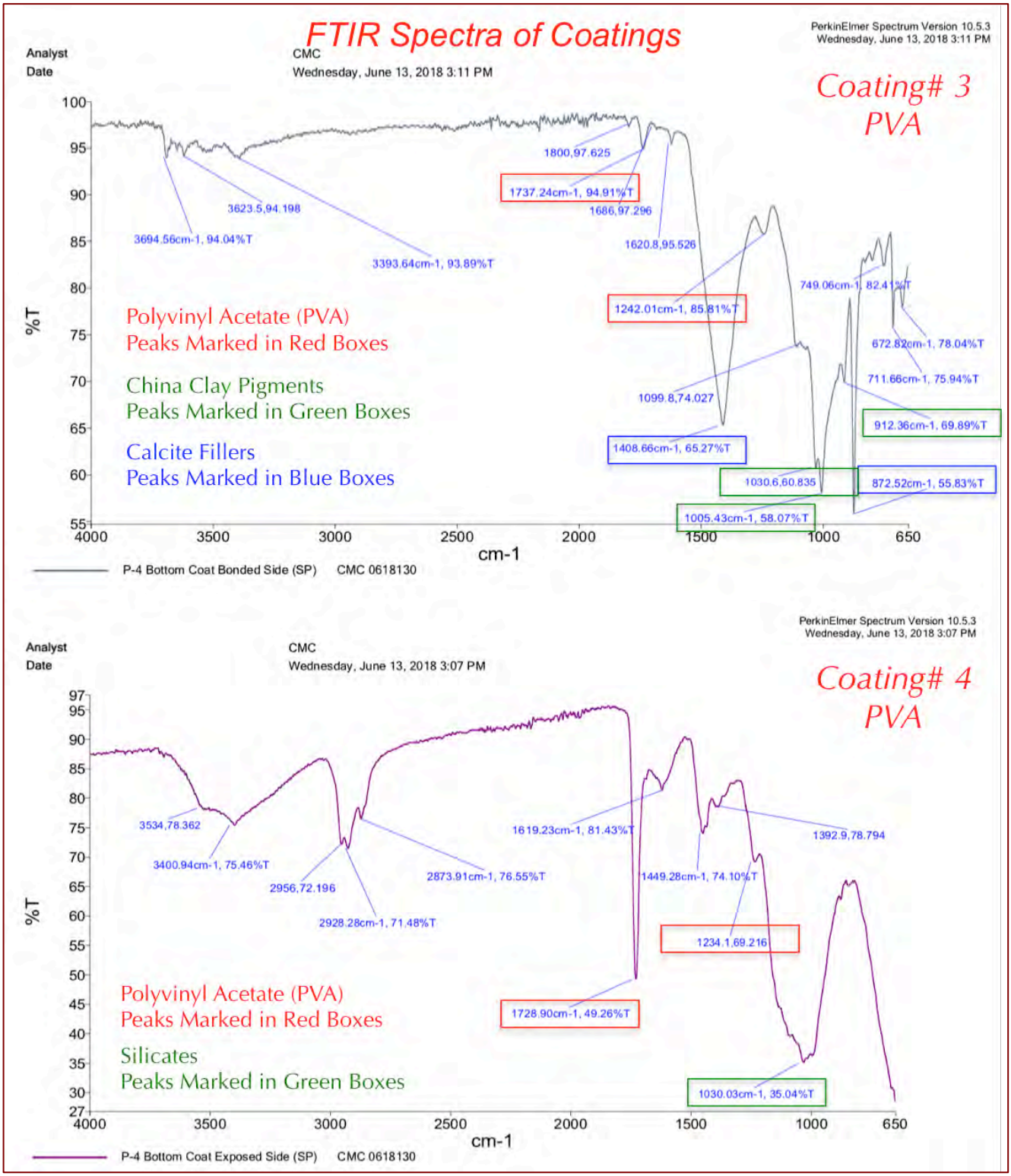

Figure 40: Coating #3 - The resin bands are small. From the bands near 1740 and 1240 cm^{-1}, the resin is most consistent with a vinyl (polyvinyl acetate, PVA). The pigmentation is china clay as indicated by the bands near 1030, 1010, 915 cm^{-1}. The bands near 1410 and 875 cm^{-1} are a carbonate material (a little low for $CaCO_3$). Coating #4 - The resin is another layer of vinyl as confirmed from bands near 1728 and 1234 cm^{-1}. The large band between 1100 and 1000 cm^{-1} is consistent with silicate materials, which, from SEM-EDS studies is judged to be from slag and fine quartz fillers.

COARSE AND FINE AGGREGATES IN CONCRETES

Table 2 summarizes types, compositions, and properties of coarse and fine aggregates in concrete in four cores.

Properties and Compositions of Aggregates	P-1	P-2	P-3	P-4
Coarse Aggregate				
Types	Compositionally similar in all four cores – crushed granite and schist (Figures 14 to 19, 24 to 29)			
Nominal maximum size	3/4 in. (19 mm)			
Rock Type	Major amounts of crushed alkali granite (quartz, alkali feldspar many shows sericitic alterations, and biotite mica) and subordinate amounts of chlorite schist (Figures 24 to 29)			
Angularity, Density, Hardness, Color, Texture, Sphericity	Angular, dense, hard, dark speckled gray to black, crystalline granular coarse-grained massive textured for granite to schistose textured for schist, equidimensional to elongated (Figures 14 to 19, 24 to 29)			
Cracking, Alteration, Coating	Unaltered, Uncoated, and Uncracked (Figures 14 to 19)			
Grading & Distribution	Well-graded and Well-distributed (Figures 14 to 19)			
Soundness	Sound			
Alkali-Aggregate Reactivity	None			
Fine Aggregate				
Types	Compositionally similar in all four cores – natural siliceous sand			
Nominal maximum size	3/8 in. (9.5 mm)			
Rock Types	Major amounts of quartz and subordinate amounts of quartzite feldspar, mafic minerals, mica, and ferruginous rock			
Cracking, Alteration, Coating	Variably colored, subangular to subrounded, dense, hard, equidimensional to elongated			
Grading & Distribution	Well-graded and Well-distributed			
Soundness	Sound			
Alkali-Aggregate Reactivity	None			

Table 2: Properties of coarse and fine aggregates of concretes.

PORTLAND CEMENT PASTES IN CONCRETES

Table 3 summarizes compositions and properties of pastes in concretes in all four cores.

Properties and Compositions of Paste	P-1	P-2	P-3	P-4
Color, Hardness, Porosity, Luster	Paste is carbonated and beige toned at the ends (Figures 14 to 19) but light gray in the interior, dense and hard, freshly fractured surfaces have subvitreous lusters and subconchoidal textures			
Residual Portland Cement Particles	Normal, 8 to 10 percent by paste volume			
Calcium hydroxide from cement hydration	Normal, 10 to 14 percent by paste volume			

Properties and Compositions of Paste	P-1	P-2	P-3	P-4
Pozzolans, Slag, etc.	None			
Water-cementitious materials ratio (*w/cm*), estimated	0.45 to 0.50; uniform throughout the depth			
Cementitious materials contents, estimated (equivalent to bags of portland cement per cubic yard)	$5^1/_2$ to 6			
Secondary Deposits	Secondary ettringite deposits lining and filling many air voids indicating presence of moisture in the concrete for prolonged periods			
Depth of Carbonation from top end, mm (Figures 14 and 15)	20	15	30	2
Depth of Carbonation from bottom end, mm (Figures 14 and 15)	35	25	45	25
Microcracking	None			
Aggregate-paste Bond	Moderately tight to tight			
Bleeding, Tempering	None			
Chemical deterioration	None			

Table 3: Properties and compositions of hardened cement pastes in four cores.

AIR ENTRIANMENTS AND AIR-VOID SYSTEMS IN CONCRETES

Table 4 shows large variations in air entrainments and air contents within and between four cores.

Core ID	Top Exposed End	Middle Interior Body	Bottom End
P-1 (Figure 16)	Top $^3/_4$ in. Air-entrained, Estimated 5-6% air	Interior $^3/_4$ to $3^3/_4$ in.: Air-entrained Estimated 9-10% air	Bottom $3^3/_4$ to $4^3/_4$ in.: Air-entrained Estimated 7-8% air
P-2 (Figure 17)	Top 1 in. Non-Air-entrained, Estimated 1-2% air	Interior 1 to 4 in.: Air-entrained Estimated 5-6% air	Bottom 4 to 5 in.: Marginally Air-entrained Estimated $1^1/_2$-$2^1/_2$%
P-3 (Figure 18)	Top $^1/_2$ in. Non-Air-entrained, Estimated 0-1%	Interior $^1/_2$ to $4^1/_2$ in.: Non-Air-entrained Estimated $1^1/_2$-$2^1/_2$%	Bottom $4^1/_2$ to $5^1/_4$ in.: Non-Air-entrained Estimated 0-1%
P-4 (Figure 19)	Top 1 in. Non-Air-entrained, Estimated 0-1%	Interior 1 to 4 in.: Air-entrained Estimated 5-6% air	Bottom 4 to 5 in.: Non-Air-entrained Estimated 1-2%

Table 4: Within and between-core variations in air contents and air entrainments. Air occur as: (a) numerous fine, discrete, spherical and near-spherical voids having sizes up to 1 mm, and (b) a few coarse, near-spherical and irregularly-shaped voids having sizes greater than 1 mm. The former voids are characteristic of intentionally introduced entrained air, whereas latter voids are characteristic of accidentally produced entrapped air.

PROTECTIVE COATINGS – SUMMARY OF OBSERVATIONS

Cores	P-1	P-2	P-3	P-4
Coating# 1 (Top) Type: Urethane, Non-breathable	Gray to Beige (Figures 20, 21), Less than 0.1 to 1.2 mm non-uniform thickness (Figures 20, 21, 30), maximum thick at the quartz filler and minimum where filler is absent; Ti-enrichment from Ti-oxide pigment (Figure 32), Mg and Si from Talc filler (Figure 32), Talc also found in FT-IR (Figures 37, 38)	Gray to Beige (Figures 20, 21), Less than 0.1 to 1.2 mm non-uniform thickness (Figures 20, 21, 30), maximum thick at the quartz filler and minimum where filler is absent; Ti-enrichment from Ti-oxide pigment (Figure 32), Mg and Si from Talc filler (Figure 32), Talc also found in FT-IR (Figures 37, 38)	Gray to Beige (Figures 20, 21), Less than 0.1 to 1.2 mm non-uniform thickness (Figures 20, 21, 30), maximum thick at the quartz filler and minimum where filler is absent; Ti-enrichment from Ti-oxide pigment (Figure 32), Mg and Si from Talc filler (Figure 32), Talc also found in FT-IR (Figures 37, 38)	Gray to Beige (Figures 20, 21), Less than 0.1 to 1.2 mm non-uniform thickness (Figures 20, 21, 30), maximum thick at the quartz filler and minimum where filler is absent; Ti-enrichment from Ti-oxide pigment (Figure 32), Mg and Si from Talc filler (Figure 32), Talc also found in FT-IR (Figures 37, 38)
Coating# 2 (Top) Type: Epoxy, Non-breathable	Gray to ash color (Figures 20, 21), 0.8 mm nominal thickness (Figures 20, 21, 30), more uniform thickness, Al enrichment, spots of slag filler in Ca, Al, Si-maps (Figure 32); Epoxy binder in FT-IR (Figures 37, 38)	Gray to ash color (Figures 20, 21), 0.5 mm nominal thickness (Figures 20, 21, 30), more uniform thickness, Al enrichment, spots of slag filler in Ca, Al, Si-maps (Figure 32); Epoxy binder in FT-IR (Figures 37, 38)	Gray to ash color (Figures 20, 21), 0.3 mm nominal thickness (Figures 20, 21, 30), more uniform thickness, Al enrichment, spots of slag filler in Ca, Al, Si-maps (Figure 32); Epoxy binder in FT-IR (Figures 37, 38)	Gray to ash color (Figures 20, 21), 0.1 mm nominal thickness (Figures 20, 21, 30), more uniform thickness, Al enrichment, spots of slag filler in Ca, Al, Si-maps (Figure 32); Epoxy binder in FT-IR (Figures 37, 38)
Coating# 3 (Bottom) Type: PVA, Non-breathable	Off-white (Figures 20, 21), 0.5 to 0.8 mm non-uniform thickness (Figures 20, 21, 31), Ti-enrichment from Ti-oxide pigment (Figure 35); also china clay pigment and calcite filler from FT-IR (Figures 39, 40); slag particles as filler too (Figure 28)	Off-white (Figures 20, 21), 0.2 to 0.5 mm non-uniform thickness (Figures 20, 21, 31), Ti-enrichment from Ti-oxide pigment (Figure 35); also china clay pigment and calcite filler from FT-IR (Figures 39, 40); slag particles as filler too (Figure 28)	Off-white (Figures 20, 21), 0.5 to 0.8 mm non-uniform thickness (Figures 20, 21, 31), Ti-enrichment from Ti-oxide pigment (Figure 35); also china clay pigment and calcite filler from FT-IR (Figures 39, 40); slag particles as filler too (Figure 28)	Off-white (Figures 20, 21), 0.4 to 0.6 mm non-uniform thickness (Figures 20, 21, 31), Ti-enrichment from Ti-oxide pigment (Figure 35); also china clay pigment and calcite filler from FT-IR (Figures 39, 40); slag particles as filler too (Figure 28)
Coating# 4 (Bottom) Type: PVA, Non-breathable	Milky-white (Figures 20, 21), 0.5 to 0.6 mm non-uniform thickness (Figures 20, 21, 31), multi-layered opaque (Figures 24, 31)	Milky-white (Figures 20, 21), 0.5 to 0.6 mm non-uniform thickness (Figures 20, 21, 31), multi-layered opaque (Figures 24, 31)	Milky-white (Figures 20, 21), 0.4 to 0.5 mm non-uniform thickness (Figures 20, 21, 31), multi-layered opaque (Figures 24, 31)	Milky-white (Figures 20, 21), 0.2 to 0.3 mm non-uniform thickness (Figures 20, 21, 31), multi-layered opaque (Figures 24, 31)

Table 5: Protective Coatings at the top and bottom ends in all four Cores.

PETROGRAPHIC EXAMINATIONS – ANCHORING GROUT

BULK MINERALOGY AND CHEMISTRY FROM XRD AND XRF

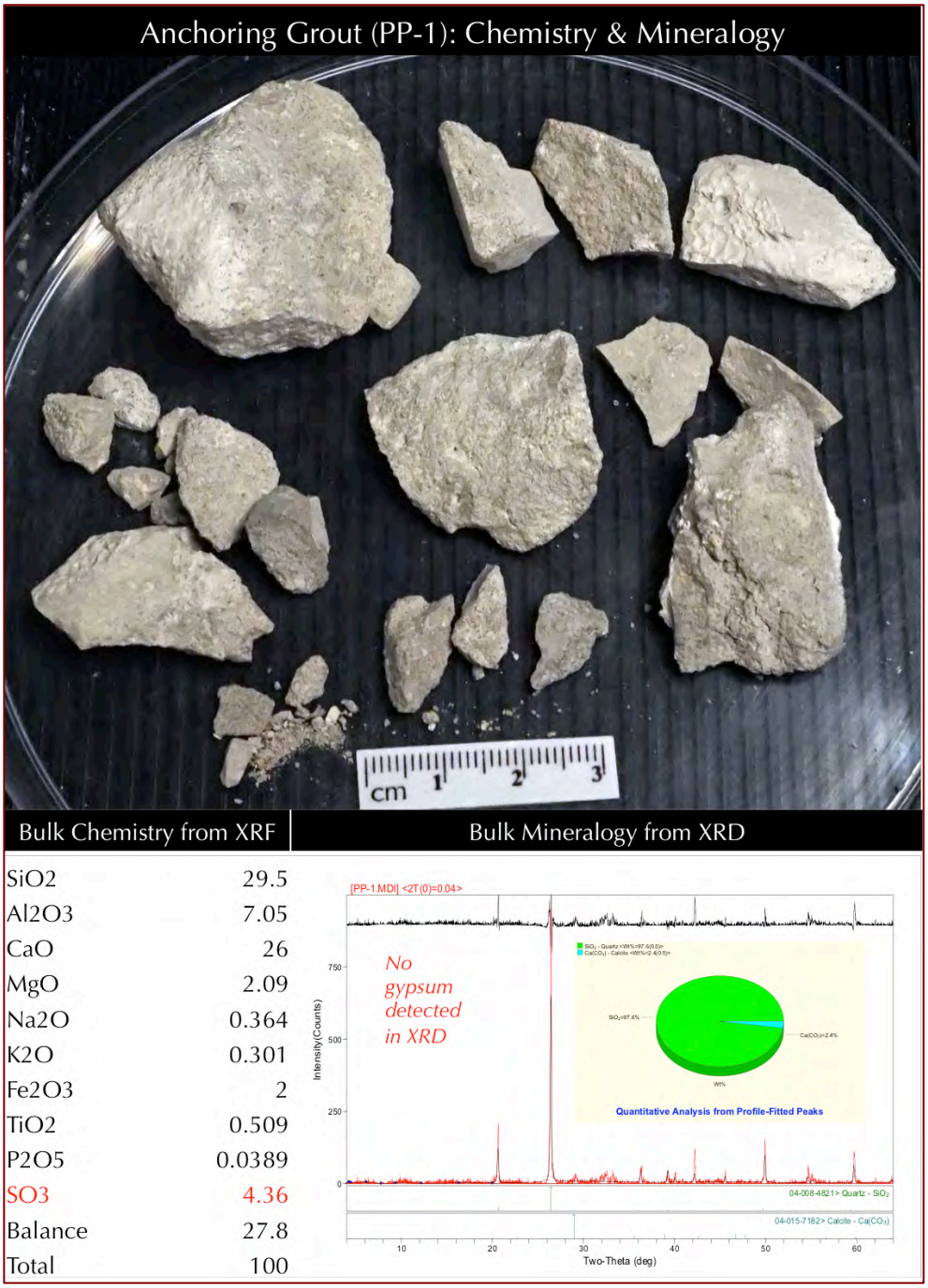

Figure 41: XRD and XRF of bulk grout to determine bulk mineralogy and chemical (oxide) composition, respectively. Sulfate content in grout indicates incorporation of a sulfate component in the binder, which, however, has not formed gypsum from hydration and hardening processes, as XRD did not find any gypsum peak. Bulk sulfate (as SO_3) content in the distressed grout is 4.3 percent, which is less than that of a gypsum-based grout but higher than that of a Portland cement-based grout, indicating presence of a sulfate component in the binder, which is not gypsum but a calcium sulfoaluminate cement.

MICROSTRUCTURE OF GROUT FROM OPTICAL MICROSCOPY OF THIN SECTION

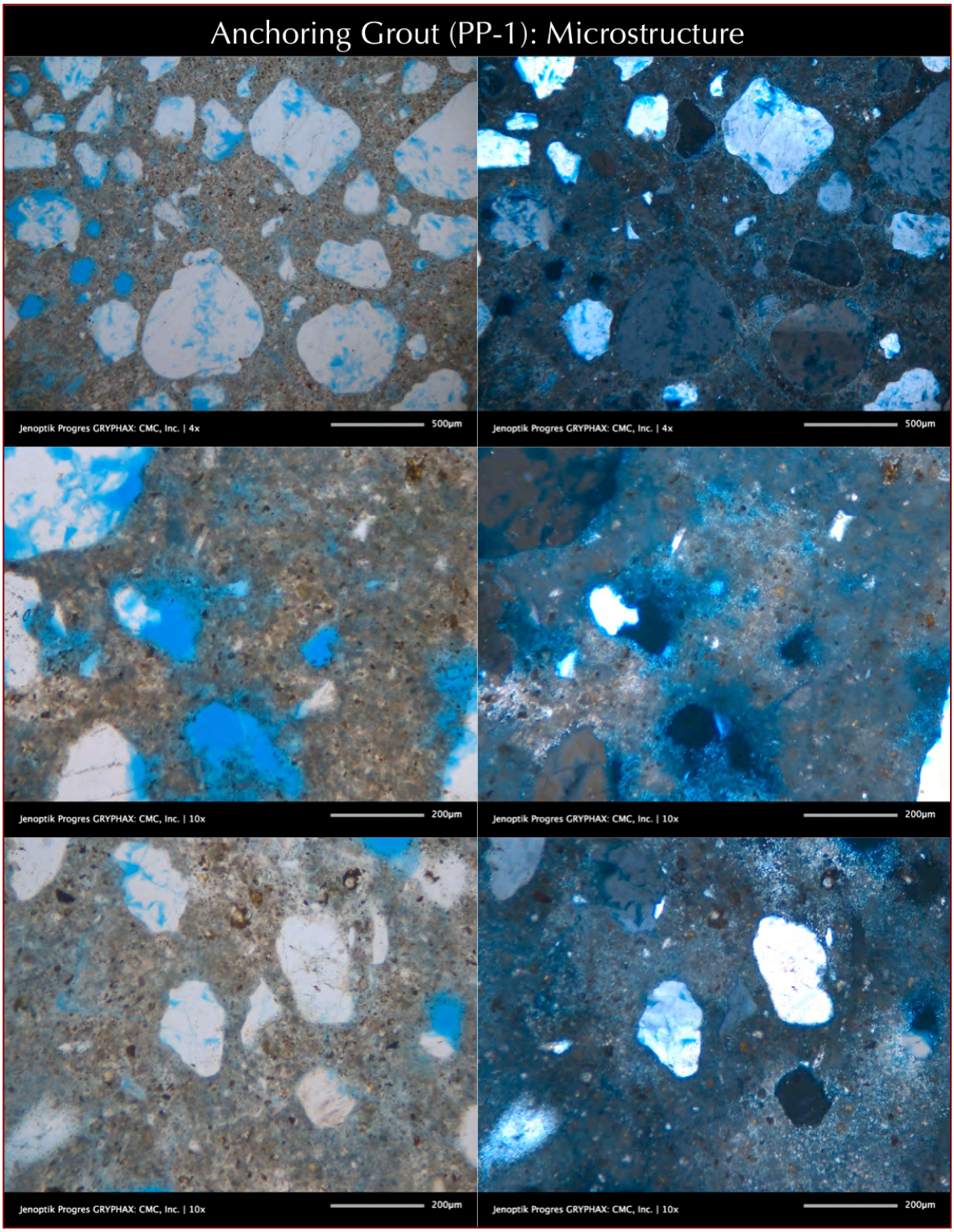

Figure 42: Photomicrographs of thin section of grout showing typical Portland cement paste composition of grout having many residual cement particles, but an overall variable density of paste from denser or porous areas as indicated by variable absorption of blue epoxy by the paste. Also present are fine silica (quartz) sand. Notice overall dense nature of grout and the absence of any visible or invisible cracking.

MICROSTRUCTURE & MICROCHEMISTRY OF GROUT FROM SEM-EDS OF THIN SECTION

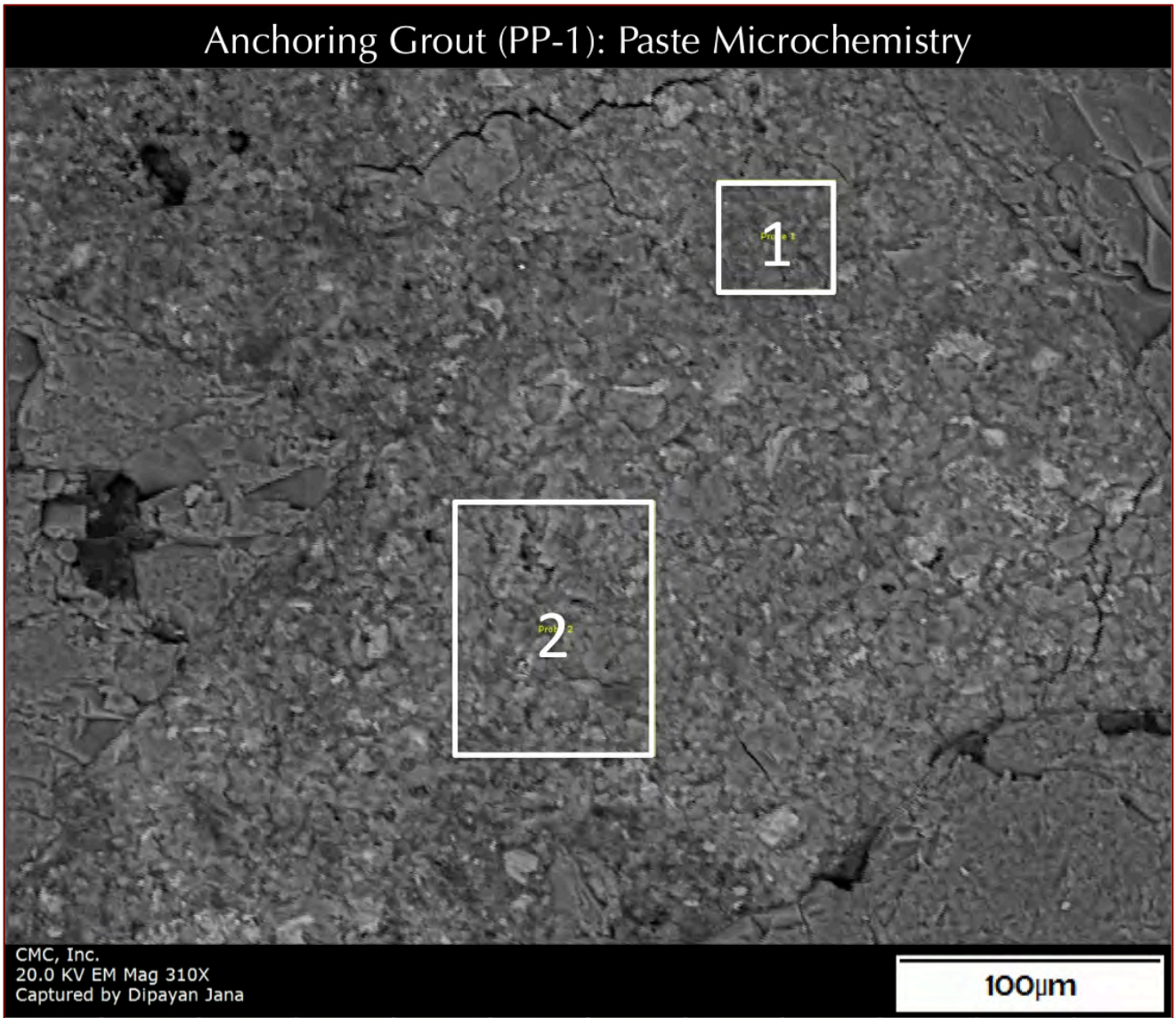

Probe	CaO	SiO2	Al2O3	Na2O	MgO	SO3	K2O	TiO2	FeO	Total	Phase
1	67.68	17.41	11.48	0.07	0.27	0.40	0.53	0.11	2.06	100.01	Paste
2	62.26	22.49	9.44	0.00	2.29	0.04	0.62	0.66	2.20	100.00	Paste

Figure 43: Backscatter electron image (top) and X-ray elemental analyses (bottom Table) of two boxed areas from the paste fraction of grout showing the typical calcium silicate composition of paste as anticipated from incorporation of Portland cement based binder with some sulfate but not high enough as found in many other gypsum-based grouts.

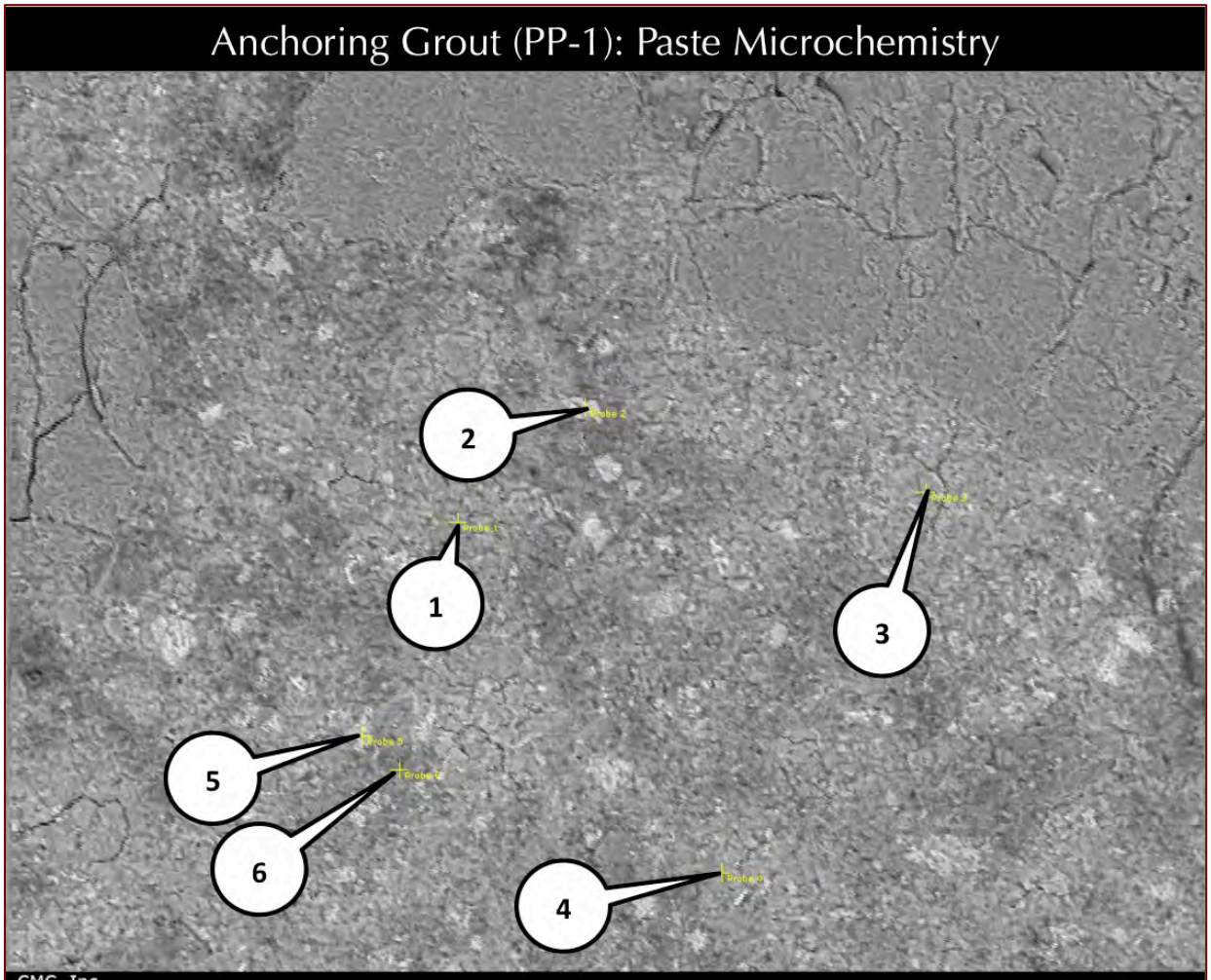

Probe	CaO	SiO2	Al2O3	Na2O	MgO	SO3	K2O	TiO2	FeO	Total	Phase
1	21.81	73.63	3.83	0.01	0.15	0.00	0.27	0.03	0.28	100.01	Grain
2	1.61	30.00	15.00	0.03	3.99	0.00	13.62	2.96	32.78	99.99	Grain
3	60.46	29.47	4.64	0.13	1.67	0.07	0.72	0.23	2.63	100.02	Paste
4	62.06	24.72	8.19	0.03	0.42	0.00	1.33	0.84	2.42	100.01	Paste
5	66.42	28.73	1.25	0.01	2.48	0.00	0.12	0.83	0.16	100.00	Paste
6	70.17	14.33	12.12	0.10	0.25	0.09	1.02	0.00	1.92	100.00	Paste

Figure 44: Backscatter electron image (top) and X-ray elemental analyses (bottom Table) of various areas from the paste fraction of grout (at the tips of callouts) showing the typical calcium silicate aluminate composition of paste from incorporation of Portland cement based binder with a calcium aluminate binder typical in many anchoring grouts. Notice the low amount or negligible sulfate in paste indicating absence of gypsum formation in paste (consistent with absence of gypsum peaks in XRD).

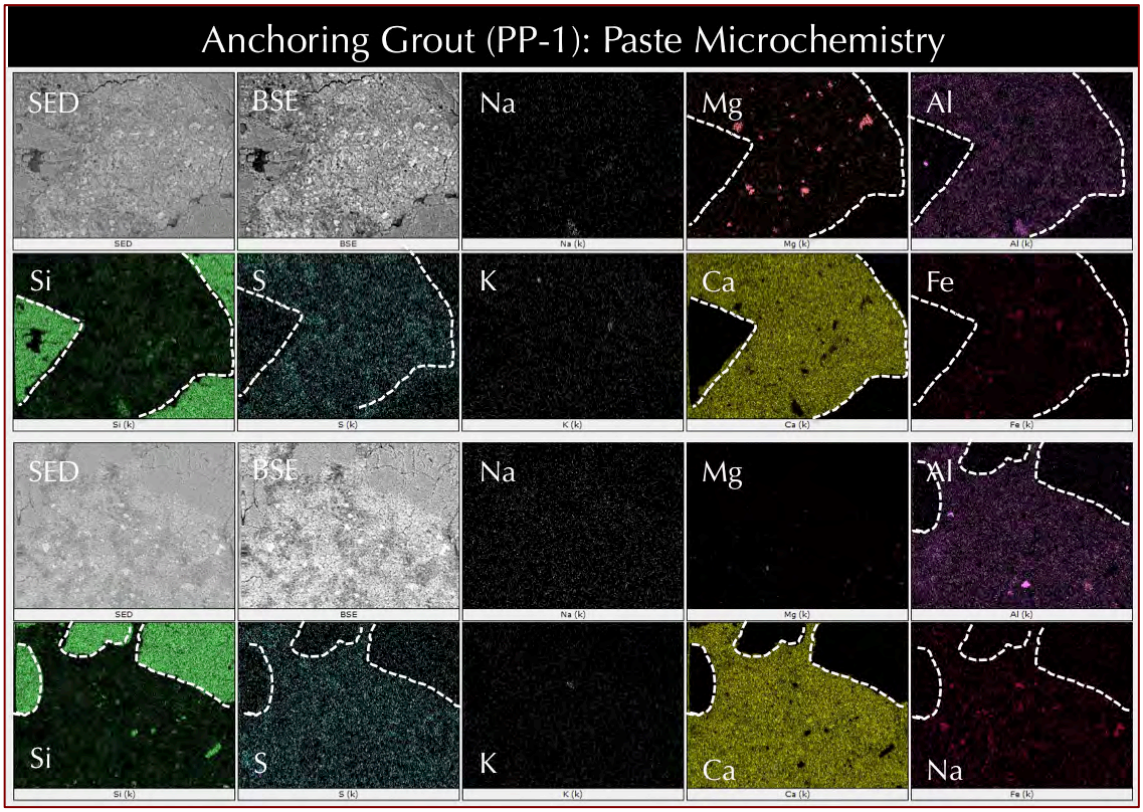

Figure 45: X-ray elemental mapping of paste around silica aggregate particles showing typical calcium, silica enrichment in paste but also some aluminum and sulfur when compared to silica sand particles indicating the presence of a binder that has provided aluminum and sulfur at levels higher than that typically come from Portland cement binder, thus indicating importation of a potential calcium sulfoaluminate component in binder along with Portland cement that is already detected from residual Portland cement particles in paste from optical microscopy (Figure 42).

Phase	CaO	SiO2	Al2O3	Na2O	MgO	SO3	K2O	TiO2	FeO	Total
PC	79.44	13.13	2.77	0.00	0.00	0.00	1.62	0.35	0.77	98.08
PC	61.14	24.60	4.14	0.03	0.64	0.00	3.16	0.64	2.70	97.05
Grout	67.68	17.41	11.48	0.07	0.27	0.40	0.53	0.11	2.06	100.01
Grout	62.26	22.49	9.44	0.00	2.29	0.04	0.62	0.66	2.20	100.00
Grout	60.46	29.47	4.64	0.13	1.67	0.07	0.72	0.23	2.63	100.02
Grout	62.06	24.72	8.19	0.03	0.42	0.00	1.33	0.84	2.42	100.01
Grout	66.42	28.73	1.25	0.01	2.48	0.00	0.12	0.83	0.16	100.00
Grout	70.17	14.33	12.12	0.10	0.25	0.09	1.02	0.00	1.92	100.00

Figure 46: Comparison of paste compositions in Portland cement concrete in Core P-4 (from Figure 36) and anchoring grout PP-1 (from Figures 43 and 44) showing higher aluminum, iron, and slightly higher sulfur in grout.

THERMAL ANALYSIS OF GROUT

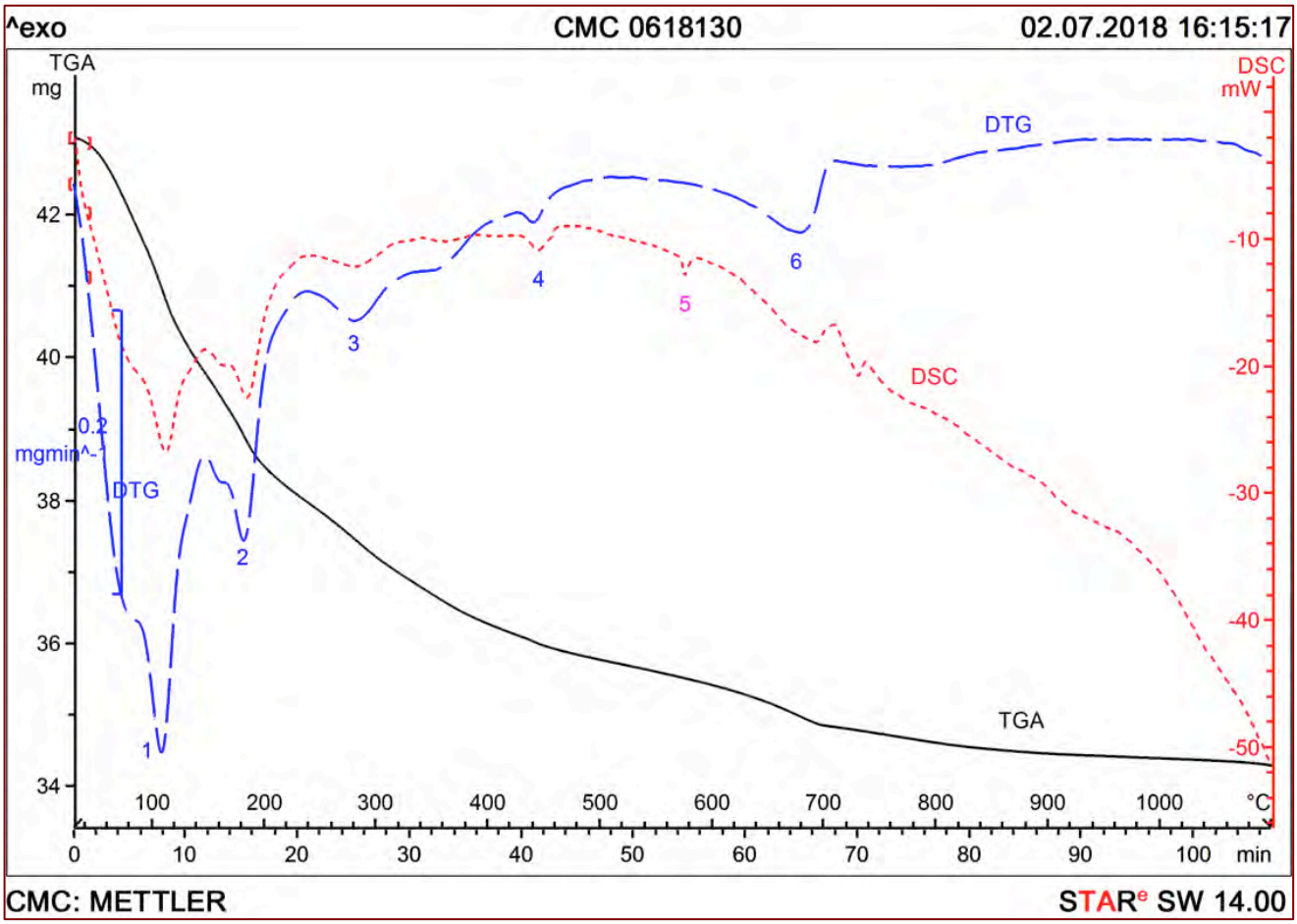

Figure 47: TGA (bold black), DSC (dotted red), and DTG (dashed blue) curves of grout showing weight loss due to thermal decompositions during controlled heating in a Mettler-Toledo's simultaneous TGA/DSC 1 unit from 30ºC to 1000ºC in a ceramic crucible (alumina 70µl, no lid) at a heating rate of 10ºC/min in a nitrogen purge at a rate of 75 mL/min. Dehydration and decarbonation reactions are marked as endothermic peaks (#1 to 6) in the superposed DSC and DTG curves. Large endothermic peaks at #1, 2, and 3 around 100ºC, 180ºC, and 280ºC, respectively, are from dehydration of CSH and calcium sulfoaluminte hydrate components of paste. Endothermic peak #4 at 440ºC is from dehydration of calcium hydroxide (portlandite) component of cement hydration. The alpha-to-beta polymorphic transition of quartz sand occurs around 575ºC, where integration of the peak area has indicated about 25 percent quartz in grout. Calcite decarbonation occurred around 680ºC and provided a low 1.6 percent calcite (which is consistent with low calcite detcted in XRD and low amount of carbonation detected in thin section photomicrograph of paste in Figure 42).

Sample	CMC 0618130											
Method	30 to 1100°C, 10°C/min, N_2 75.0 ml/min, Alumina Crucible (70µl, no lid)											
Phases	**1 (Water)**		**2 (Sulfates)**		**3**		**4 (Portlandite)**		**5 (Quartz)**		**6 (Calcite)**	
TGA	Step	-5.76%	Step	-3.20%	Step	-1.87%	Step	-0.45%			Step	-1.20%
		-2.4884 mg		-1.3828 mg		-0.8058 mg		-0.1963 mg				-0.5201 mg
	Left Limit	67.12 °C	Left Limit	161.06 °C	Left Limit	243.02 °C	Left Limit	424.95 °C			Left Limit	612.52 °C
	Right Limit	139.92 °C	Right Limit	238.03 °C	Right Limit	309.01 °C	Right Limit	459.19 °C			Right Limit	703.70 °C
	Step	-2.65%	Step	-1.48%	Step	-1.07%	Step	-0.17%			Step	-0.82%
		-1.1458 mg		-0.6410 mg		-0.4612 mg		-72.3686e-03 mg				-0.3528 mg
	Onset	91.10 °C	Onset	171.46 °C	Onset	262.01 °C	Onset	438.16 °C			Onset	645.87 °C
	Left Limit	67.12 °C	Left Limit	161.06 °C	Left Limit	243.02 °C	Left Limit	424.95 °C			Left Limit	612.52 °C
	Right Limit	139.92 °C	Right Limit	238.03 °C	Right Limit	309.01 °C	Right Limit	459.19 °C			Right Limit	703.70 °C
											% (SH, sf 2.27)	**-2.73%**
											% (ST, sf 2.27)	**-1.85%**
DTG	Integral	-0.45 mg	Integral	-33.73e-03 mg	Integral	-76.08e-03 mg	Integral	-21.14e-03 mg			Integral	-0.21 mg
	normalized	-1.04%	normalized	-7.81E-04	normalized	-0.18%	normalized	-4.90E-04			normalized	-0.49%
	Onset	82.07 °C	Onset	163.92 °C	Onset	248.20 °C	Onset	428.48 °C			Onset	624.08 °C
	Peak	**103.11 °C**	**Peak**	**178.70 °C**	**Peak**	**279.63 °C**	**Peak**	**441.45 °C**			**Peak**	**679.08 °C**
	Left Limit	67.12 °C	Left Limit	161.06 °C	Left Limit	243.02 °C	Left Limit	424.95 °C			Left Limit	612.52 °C
	Right Limit	139.92 °C	Right Limit	238.03 °C	Right Limit	309.01 °C	Right Limit	459.19 °C			Right Limit	703.70 °C
											% (sf 2.27)	**-1.11%**
DSC	Integral	-1512.67 mJ	Integral	-306.80 mJ	Integral	-266.56 mJ	Integral	-145.24 mJ	Integral	-45.33 mJ	Integral	-570.80 mJ
	normalized	-35.03 Jg^-1	normalized	-7.10 Jg^-1	normalized	-6.17 Jg^-1	normalized	-3.36 Jg^-1	normalized	-1.05 Jg^-1	normalized	-13.22 Jg^-1
	Onset	82.88 °C	Onset	166.07 °C	Onset	280.42 °C	Onset	432.06 °C	Onset	571.40 °C	Onset	638.00 °C
	Peak	**106.36 °C**	**Peak**	**181.42 °C**	**Peak**	**281.82 °C**	**Peak**	**444.43 °C**	**Peak**	**574.81 °C**	**Peak**	**680.74 °C**
	Left Limit	67.12 °C	Left Limit	161.06 °C	Left Limit	243.02 °C	Left Limit	424.95 °C	Left Limit	570.50 °C	Left Limit	612.52 °C
	Right Limit	139.92 °C	Right Limit	238.03 °C	Right Limit	309.01 °C	Right Limit	459.19 °C	Right Limit	584.34 °C	Right Limit	703.70 °C
									% (Pure quartz 4.30 Jg^-1)	**24.4**	% (Pure Calcite 1340 Jg^-1)	**0.98%**
Average Content, %									**Quartz**	**24.4**	**Calcite**	**1.67**

Figure 48: Results obtained from various endothermal and polymorphic transition peaks in TGA, DSC, and DTG curves in Figure 46.

CONCLUSIONS

CONCRETE

Concrete present in all four cores are compositionally similar to each other and made using essentially similar concrete ingredients, e.g., (a) crushed granite and crushed chlorite schist coarse aggregate (alkali granite content is higher than chlorite schist) having nominal maximum sizes of $^3/_4$ in. in. (19 mm) (b) natural siliceous (quartz-quartzite) sand fine aggregate having nominal maximums sizes of $^3/_8$ in. (9.5 mm); (c) Portland cement pastes having water-cement ratios similar within and between cores and estimated to be 0.45 to 0.50 and cement contents similar between cores and estimated to be from $5^1/_2$ to 6 bags per cubic yard; and (d) air contents variable within and between the cores indicating variable air-void systems from non-air-entrained concrete at the ends to air-entrained concrete in the interior where absence of air especially at the top and/or bottom ends of cores have created essentially a non-air-entrained appearance of concrete as opposed to detection of higher amount of 'entrained' air in the body to indicate potential air entrainment in the body (e.g., in Cores P-2, and P-4), or, to even absence of any air entrainment all throughout the depth of a core (e.g., in Core P-3), or adequate air entrainment throughout the

depth (in Core P-1). Therefore, air content and air entrainment showed lack of quality assurance of concrete being delivered at the locations of examined cores. Carbonation of concrete has occurred from both top and bottom ends and measured to be from as low as 2 mm in Core P-4 to as high as 30 mm in Core P-3 (15 to 20 mm in Cores P-1 and P-2) from their top ends, and, from 25 mm (in Cores P-2 and P-4) to 35 mm in Core P-1 and as deep as 45 mm in Core P-3 from their bottom ends. Besides carbonations to as deep as 15 to 30 mm from the exposed end of the cores (which are higher than that normally anticipated for a well-consolidated concrete impermeable to atmospheric carbon dioxide) there is no evidence of any chemical or physical deterioration of concrete detected in the concrete in all cores. Despite lack of air entrainment at the exposed surface ends of some cores to depths of $^1/_2$ to 1 in. (e.g., in Cores P-2, P-3, and P-4) and reported exposure to possible freezing, there is, however, no evidence of any cracking of other distress in the concrete at the exposed surface ends that could be contributed to cyclic freezing and thawing or a non-air-entrained concrete at critically saturated conditions. Carbonation is the only mechanism detected in the cores from prolonged exposures to atmospheric carbon dioxide that has penetrated deep enough to promote potential carbonation-induced corrosion of reinforcing steel, if steel is present within the carbonated zone, especially when the concrete cover over steel is shallow. Pastes in the concrete have water-cement ratios and consolidation that have promoted deep penetration of atmospheric carbon dioxide. Carbonation-induced corrosion of steel especially over shallow concrete cover can cause cracking and delamination of concrete cover over the exposed corroded steel. Both coarse and fine aggregates are present in sound condition and did not contribute to any distress.

PROTECTIVE COATING

All four cores showed two protective coatings at their exposed ends (Coat #1 and 2), and, two protective coats at the bottom ends (Coat #3 and 4) that are compositionally similar for each coat across the cores. Coat #1 is an elastomeric non-breathable urethane waterproofing membrane, gray to beige in color, less than 0.1 to 1.2 mm non-uniform thickness (maximum thickness is at the locations of quartz filler and minimum where filler is absent), showing characteristic titanium-enrichment from Ti-oxide pigment, and magnesium and silica in SEM-EDS and characteristic FT-IR absorption bands from Talc filler. Coat #2 beneath #1 at the top end is directly adhered to concrete, which is a non-breathable epoxy-based binder, gray to ash in color, 0.8 mm nominal thickness, more uniform in thickness than Coat #1 due to the absence of any coarse quartz fillers, but contains potential silicate (slag, fine silt-sized quartz) fillers as detected in SEM-EDS and silicate absorption bands in FT-IR studies. Coat #3 at the bottom end is directly adhered to concrete, which is a non-breathable poly-vinyl acetate (PVA)-based paint, off-white in color, 0.5 to 0.8 mm non-uniform thickness, showing characteristic titanium-enrichment from Ti-oxide pigment in SEM-EDS studies and also characteristic absorption bands for china clay pigment, silicate (slag, fine silt-sized quartz) and calcite fillers from FT-IR studies. Coat #4 applied over #3 at the bottom end directly exposed to the environment is another PVA-based paint, milky white in color, 0.5 to 0.6 mm and non-uniform thickness, showed multi-layered applications that appeared opaque in transmitted plane-polarized light observations in a petrographic microscope. FT-IR studies showed characteristic absorption bands for urethane in Coat #1, epoxy in

Coat #2, and PVA in Coat #3 and 4. Protective coatings are mostly well-bonded to each other and to concrete for those directly applied on concrete surfaces over the area of examinations in the cores.

ASSESSMENT OF CONCRETE CONDITION AT CORE LOCATIONS

Core Nos. P-1 and P-2 were reportedly collected respectively from areas exhibiting: (a) extensive delaminations; near excavation revealed severe rebar corrosion at the location of P-1, and (b) nearby walkway soffit delamination at the location of P-2; low cover soffit reinforcement is corroded – higher cover rebar minimally corroded in nearest excavation. No visible distress was noted at the locations of Cores P-3 and P-4.

As mentioned, except carbonation of concrete to depths as deep as 30 mm from top exposed end and 45 mm from bottom end and potential carbonation-induced corrosion of steel in concrete if steel is present within the carbonated zone (especially at the locations of shallow concrete covers over top layer of steel) there is no other evidence of any chemical or physical deterioration of concrete detected in the cores. Reported field evidence of extensive delaminations over severely corroded rebar at the location of P-1, and walkway soffit delamination at the location of P-2 over low cover, and minimal rebar corrosion over higher concrete cover over rebar are consistent with petrographic observations.

ANCHORING GROUT

Properties & Types

Properties that are vital for use of a proprietary prepackaged anchoring grout in railing posts are:

- Non-shrink behavior when set and hardened (hence also called nonshrink, or, shrinkage-compensating grout), which is achieved by an expansion at the plastic state (*pre-hardening expansion*) to fill available open or void spaces around railing post to provide successful anchorage and load-transfer from the railing to the surrounding concrete. Pre-hardening expansion reduces or eliminates subsequent shrinkage during hardening that a traditional Portland-cement-only grout system undergoes. Usually, the mechanism that provides the early expansion at the plastic state and thus the nonshrink behavior, if continues after hardening, contributes to the *post-setting/hardening expansions* with the failure of the grout system and/or the surrounding medium.
- Quick setting and high early strength, in order to reduce the time that posts are needed to be supported. Traditional Portland-cement-only grouts provide slow setting and strength gain, hence are commonly replaced by many newer-generations of proprietary grout products offering very fast setting and high early strengths.

The present examined grout is judged to be similar to many nonshrink grouts in the market that advertises quick setting and high early strength as two advantages if grout is installed according to manufacturer's recommendation and is not exposed to moisture during service.

The newer generations of nonshrink anchoring grouts are broadly classified into:

- Polymer Grouts (e.g., nonshrink epoxy grouts) that contain a filler and a polymer binder, or, a Polymer-Modified Grout, where a cementitious system is further densified with an impregnated polymer, or,
- Cementitious Grouts.

The present examined grout belongs to the category of cementitious grouts.

Cementitious grouts can have one of the following three primary types of binders that are traditionally used for repair materials, or, anchoring:

- Portland cement-based repair grouts, where Portland cement constituents the dominant binder component. Due to the requirements of shrinkage-compensation, quick setting, and high early strength during anchoring applications, Portland-cement-only grout systems, as mentioned, are less common than the following two types. A Type III Portland cement, being more finely ground than Type I/II can provide high early strength, hence a better choice in a cement-grout.
- Gypsum-based, which provide fast, early set, which may contain gypsum as the sole binder component, or gypsum with a minor amount of Portland cement (usually less than 10 percent cement to provide some passivation of embedded metals, which, however, can also cause formation of deleteriously expansive compounds like ettringite, a calcium sulfoaluminate hydrate, after initial hardening, if exposed to moisture during service, resulting in cracking of the grout itself and/or of the surrounding medium),
- Blended Portland cement and Calcium Aluminate Cement-based, or expansive calcium sulfoaluminate cement system, where sulfate-aluminate reactions during setting provide the necessary nonshrink behavior, which, however, can also contribute to the distress if this reaction continues after setting i.e. during service in the continued presence of moisture.

The present examined grout belongs to the third category of blended Portland cement and calcium aluminate/sulfoaluminate cement-based *cementitious grout, which is determined to contain no gypsum as a major binder component as found in the second category, but Portland cement as the major hydraulic cement along with possible presence of a calcium aluminate and/or sulfoaluminate-based binder. Bulk sulfate (as SO_3) content in the distressed grout is 4.3 percent, which is less than that of a gypsum-based grout but higher than that of a Portland cement-based grout, indicating presence of a sulfate component in the binder, which is not gypsum but a calcium sulfoaluminate cement.*

Both gypsum-based grouts and blended Portland cement/calcium aluminate cement-based grouts offer the necessary shrinkage compensation characteristic of a nonshrink grout. Many proprietary grout products contain other shrinkage compensation additives, such as:

- A shrinkage-compensating (expansive) cement, e.g., a Type K sulfoaluminate-type expansive cement, or a Type M expansive cement, which is a mixed Portland cement plus calcium aluminate cement plus calcium sulfate,

or, a Type S expansive cement, which is a very high C_3A, as high as 20% C_3A Portland cement containing a stoichiometrically high amount of calcium sulfate - all of which undergo an expansive formation of ettringite during hydration thus provide the shrinkage-compensation (expansion) during the early hardening period after setting, and all are specified in ASTM C 845.

- A shrinkage-compensating/reducing chemical (e.g., organic, water-soluble) admixture (SRAs, however, are not covered in ASTM C 494 specifications for chemical admixtures), which operates by interfering with the surface chemistry of the air/water interface within the capillary pores, reducing surface tension of water in the capillary pores (which is the prime factor for drying shrinkage of Portland cement-based systems), and consequently reducing the shrinkage as water evaporates from within the grout or concrete.
- Oxidizing iron aggregate, or metallic powders (aluminum).

Problems

Three common types of problems of many anchoring grout systems related to *post-hardening expansions* are:

- Volume instability when exposed to moisture after hardening i.e. during service, resulting in expansion or degradation of the product itself,
- Migration into and reaction with the surrounding concrete, again, in the presence of moisture during service that causes dissolution of potentially deleterious water-soluble components from the grouts to the concrete, resulting in the formation of expansive chemical compounds and deterioration of concrete as cracking and spalling; and,
- Lack of passivation of embedded metal, particularly aluminum causing corrosion of metal.

Based on detailed petrographic examinations, the present grout is judged to have experienced at least both of the first two types of distress, and, possibly also of the third type that can be verified from field survey. Additionally, from the fragmented (but not soft powdery as for many grouts made using excess water) yet dense appearance of the grout, as well as from the dense paste microstructure of the grout (as opposed to very soft, porous microstructure of grouts having evidence of excess water in the mix), the grout is determined to have been prepared with proper amount of water. Excess water if left from mixing and setting, can cause softening, subsequent recrystallization during drying, expansion, and disintegration of the grout, as well as deleterious expansive reactions with the aluminate components either within the grout (i.e. from the minor amount of added hydraulic cement) and/or from the surrounding concrete.

Excess Calcium Sulfates & Mechanisms of Post-Hardening Expansions and Distress

The primary cause for post-hardening expansion and associated distress of the grout and/or of the surrounding concrete is the presence of: (i) free calcium sulfate in the hardened grout, and (ii) moisture during service.

- After the rapid-setting/hardening grout has set, free calcium sulfate, if present dissolves if exposed to moisture during service, and then precipitates out as calcium sulfate again, when the material dries. After precipitation, the calcium sulfate is more loosely packed and occupies more space than the original free calcium sulfate, resulting in a friable deposit that expands within the material. This phenomenon is similar when a drywall, which is mostly calcium sulfate, gets wet and then dries out, forming an expanded, flaky residue.
- Also, when calcium sulfate is dissolved in water, it can migrate into the surrounding concrete, where it can react with the aluminates in the cement, resulting in deleterious expansions from sulfate-aluminate reactions and formation of secondary ettringite deposits.

From the absence of free gypsum in SEM-EDS or XRD studies, both of the above mechanisms are judged NOT to have played roles in causing disintegration of the present grout, which is common in many gypsum-based grouts. However, moisture-induced freezing and post-hardening moisture-induced sulfate-aluminate reactions during service are judged to have contributed to the reported expansion of this grout in the field.

For Portland-cement-only grouts, calcium sulfate originally present in the Portland cement (usually less than 3% by mass of cement when C_3A content of cement is 8% or less, or, less than 3.5% by mass of cement when C_3A content is greater than 8%) for set-controlling purposes (to control the flash set of C_3A in cement) is consumed during initial hydration of cement in the plastic state. If, however, 'excess' calcium sulfate is present after hydration that can, when exposed to moisture during service, cause several distress mechanisms in grout and/or surrounding concrete. That 'excess' calcium sulfate can: (a) readily dissolve in the moisture during service, and when the system dries out, it can recrystallize, thus occupying more volume than before it was wetted, thus causing disintegration of the grout. Additionally: (b) excess calcium sulfate in the hardened grout can migrate out to the surrounding concrete to form deleteriously expansive materials by sulfate-aluminate reactions, leading to cracking and spalling of concrete. *The present grout does not belong to the above category.*

For gypsum-based grouts that, by definition, contain abundant free calcium sulfate at the hardened state, the system, though fast-setting, is extremely vulnerable to moisture during service, for the same reasons as mentioned for the fate of excess calcium sulfate in the Portland-cement-only grouts during service in a moist environment. Gypsum can: (a) expand during wetting (ready dissolution in water) and drying (recrystallization to larger masses); (b) gypsum can participate in deleterious expansive reaction with aluminates in Portland cement, if the grout formulation contains a minor cement additive, or with the hydrates of aluminate in the Portland cement in the surrounding concrete; (c) gypsum can cause expansive corrosion of aluminum posts, anchors, and clips that they may be in contact with when exposed to moisture during service; and (d) gypsum in a confined space can absorb a lot of moisture in the moist outdoor condition and expand during freezing at the moist state. *The present grout does not belong to the above category.*

For blended cement systems containing Portland cement and calcium aluminate cement, or an expansive (e.g., calcium sulfoaluminate) cement, pre-hardening expansion is achieved by sulfate-aluminate reactions and abundant primary ettringite formation from hydration of such systems, which provide the necessary expansion at the plastic state. Both Portland cement and calcium aluminate cement contain calcium sulfate for set-controlling purposes (3-3.5% maximum SO_3 for Portland cement and 2.5-15% SO_3 for calcium aluminate cement), where the former has a much tighter control on chemistry and a well-established ASTM standard (C 150) than the latter (which has no ASTM standard or a control of SO_3 content). Hence sulfate content in calcium aluminate cement can vary between products and formulations depending on the desired performance in a particular application. Hence two different products having the same SO_3 content may behave differently i.e. one could be expansive when exposed to moisture, while the other may not. Due to such uncontrolled, inconsistent calcium sulfate contents, it is difficult to know if a given batch will be durable prior to use. The binder in these newer-generation of grouts can also contain fly ash, limestone fines, silica fume, and other additives. *The present grout belongs to this category, where moisture-induced freezing and post hardening moisture-induced sulfate-aluminate reactions during service are judged to have contributed to the reported expansion of this grout in the field.*

Mix Proportioning & Curing

In addition to the type of binder present, a control on the amount of mix water added and adequate moist curing are critical. Sufficient mix water is needed for mixing and sulfate-aluminate reactions at the plastic state to achieve the non-shrink behavior, but 'excess' water can cause physical and/or chemical segregation, e.g., of aggregates at the bottom from binder at the top and/or different layers of compounds, respectively. It is crucial to follow manufacturer's recommended amount of mix water. For blended cement systems, adequate moist curing is important since inadequate curing may cause reversal of chemical reactions changing the resulting chemical compounds to more expansive and lower-strength compounds (Papas 2014).

ASTM Specifications & Tests

Presently, there is no ASTM standard that specifically addresses rapid-hardening grouts, particularly for use in an exterior environment where the hardened material will be exposed to moisture in service, *such as the case for the present grout*. The ASTM standards commonly associated with the repair and anchorage grout systems are:

- ASTM C 928, "Standard Specification for Packaged, Dry, Rapid-Hardening Cementitious Materials for Concrete Repairs," which covers packaged, dry, cementitious mortar or concrete materials for rapid repairs to hardened hydraulic-cement concrete pavements and structures i.e. elements that could be exposed to moist exterior environments during service.
- ASTM C 1107, "Standard Specification for Packaged, Dry, Hydraulic Cement Grout (Nonshrink)" is the specification that is often cited by manufacturers of prepackaged grouts, where the specification covers as stated in the scope "packaged dry, hydraulic cement material (nonshrink) intended for use under applied load (such

as to support a structure, a machine, and the like) where a change in height below the initial placement heights is to be avoided." Many anchoring grout systems advertised to meet C 1107, however, are not consistent with intended use mentioned in the scope of C 1107.

Both standards require length change measurements at specific ages, but do not necessarily simulate the conditions that an anchoring grout may face during service. For example, ASTM C 928 uses mortar bars cured in both air and water but the length change is measured only at a single age of 28 days, which does not provide sufficient information to predict expansion potential of an anchoring grout. ASTM C 1107 uses a cylindrical specimen that is stored restrained for 56 days, which may simulate semi-restrained condition of anchoring grout but does not simulate the conditions that a repair grout in a deteriorated concrete would be exposed to after removal of the forms.

Two ASTM Tests followed by manufacturers of many nonshrink cementitious grouts are:

- ASTM C 827, "Standard Test Method for Change in Height at Early Ages of Cylindrical Specimens from Cementitious Mixtures;" and,
- ASTM C 1090, "Standard Test Method for Measuring Change in Height of Cylindrical Specimens for Hydraulic-Cement Grout."

ASTM C 827 evaluates vertical height change of nonshrink grout at the plastic state prior to hardening, where up to 90% of shrinkage can occur following the initial expansion; therefore, C 827 has been used widely as the starting point for specification of nonshrink grout. ASTM C 1107 sets the maximum height change requirements in the plastic state to be 4.0% when tested in accordance with C 827, but C 1107 does not set a minimum requirement for height change in the plastic state. Therefore, a grout can exhibit shrinkage in the plastic state and still meet the requirements of C 1107. Typical values of height change of nonshrink grouts tested *a la* C 827 and conforming to C 1107 are from 1% minimum to 4% maximum.

REFERENCES

ACI Committee Report 116R-00, Guide to Durable Concrete, *ACI Manual of Concrete Practice*, Vol. 1, American Concrete Institute, 2008.

ACI Committee Report 201.2R, Guide to Durable Concrete, *ACI Manual of Concrete Practice*, Vol. 1, American Concrete Institute, 2008.

ASTM C 457 "Standard Test Method for Microscopical Determination of Parameters of the Air-Void System in Hardened Concrete," Vol. 4.02, ASTM International, West Conshohocken, PA, 2010.

ASTM C 856 "Standard Practice for Petrographic Examination of Hardened Concrete," Vol. 4.02, ASTM International, West Conshohocken, PA, 2014.

ASTM C 1152: "Standard Test Method for Acid-Soluble Chloride In Mortar and Concrete," Vol. 4.02, ASTM International, West Conshohocken, PA, 2012.

Jana, D., and Cole, A.A., "Microscopy: A Practical Solution to Concrete Problems," *Bulletin of Concrete Industry Board*, September 1997a, pp. 18-22.

Jana, D., "Petrography: A Powerful Tool For Solving Common Concrete Problems," *Civil Engineering NEWS*, March 1997b, pp. 40-44.

Jana, D., and Erlin, B., "Scaling Revisited," Letters, *Concrete International*, American Concrete Institute, September 2001, pp. 25-26.

Jana, D., "Concrete, Construction or Salt – Which Causes Scaling? Part I: Importance of Air-Void System in Concrete," *Concrete International*, American Concrete Institute, November 2004a, pp. 31-38.

Jana, D., "Petrography and Concrete Repair – A Link is Needed," Point of View Publication in *Concrete International*, American Concrete Institute, pp. 37-39, January 2005a.

Jana, D., Erlin, B., and Pistilli, M., "A Closer Look at Entrained Air in Concrete," *Concrete International*, American Concrete Institute, June 2005b, pp. 31-38.

Jana, D., "Sample Preparation Techniques in Petrographic Examinations of Construction Materials: A State-of-the-art Review," *Proceedings of the 28th Conference on Cement Microscopy*, International Cement Microcopy Association, Denver, Colorado, pp. 23-70, 2006.

Jana, D., "Concrete Scaling – A Critical Review," *Proceedings of the 29th Conference on Cement Microscopy*, Quebec City, PQ, Canada, 2007.

Jana, D., and Erlin, B., "Delamination: A Sometime Curse of Entrained Air," *Concrete Construction*, January 2005, pp. 101-107.

Jana, D., "Delamination – A State-of-the-Art Review," *Proceedings of the 29th Conference on Cement Microscopy*, ICMA, Quebec City, Canada, 2007, pp. 135-167.

Jana, D., Erlin, B., "Carbonation as an Indicator of Crack Age," *Concrete International*, May 2007, pp. 61-64.

Papas, S. M., "Cementitious Concrete Repair Materials and Grouts: When is Fast Too Fast?" Interface, pp. 18-24, April 2014.

✪ ✪ ✪ END OF TEXT ✪ ✪ ✪